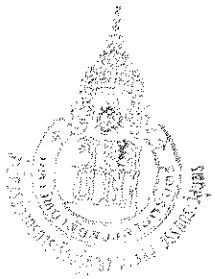

Titanium Dioxide Photocatalysts: Syntheses, Antimicrobial Activities, and Dye Degradations

Uraiwan Sirimahachai

A Thesis Submitted in Fulfillment of the Requirements

for the Degree of Doctor of Philosophy in Chemistry

Prince of Songkla University

2010

Thesis Title	Titanium Dioxide Photocatalysts: Syntheses, Antimicrobial Activities, and Dye Degradations
Author	Mrs Uraiwan Sirimahachai
Major Program	Chemistry

Major Advisor:

Sumpun Wongnawa
(Assoc. Prof. Dr. Sumpun Wongnawa)

Co-advisor:

Souwalak Phongpaichit
(Assoc. Prof. Dr. Souwalak Phongpaichit)

Examining Committee:

Apisit Songsasen ..... Chairperson
(Assoc. Prof. Dr. Apisit Songsasen)

Sumpun Wongnawa
(Assoc. Prof. Dr. Sumpun Wongnawa)

Souwalak Phongpaichit
(Assoc. Prof. Dr. Souwalak Phongpaichit)

Lek Sikong
(Assoc. Prof. Dr. Lek Sikong)

Walailak Puetpaiboon
(Dr. Walailak Puetpaiboon)

The Graduate School, Prince of Songkla University, has approved this thesis as fulfillment of the requirements for the Doctor of Philosophy Degree in Chemistry

A. Phongdara
(Prof. Dr. Amornrat Phongdara)
Dean of Graduate School

ATCC25922, *Pseudomonas aeruginosa* ATCC28753, *Bacillus subtilis* BGA, *Staphylococcus aureus* ATCC25923 และ Methicillin-resistant *Staphylococcus aureus* DMST2054) และแบบเชิงคุณภาพกับยีสต์ 2 ชนิด (*Candida albicans* ATCC90028 และ *Cryptococcus neoformans* ATCC 90112) ซึ่งทำการศึกษาที่ความเข้มข้นไทเทเนียมไดออกไซด์สูงสุด คือ 100 มิลลิกรัมต่อมิลลิลิตร และเวลาที่ใช้ในการฉายแสงสูงสุด คือ 120 นาที พบว่าไทเทเนียมไดออกไซด์ทุกชนิดที่เตรียมขึ้นมีฤทธิ์ต้านเชื้อแบคทีเรียได้แต่ในระดับที่แตกต่างกัน โดย 2 ชนิด แสดงฤทธิ์ที่ดีกว่า Degussa P25 ซึ่งเป็นไทเทเนียมไดออกไซด์เชิงพานิชย์ที่นิยมใช้เป็นตัวเร่งปฏิกิริยาด้วยแสง ส่วนกรณีที่ทำการศึกษาไทเทเนียมไดออกไซด์กับยีสต์ พบว่าไทเทเนียมไดออกไซด์ที่เตรียมขึ้นมีผลในการหน่วงการเจริญเติบโตของยีสต์เท่านั้น ซึ่งให้ผลดีใกล้เคียงกับ Degussa P25 แต่ให้ผลดีกว่าไทเทเนียมไดออกไซด์เชิงพานิชย์ Anatase และ Rutile

ในส่วนที่ 2 เป็นการศึกษาการเตรียมไทเทเนียมไดออกไซด์อนุภาคระดับนาโน(2 นาโนเมตร) เคลือบบนซิลิคอนไดออกไซด์รูปทรงกลมขนาด 300-400 นาโนเมตร(TiO_2/SiO_2) ด้วยกระบวนการโซล-เจลที่อุณหภูมิต่ำ (60 องศาเซลเซียส) ในขั้นตอนการเตรียมมีการควบคุมอัตราส่วนของปริมาณไทเทเนียมไดออกไซด์ที่เคลือบบนผิวทรงกลมของซิลิคอนไดออกไซด์โดยแปรเปลี่ยนปริมาณของไทเทเนียมโซลที่จะนำไปเคลือบบนซิลิคอนไดออกไซด์เป็นเปอร์เซ็นต์น้ำหนักของไทเทเนียมไดออกไซด์ คือ 30%, 50% และ 75% TiO_2 ที่เคลือบบนผิวทรงกลมซิลิคอนไดออกไซด์ (TiO_2/SiO_2) ตามลำดับ จากนั้นทำการศึกษาสมบัติทางกายภาพและทางเคมีของไทเทเนียมไดออกไซด์ที่เคลือบบนซิลิคอนไดออกไซด์ที่เตรียมได้ด้วยเทคนิค X-ray Diffraction Spectrometry (XRD), X-ray Photoelectron Spectroscopy (XPS), Scanning Electron Microscopy (SEM), Energy-Dispersive X-ray Spectrometry (EDX), Transmission Electron Microscopy (TEM),

Brunauer-Emmett-Teller (BET) และ Fourier-Transformed Infrared Spectrometry (FT-IR) นอกจากนี้ยังได้ศึกษาความสามารถในการเป็นตัวเร่งปฏิกิริยาด้วยแสงของ TiO_2/SiO_2 ที่เตรียมได้โดยใช้สลายสีย้อมเมทิลีนบลู พบว่า TiO_2/SiO_2 ที่เตรียมขึ้นสามารถสลายสีย้อมได้ดีและ TiO_2/SiO_2 ทุกสัดส่วนให้ผลในการสลายสีย้อมเมทิลีนบลูได้ดีกว่า ไทเทเนียมไดออกไซด์บริสุทธิ์ โดยเฉพาะ 50% TiO_2/SiO_2 มีความสามารถในการสลายสีย้อมเมทิลีนบลูได้ดีกว่าไทเทเนียมไดออกไซด์บริสุทธิ์ถึง 6 เท่า

Thesis Title	Titanium Dioxide Photocatalysts: Syntheses, Antimicrobial Activities, and Dye Degradations
Author	Mrs Uraiwan Sirimahachai
Major Program	Chemistry
Academic Year	2010

ABSTRACT

The first part of the thesis dealt with the syntheses of titanium dioxide and M(III)-doped titanium dioxide photocatalysts and studied their antimicrobial activities. The catalysts were prepared by the sol-gel process at low temperature (80 °C and 95 °C) without calcination, by varying the reaction conditions, acids, water content, and M(III) dopants. The characterizations of products were determined by X-ray Diffraction Spectrometry (XRD), Scanning Electron Microscopy (SEM), Brunauer-Emmett-Teller (BET), Fourier-Transformed Infrared Spectrometry (FTIR), Energy-Dispersive X-ray Spectrometry (EDX), and UV-vis Spectroscopy. Compositions of these samples were mainly an amorphous phase with small amount of anatase, rutile, or a mixture of anatase and rutile. The crystallite sizes of all samples were about 5 – 10 nm. The antimicrobial activities of the synthesized TiO_2 samples were investigated quantitatively against five strains of bacteria, *Escherichia coli* ATCC25922, *Psudomonas aeruginosa* ATCC27853, *Bacillus subtilis* BGA, *Staphylococcus aureus* ATCC25923, and methicillin-resistant *S. aureus* (MRSA) DMST 2054 by agar dilution method. In addition, qualitative inhibitory activities were carried out with two species of yeasts, *Candida albicans* ATCC90028 and *Cryptococcus neoformans* ATCC90112, by agar dilution method upon the highest concentration of titania (100 mg/mL) and highest irradiation time (120 min). In case of bacteria, all the synthesized samples showed inactivation activity with varying degree of efficiency. Two of them showed much higher activity than Degussa P25 which is the popular commercial photocatalyst. Besides, the prepared titania showed retarded the growth of yeast favorably with Degussa P25. However, the inhibitory

growth of yeast by the synthesized TiO_2 samples were greater than commercial anatase and rutile.

In the second part, the nanosized TiO_2 and nano anatase TiO_2 (*ca.* 2 nm) decorated on SiO_2 sphere core-shell (*ca.* 300-400 nm) were synthesized by using sol-gel method at low temperature (60 °C). In the synthesis procedure, the control of titanium dioxide sol decorated on silicon dioxide sphere was done by varying the relative weight percentage of TiO_2 sol grafted on SiO_2 sphere as 30%, 50%, and 75% TiO_2/SiO_2. The synthesized pristine TiO_2 nanoparticle, TiO_2 grafted on SiO_2 sphere with various ratios have been characterized for their structures and morphologies by X-ray Diffraction Spectrometry (XRD), X-ray Photoelectron Spectroscopy (XPS), Scanning Electron Microscopy (SEM), Energy-Dispersive X-ray Spectrometry (EDX), Transmission Electron Microscopy (TEM), Brunauer-Emmett-Teller (BET), and Fourier-Transformed Infrared Spectrometry (FT-IR). The photocatalytic activities of all nanocomposites were investigated by using methylene blue as a model dye pollutant. The synthesized TiO_2/SiO_2 particles appeared to be very efficient toward degradation of methylene blue pollutant as compared to pure TiO_2 particles. Especially, the 50% TiO_2/SiO_2 powder was a capable photocatalyst in this series to decolorize methylene blue with an activity about 6 times higher than that of pristine TiO_2.

ACKNOWLEDGEMENTS

I would like to express my sincere gratitude and appreciation to my advisor, Assoc. Prof. Dr. Sumpun Wongnawa, for his numerous guidance, support and patience towards the completion of this work without which I would have been unable to complete this work.

I wish also to express my sincere thanks to my co-advisor, Assoc. Prof. Dr. Souwalak Phongpaichit, for her advice and assistance. I am also grateful to Assoc. Prof. Dr. Apisit Songsasen, Assoc. Prof. Dr. Lek Sikong, and Dr. Walailak Puetpaiboon, the examining committee for their kind comments and correction to the report. Special thanks are addressed to Prof. Dr. Mark A. Shannon (University of Illinois at Urbana-Champaign, USA) for his valuable guidance, excellent suggestion and understanding which kept me going while so far away from home. I am also very grateful to all members of the academic and technical staff of both Prince of Songkla University and University of Illinois at Urbana-Champaign who have helped me in various ways throughout this research. In addition, my acknowledgements are extended to all of my collaborators who helped create an enjoyable atmosphere to be working in and for their many helpful in many countless ways throughout the years.

This research was made possible by the Songklanagarind Scholarship for Graduate Study from the Prince of Songkla University and the Thesis Research Fund through the Graduate School-PSU. I am also indebted to the NSF Science and Technology Center of Advanced Materials for Purification of Water with Systems (WaterCAMPWS), University of Illinois at Urbana-Champaign for partial financial support.

Finally, I would like to thanks my husband Keerati and our little boy Kenji for their unconditional love and sacrifices in order to make this work a reality. Also, my parents and the rest of my family, who are always loving and supporting me in their characteristic style, deserve more gratitude than I can ever express.

Uraiwan Sirimahachai

CONTENTS

CONTENTS (Continued)

CONTENTS (Continued)

LIST OF TABLES

LIST OF ILLUSTRATIONS

LIST OF ILLUSTRATIONS (Continued)

LIST OF ILLUSTRATIONS (Continued)

LIST OF ILLUSTRATIONS (Continued)

LIST OF SCHEMES

ABBREVIATIONS AND SYMBOLS

eV	=	Electron volt
g	=	Gram
hr	=	Hour
nm	=	Nanometer
min	=	Minute
mL	=	Milliliter
mg/mL	=	Milligram per milliliter
mol/L	=	Mole per liter
ppm	=	Part per million
^{o}C	=	Degree celcius
λ_{max}	=	Maximum wavelength
MIC	=	Minimum inhibitory concentration (mg/mL)
DBPs	=	Disinfection by-products
MB	=	Methylene blue
TTIP	=	Titanium tetraisopropoxide
MTMS	=	Methyl-trimethoxysilane
OEt	=	Etoxide
OPr^{i}	=	Isopropoxide
BET	=	Brunauer-Emmett-Teller
EDX	=	Energy dispersive X-ray
FTIR	=	Fourier transform infrared
SEM	=	Scanning electron microscope
UV-Vis	=	Ultraviolet-Visible
XRD	=	X-ray diffractrometer
XPS	=	X-ray photoelectron spectroscopy
ROS	=	Reactive Oxygen Species
VB	=	Valence band
CB	=	Conduction band

Part I

Synthesis and Evaluation of Antimicrobial Activity of Titanium Dioxide Photocatalysts

CHAPTER 1

INTRODUCTION

1.1 Introduction

An exploration of a new technology is undertaken in the hope that eventually its practical applications will generate revenue. Yet, interest in some topics remains high over a period of years despite the absence of profitable commercial deployment. Heterogeneous photocatalysis is one of this topic which has attracted great attention as an alternative method for water and air purification processes. Fundamental and applied research on this subject has been performed extensively during the last three decades, and this is illustrated by the vast numbers of scientific and technical publication on this topic. Nowadays, the main goal of research and development in the area is the use of the technique for air purification and waste water treatment known as photocatalytic oxidation (PCO) process. This method offer the advantage of destroying the pollutants, in contrast to conventional techniques such as activated carbon or air stripping that only transfer the contaminants from one phase to another. PCO is a room temperature combustion process which involves the use of UV radiation with titanium dioxide (TiO_2) as a photocatalyst. In this way, organic and inorganic compounds and even microorganisms, are degraded or transformed into less harmful substances, CO_2 and H_2O (Fujishima, *et al.*, 1999).

An ideal photocatalyst for photocatalytic oxidation is characterized by the following attributes (Carp, *et. al.*, 2004):

(a) Photo-stability.

(b) Chemically and biologically inert nature.

(c) Availability and low cost.

(d) Capability to adsorb reactants under efficient photonic activation ($h\nu \geq E_g$)

Titania is the most widely employed nanomaterial in photocatalytic processes, although there are several nanomaterials currently considered as photocatalysts and/or supports for photocatalysis aside from titania. These include related metal oxides, metal chalcogenides, zeolites (as supports), etc. However, among these nanomaterials TiO_2 has proven to be the most suitable for widespread environmental application because its characteristic in terms of chemical stability, endurance, thin film transparency, and lower production costs over other similar photocatalyst (Hoffmann, *et al.*, 1995; Fox and Dulay, 1993). Good catalytic property is governed by two major opposing physical properties: surface area and crystallinity of the catalysts. The high surface area helps facilitate adsorption of the target molecules onto the surface of the catalyst, consequently as the higher number of molecules are adsorbed the faster the rate of reaction. The high crystallinity helps prolong the recombination rate of the photoexcited electron and positive hole resulting in strong reducing of oxidizing power of the catalyst (Ohtani, *et al.*, 1997). Among the two properties, crystallinity and surface area, one has to decide and choose one over the other since both cannot be had simultaneously from the syntheses. It has been reported that the different methods for the syntheses of TiO_2 result in products with different structures (anatase or rutile), crystallinity, and contaminants. Consequently, the surface properties of TiO_2 strongly depend on the preparation techniques (Zhang, *et al.*, 1999; Reddy, *et al.*, 2001). In preparing oxide materials, the sol-gel method can provide a number of advantages over conventional methods.

Another important application related to photocatalysis is disinfection. Well-known disinfection processes like chlorination, UV-irradiation, membrane filtration, and ozone all have their advantages and disadvantages. The most widely used disinfection process is chlorination, because of its high disinfection rate, residual effect, and low cost. However, due to natural organic matter (NOM) found in the water, disinfection by-products (DBPs) generated may present a health risk (Urbansky and Magnuson, 2002: Freuze, *et. al.*, 2005). Other frequently used processes are ozonation and irradiation by germicidal lamps (254 nm), which also have problems and limitations, such as lack of residual effect (Masschelin, 2002) and generation of toxic disinfection by-product by ozonation (Huang, *et. al.*, 2005). Therefore, there is

a growing interest in developing alternative, effective low-cost disinfection technologies. The photocatalytic disinfection is such a technology. Killing microbial cells through the use of photoexcited semiconductor powder was first reported by Matsunaga and his colleague (Matsunaga, *et al.*, 1985). They reports that microbial cells could be killed by contact with TiO_2-Pt catalyst under illumination with near UV light for 60 to 120 min. Since then, an increasing number of scientific contributions have developed new materials, supported photocatalysts, photoreactors, and procedures for both gas and aqueous-phase purification and disinfection. Viruses, bacteria, fungi, algae, and cancer cells are included in the wide spectrum of organisms that were inactivated using this technique (Blake, *et al.*, 1999).

In our earlier work (Randorn, *et al.*, 2004), we found that the amorphous form, previously thought rather inactive, with small amount of crystalline anatase form also showed photocatalytic properties. This amorphous form could be synthesized by a simple precipitation method to produce TiO_2, however, the subsequent calcination was excluded. Since no calcination was employed, the product powder was mostly present in an amorphous form with some hydrated water molecules. Its surface area was also significantly higher than that of commercially available anatase/rutile or P25 due to its amorphous morphology.

Another previous work was done by Kanna (Kanna and Wongnawa, 2008) showed some good results in photocatalytic activity of mixed titanium dioxide powders with various dyes. These mixed TiO_2 powders consist of various amorphous-anatase-rutile contents were prepared by acid-catalyzed sol-gel method at 80 °C without calcination. Some of those mixed TiO_2 powders, with good photodecolorization of dye, were freshly synthesized and studied their antimicrobial activities in this work.

This research was focused on the preparation of TiO_2 powder with various amorphous-anatase-rutile contents by using sol-gel method under different acids as hydrolysis catalysts without annealing at high temperature, based on the above mentioned previous works. As a spin-off from our previous studies involving

dye degradation, the products obtained in this work were investigated for their antimicrobial activities instead.

1.2 Review of literatures

1.2.1 Titanium dioxide

(1) General background

The semiconductor TiO_2 is the most widely studied photocatalyst. The photosensitizing action of titanium dioxide was first observed in 1929, when as a pigment used in paint, it was found to be responsible for paint fading. This paint fading caused from the photodegradation of the polymer organic binder of the paint by the action of TiO_2. However, works toward the development of photocatalytic theory, using titanium dioxide as a photocatalyst, gained momentum in the late 1960s (Vohra, *et al.*, 2005).

Titanium dioxide (TiO_2) belongs to the family of transition metal oxides. In the beginning of the 20^{th} century, industrial production started with titanium dioxide replacing toxic lead oxides as pigments for white paint. At present, the annual production of TiO_2 exceeds 4 million tons. It is used as a white pigment in paints (51% of total production), plastic (19%), and paper (17%), which represent the major end-use sectors of TiO_2. The consumption of TiO_2 as a pigment increased in the last few years in a number of minor end-use sectors such as textiles, food (it is approved in food-contact applications and as food coloring) under a EU legislation on the safety of the food additives, leather, pharmaceuticals (tablet coatings, toothpastes, and as a UV absorber in sunscreen cream with high sun protection factors and other cosmetic products), and various titanate pigments (mixed oxides such as $ZnTiO_3$, $ZrTiO_4$, etc) (Carp, *et al.*, 2004).

(2) Crystal structures and properties

Titanium dioxide exists naturally in three distinct crystallographic modifications, namely, anatase, rutile, and brookite (Fig. 1). The structures of rutile, anatase and brookite can be discussed in terms of (TiO_6^{2-}) octahedrals. The three crystal structures differ by the distortion of each octahedral and by the assembly patterns of the octahedral chains. Anatase can be regarded to be built up from octahedrals that are connected by their vertices, in rutile the edges are connected, and in brookite both vertices and edges are connected. Some of the most important bulk properties of TiO_2 are given in Table 1.

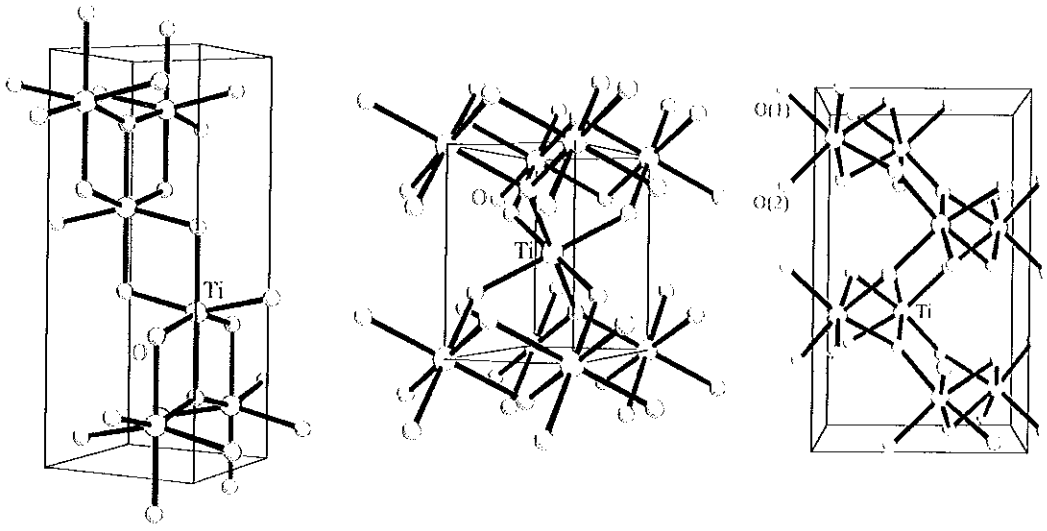

(a) Anatase (b) Rutile (c) Brookite

Figure 1. Crystal structures of TiO_2: (a) anatase, (b) rutile, and (c) brookite (Kanna, 2008).

Table 1. Some bulk properties of the three main polymorphs of titanium dioxide (Carp, *et al.*, 2004).

Crystal structure	System	Space group	Lattice constants (nm)			
			a	b	c	c/a
Rutile	Tetragonal	D^{14}_{4h}-P_4/mmm	0.4584	-	0.2953	0.644
Anatase	Tetragonal	D^{19}_{4h}-$I4_1/amd$	0.3733	-	0.937	2.51
Brookite	Rhombohedral	D^{15}_{2h}-$P_4/Pbca$	0.5436	0.9166	-	0.944

Density (kg/m^3)	
Rutile	4240
Anatase	3830
Brookite	4170

Melting Point (°C)	
Rutile	1840±10
Anatase	Change to rutile
Brookite	Change to rutile

Dielectric properties	Frequency (Hz)	Temperature (K)	Dielectric constant
Rutile, perpendicular to optical c-axis	10^8	290-295	86
Rutile, parallel to optical c-axis	-	290-295	170
Rutile, along c-axis	10^7	303	100
Anatase, average	10^4	298	55

Refractive index	n_g	n_p
Rutile	2.9467	2.6506
Anatase	2.5688	2.6584
Brookite	2.809	2.677

Nanometric size titania is by far the most widely employed system in photocatalysis due to its comparatively higher photocatalytic activity, low toxicity, chemical stability and very low cost. The anatase form of titania is reported to give the best combination of photoactivity and photostability (Zeltner and Tompkin, 2005).

Nearly all studies have focused on the crystalline forms of titania, namely anatase and rutile. The minimum band gap energy required for photon to cause photogeneration of charge carriers over TiO_2 semiconductor (anatase form) is 3.2 eV corresponding to a wavelength of 388 nm (Perkowski, *et al.*, 2006). Practically, TiO_2 photoactivation takes place in the range of 300-388 nm. The photoinduced transfer of electrons occurring with adsorbed species on semiconductor photocatalysts depends on the band-edge position of the semiconductor and the redox potentials of the adsorbates (Fujishima, *et al.*, 2000). The schematic diagram of band position for various semiconductors is shown in Fig. 2.

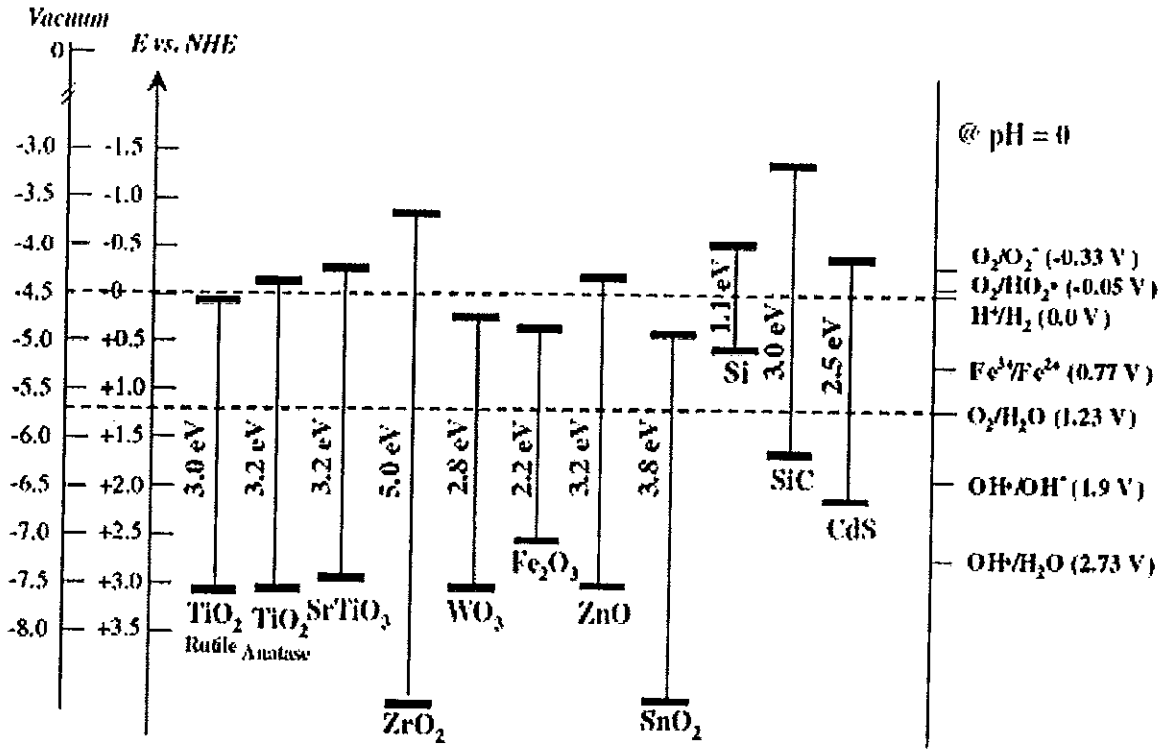

Figure 2. Diagram of conduction band and valence band energy positions for common semiconductors at pH = 0. The values noted on the right axes are the redox potentials for certain common redox couples of interest in water purification (Chandrasekharan, 2008).

(3) Synthesis of titanium dioxide via a sol-gel method

Titanium dioxide can be prepared in the form of powder, crystal, or thin film. Both powder and film can be built up from crystallites ranging from a few nanometers to several micrometers (Carp, *et al.*, 2004).

The sol-gel method involves the transition of system from a liquid "sol" into solid "gel" phase. An overview of the sol-gel product is presented in Fig. 3. The starting materials in the preparation of the "sol" are usually inorganic metal salts or metal organic compounds. In a typical sol-gel method, the precursor is subjected to a series of hydrolysis and polymerization (condensation) reactions to form a colloidal suspension or a "sol". Further processing of the "sol" enables one to make ceramic materials in different forms. Thin films can be prepared on a piece of substrate by spin coating or dip coating. When the "sol" is cast into a mold, a wet "gel" forms. With further drying and heat-treatment, the "gel" is converted into dense ceramic or glass articles. If the liquid in a wet "gel" is removed under a supercritical condition, a highly porous and extremely low density material called "aerogel" is obtained. As the viscosity of a "sol" is adjusted into a proper viscosity range, ceramic fibers can be drawn from the "sol". Ultra-fine and uniform ceramic powders are formed by precipitation, spray pyrolysis, or emulsion techniques (Chemat Technology, Inc., 1998).

In preparing oxide materials, the sol-gel method offers many advantages in easily control and strongly influenced by the synthesis conditions. The homogeneous property of the products prepared by this method is very satisfactory (Ding and Liu, 1997; Suresh, *et al.*, 1998). Moreover, in these method precursor materials are metallic halide or alkoxide that favor the building of a solid network in a gel which eventually become a stable solid (Sanchez, *et al.*, 1996).

In sol-gel processes, titania is usually prepared by the hydrolysis and polycondensation reactions of titanium alkoxide. It is well known that titanium alkoxide hydrolyze vigorously in water, and many catalysts typically various simple acids, e.g., nitric acid, hydrochloric acid, sulfuric acid (Ding and Liu, 1997; Zaban, *et al.*, 2000; Yamazaki, *et al.*, 2001; Baolong, *et al.*, 2003; Samantaray, *et al.*, 2003), and

acetic acid, have been applied to lower the reaction rates. Furthermore, this work used titanium tetrachloride ($TiCl_4$) as precursor for preparation TiO_2 powders due to inorganic compounds are more economical than alkoxides (Zhang, *et al.*, 1999).

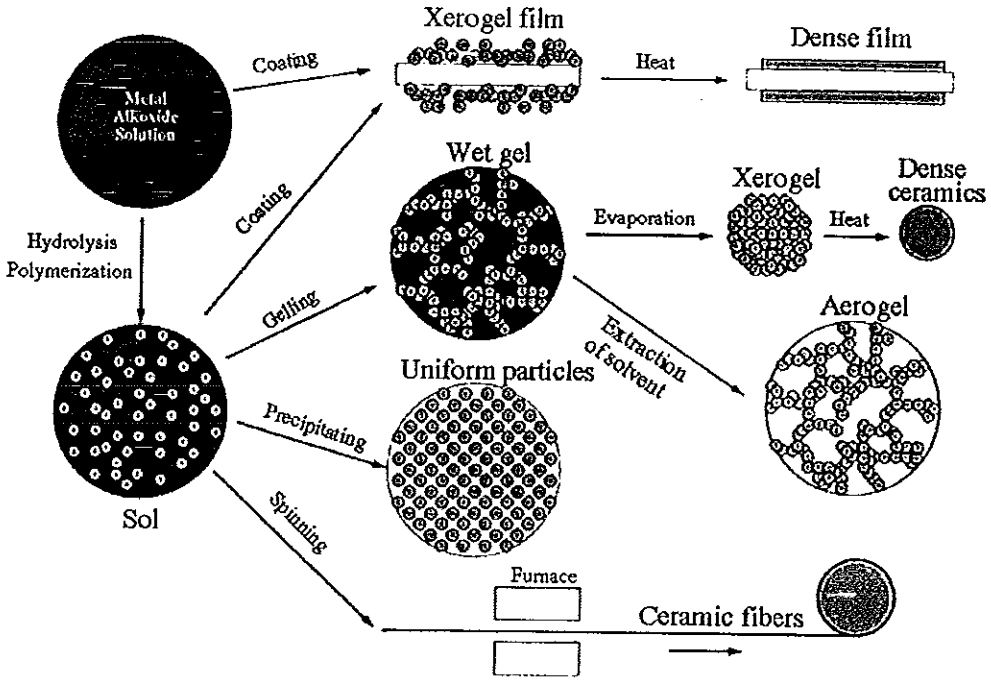

Figure 3. An overview of products prepared by sol-gel methods (http://sariyusriati.files.wordpress.com/2008/10/flowchat-sol-gel1.jpg).

As is well known, Degussa P25 is the most popular and promising photocatalysts due to its efficiency and has often been proposed for the degradation of pollutants in water or air. It has found that the mixture phase of anatase and rutile was an important factor for the photoactivity of TiO_2 as we can see from Degussa P25, which consist of anatase 75% and rutile 25%. In addition, it has been found that a mixture of anatase and rutile TiO_2 nanoparticles has a much higher photocatalytic activity than pure anatase or pure rutile TiO_2 nanoparticles (Ding and Liu, 1997; Zhang and Gao, 2001). Therefore, it is interesting to synthesize TiO_2 that exhibits high photoactivity with a good combination of anatase-rutile mixture phase and surface area.

Most of the literature works usually used the precalcined titanium dioxide at around 300-400°C to induce crystallinzation of the anatase form. It has been reported that the different methods for the syntheses of titanium dioxide result in products with different structures (anatase or rutile), crystallinity, and contaminants. As a consequence, the surface properties of TiO_2 strongly depend on the preparation techniques (Zhang, *et al.*, 1999; Reddy, *et al.*, 2001). There have been some works reported the synthesis of mixture phase TiO_2, for example, Gopal, *et al*, (1997) prepared crystalline TiO_2 powder either rutile or anatase from titanium isopropoxide at temperature below 100°C. The precipitate sizes were between 50 and 100 nm. Wang, *et al.*, (2000) prepared a mixture of anatase and rutile-type TiO_2 from poly-peroxotitanic acid gel obtained by addition of $Ti(OBu^n)_4$ to H_2O_2 solution. The gel was heat-treated in air at temperatures ranging from 150°C to 750°C. Zhang, *et al.*, (1999) obtained nanocrystalline TiO_2 in anatase or mixed phases from controlling the hydrolysis of $TiCl_4$. The addition of small amount $(NH_4)_2SO_4$ promotes occurrence of anatase phase, however, these were not studied for photocatalytic activity.

In this work, samples of nanosized TiO_2 powder were synthesized by the sol-gel method using $TiCl_4$ as a starting material at temperature below 100°C. Several acids, such as nitric acid and sulfuric acid, were used as hydrolysis catalysts.. Furthermore, to extend the range as wide as possible the preparation of Al^{3+}-doped TiO_2 and B^{3+}-doped TiO_2 powders were also prepared and included in all experiments for comparison.

1.2.2 Microorganism and the evaluation of antimicrobial activity

1.2.2.1 Microorganism

A microorganism or microbe is an organism that is microscopic (usually too small to be seen by the naked human eye). The study of microorganisms is called microbiology, a subject that began with Anton van Leeuwenhoek's discovery of microorganism in 1675, using a microscope of his own design.

Microorganisms are very diverse; they include bacteria, fungi, archaea, and protists; microscopic plants (called green algae); and animals such as plankton

and the planarian. Some microbiologists also include viruses, but others consider these as non-living. Most microorganisms are unicellular (single-celled), but this is not universal, since some multicellular organisms are microscopic, while some unicellular protists and bacteria are macroscopic and visible to the naked eye.

Microorganisms live in all parts of the biosphere where there is liquid water, including soil, hot springs, on the ocean floor, high in the atmosphere and deep inside rocks within the Earth's crust. Microorganisms are critical to nutrient recycling in ecosystems as they act as decomposers. As some microorganisms can fix nitrogen, they are a vital part of the nitrogen cycle, and recent studies indicate that airborne microbes may play a role in precipitation and weather (Christner, et al. 2008). Microbes are also exploited by people in biotechnology, both in traditional food and beverage preparation, and in modern technologies based on genetic engineering. However, pathogenic microbes are harmful, since they invade and grow within other organisms, causing diseases that kill millions of people, other animals, and plants.

Microorganisms can be found almost anywhere in the taxonomic organization of life on the planet. Bacteria and archaea are almost always microscopic, while a number of eukaryotes are also microscopic, including most protists, some fungi, as well as some animals and plants. Viruses are generally regarded as not living because of their noncellular structure, viruses are considered neither eukaryotic nor prokaryotic and are placed in a separated category, although the field of microbiology also encompasses the study of viruses (Jawetz, *et al.*, 1984; McKane and Kandel, 1985).

Microorganism can be classified as follows.

(1) Prokaryotes

1.1 Bacteria

1.1.1. Gram-negative

1.1.2. Gram-positive

1.2 Cyanobacteria

1.3 Archaea

(2) Eukaryotes

2.1 Protists (algae, fungi, protozoa, slime molds)

2.2 Plant cells

2.3 Animal cells

1.2.2.1.1 Bacteria

Focusing on bacteria, the structure, components, and functions of the cell wall was used to distinguish Gram-positive from Gram-negative bacteria as shown in Fig. 4. The important differences in membrane characteristics are outlined in Table 2. The cytoplasmic membranes of most prokaryotes are surrounded by rigid peptidoglycan (murein) layers. The exceptions are *Archaeobacteria* organisms (which contain pseudoglycans or pseudomureins related to peptidoglycan) and mycoplasmas (which have no cell walls at all). Because the peptidoglycan provides rigidity, it also determines the shape of the particular bacterial cell. Gram-negative bacteria are also surrounded by outer membranes.

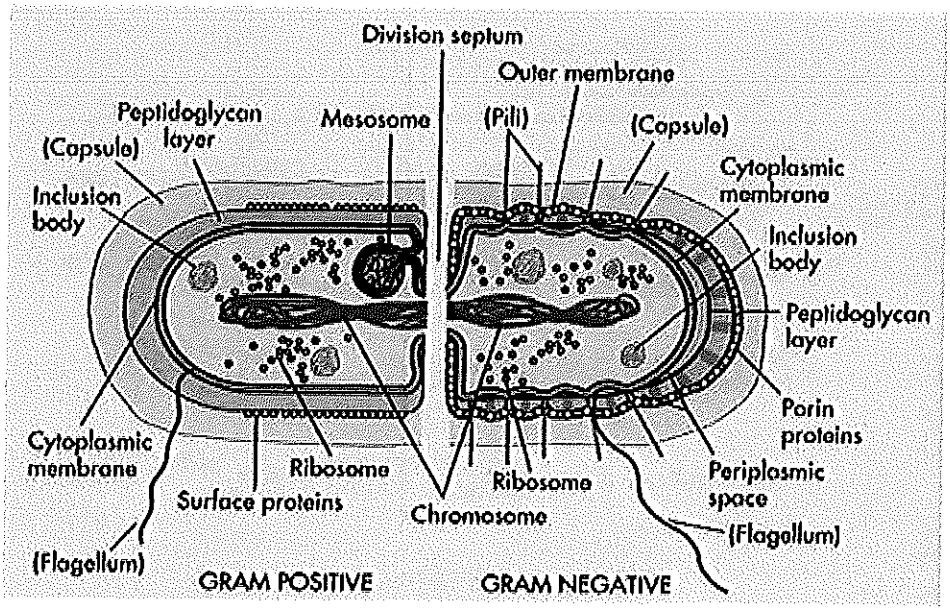

Figure 4. Gram-positive and Gram-negative bacteria. A Gram-positive bacterium has a thick layer of peptidoglycan (left). A Gram-negative bacterium has a thin peptidoglycan layer and an outer membrane (right).
(http://micro.digitalproteuscom/morphology2.php)

The difference in staining behavior between Gram-positive and Gram-negative cells is due to differences in the physical structure of their cell walls as indicated in Table 2 and Fig. 5.

Table 2. Structural comparison between Gram-positive and Gram-negative bacterial cell wall (Jawetz, *et al.*, 1984).

Structure	Chemical Constituents
Cell wall	
Gram-positive bacteria	
- Peptidoglycan	- Glycan chains of N-Acetylglucosamine (GlcNAc) and N-acetylmuramic acid (MurNAc) crosslinked by peptide bridge.
- Teichoic acid	- Polyribitol phosphate or glycerol phosphate crosslinked to peptidoglycan.
- Lipoteichoic acid	- Lipid linked teichoic acid.
Gram-negative bacteria	
- Peptidoglycan	- Thinner version of that found in Gram-positive bacteria.
- Periplasmic space	- Enzymes involved in transport, degradation, and synthesis.
- Outer membrane	- Phospholipids with saturated fatty acids.
- Proteins	- Porins, lipoprotein, transport proteins.
- Lipopolysaccharide (LPS)	- Lipid A, core polysaccharide, O antigen.

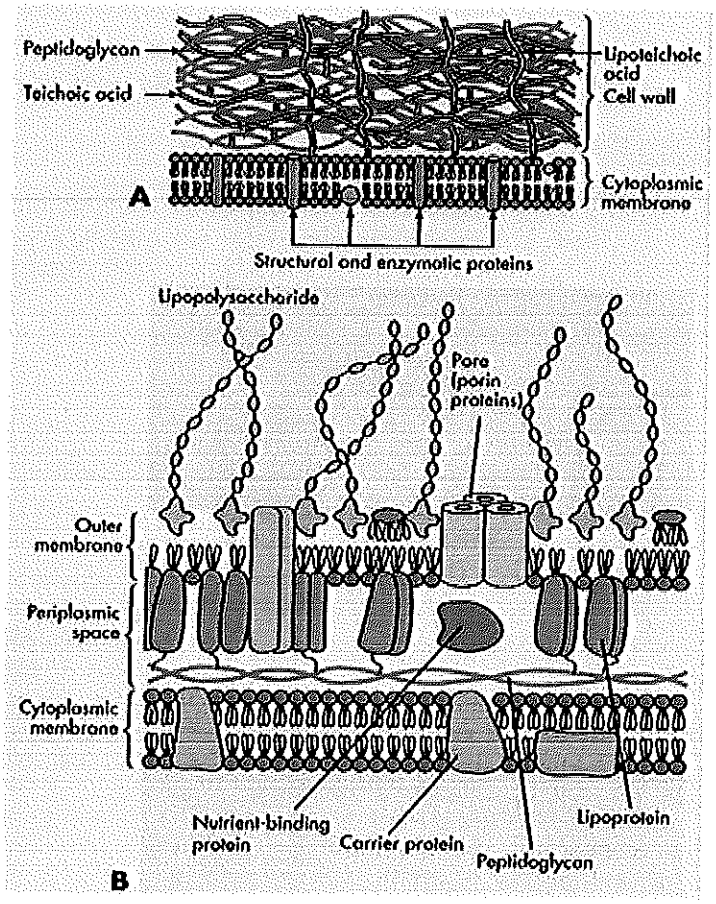

Figure 5. Comparison of the Gram-positive (A) and Gram-negative (B) bacterial cell walls (http://micro.digitalproteuscom/morphology2.php).

A Gram-positive bacterium has a thick, multilayered cell wall consisting mainly of peptidoglycan (150 to 500 Å) surrounding the cytoplasmic membrane. The peptidoglycan is a meshlike exoskeleton similar in function to the exoskeleton of an insect. Unlike the exoskeleton of the insect, however, the peptidoglycan of the cell is sufficiently porous to allow diffusion of metabolites to the plasma membrane. The peptidoglycan is essential for the structure, for replication, and for survival in the normally hostile conditions in which bacteria grow. During infection, the peptidoglycan can interfere with phagocytosis, is mitogenic (stimulates mitosis of lymphocytes), and has pyrogenic activity (induces fever).

The peptidoglycan can be degraded by treatment with lysozyme. Lysozyme, an enzyme in human tears and mucus, is also produced by

bacteria and other organisms. Lysozyme degrades the glycan backbone of the peptidoglycan. Without the peptidoglycan, the bacteria succumb to the large osmotic pressure difference across the cytoplasmic membrane and lyse. Removal of the cell wall produces a protoplast that lyses unless it is osmotically stabilized (McKane and Kandel, 1985).

The Gram-positive cell wall may also include other components such as teichoic and lipoteichoic acids and complex polysaccharides (usually called C polysaccharides). Protein such as the M protein of streptococci and R protein of staphylococci also associate with the peptidoglycan. Teichoic acids are large molecules composed of repeating units of sugar and phosphates. They are found only in the cell walls and cell membranes of Gram-positive bacteria as shown in Fig. 5. Teichoic acids give the cell surface a negative charge, which may be important in determining the types of substances attracted to and ultimately transported into the cell (McKane and Kandel, 1985).

Gram-negative cell walls are more complex than Gram-positive cell walls, both structurally and chemically, as shown in Fig. 5. Structurally, a Gram-negative cell wall contains two layers external to the cytoplasmic membrane. Immediately external to the cytoplasmic membrane is a thin peptidoglycan layer, which accounts for only 5% to 10% of the Gram-negative cell wall by weight. There are no teichoic or lipoteichoic acids in the Gram-negative cell wall. External to the peptidoglycan layer is the outer membrane, which is unique to Gram-negative bacteria. The area between the external surface of the cytoplasmic membrane and the internal surface of the outer membrane is referred to as the periplasmic space. This space is actually a compartment containing a variety of hydrolytic enzymes, which are important to the cell for the breakdown of large macromolecules for metabolism. These enzymes typically include proteases, phosphatases, lipases, nucleases, and carbohydrate-degrading enzymes. In the case of pathogenic Gram-negative species, many of the lytic virulence factors such as collagenases, hyaluronidases, proteases, and beta-lactamase are in the periplasmic space. Together these layers provide a protective coating around the cell that resists penetration by some potentially toxic chemicals (McKane and Kandel, 1985).

The outer membrane maintains the bacterial structure and is a permeability barrier to large molecules (e.g., proteins such as lysozyme) and hydrophobic molecule. The surface of the outer membrane contains molecules of lipopolysaccharide (LPS). LPS consists of a molecule called *lipid A* covalently linked to a polysaccharide (a large molecule composed of repeating sugar subunits). LPS has important medical consequences. When a Gram-negative bacterium is destroyed within the human body, the lipid A portion of LPS is released from the disrupted cell wall and elicits toxic reactions in the host. These reactions include fever, diarrhea, and potentially fatal shock. Because of its ability to injure a host and because it is an integral part of the bacterial cell wall, lipid A is commonly referred to as "endotoxin". The presence of endotoxin enables Gram-negative pathogens to produce symptoms of disease that are rarely provoked by infection with Gram-positive bacteria (McKane and Kandel, 1985).

The polysaccharides that extend outward from the lipid A are the outermost molecules of the cell wall and are major surface antigens of the Gram-negative bacterial cell. Antibodies directed against one Gram-negative bacterium usually do not protect against another Gram-negative species (McKane and Kandel, 1985).

In this research, five strains of bacteria; *Escherichia coli* ATCC25922, *Pseudomonas aeruginosa* ATCC28753, *Bacillus subtilis* BGA, *Staphylococcus aureus* ATCC25923, and Methicillin-resistant *Staphylococcus aureus* DMST2054 were used as a model of microorganism. Two species of yeast; *Candida albicans* ATCC90028 and *Cryptococcus neoformas* ATCC90112 were also used to study the photoccatalytic disinfection of TiO_2.

(a) *Escherichia coli*

Escherichia coli (*E. coli*) is a Gram-negative bacterium, facultatively anaerobic, rod prokaryote, that is commonly found in the lower intestine of warm-blooded organisms (endotherms). Most *E. coli* strains are harmless, but some, such as serotype O157:H7, can cause serious food poisoning in humans, and

are occasionally responsible for costly product recalls. The harmless strains are part of the normal flora of the gut, and can benefit their hosts by producing vitamin K_2 (Bently and Meganathan, 1982), or by preventing the establishment of pathogenic bacteria within the intestine (Hudault, *et al.*, 2001; Reid, *et al.*, 2001).

E. coli are not always confined to the intestine, and their ability to survive for brief periods outside the body makes them an ideal indicator organism to test environmental samples for fecal contamination. The bacteria can also be grown easily and its genetics are comparatively simple and easily-manipulated or duplicated through a process of metagenics, making it one of the best studied prokaryotic model organisms, and an important species in biotechnology and microbiology (Feng, *et al.*, 2002).

E. coli has been used in several research articles. In 1985, Matsunaga and coworkers (1985) reported that microbial cells, e.g. *E. coli*, in water could be killed by contact with a TiO_2-Pt catalyst upon illumination with near-UV light for 60-120 min. Kikuchi, *et al.*, (1997) investigated the role of active oxygen species in the photocatalytic bactericidal effect by using a thin transparent TiO_2 film with applied the viable number of *E. coli*. Maness, *et al.*, (1999) presented the first evidence that lipid peroxidation reation was the underlying mechanism of death of *E. coli* K-12 cells that were irradiated in the presence of the TiO_2 photocatalyst. Rincón and Pulgarin (2004) discussed the effect of different chemical parameters on photocatalytic inactivation of *E. coli* K12 by TiO_2 P-25 Degussa photocatalyst. Nadtochenko, *et al.*, (2005) studied *E. coli* photokilling due to the TiO_2 under light irradiation in a batch reactor by using attenuated total reflection Fourier transform infrared spectroscopy (ATR-FTIR) and atomic force microscopy (AFM).

(b) *Pseudomonas aeruginosa*

Pseudomonas aeruginosa (*P. aeruginosa*) is a Gram-negative, aerobic, rod-shaped bacterium with unipolar motility (Ryan and Ray, 2004). *P. aeruginosa* is a common bacterium which can cause disease in animals and humans. It is found in soil, water, skin flora and most man-made environment throughout the

world. It thrives not only in normal atmospheres, but also with little oxygen, and has thus colonized many natural and artificial environments. It uses a wide range of organic material for food; in animals, the versatility enables the organism to infect damaged tissues or people with reduced immunity. The symptoms of such infections are generalized inflammation and sepsis. If such colonisations occur in critical body organ such as the lungs, the urinary tract, and kidneys, the results can be fatal (Balcht and Smith, 1994).

P. aeruginosa has also been used in several research articles. Amézaga-Madrid, *et al.*, (2002) studied the photoinduced bactericidal capacity of TiO_2 based films by using *P. aeruginosa* as model organism. Amézaga-Madrid, *et al.*, (2003) reported the antibacterial activity of longwave UV-irradiatd TiO_2 thin films as well as the ultrastructural damage on bacterial cells using *P. aeruginosa* as a model. Ibánez, *et al.*, (2003) investigated the bactericidal action of heterogeneous photocatalysis (UV-A/TiO_2) on *P. aeruginosa.* Robertson, *et al.*, (2005) also demonstrated an effective bactericidal activity of TiO_2 when exposed to UV-A light.

(c) *Bacillus subtilis*

Bacillus subtilis (*B. subtilis*), known as the hay bacillus or grass bacillus, is a Gram-positive, catalase-positive bacterium commonly found in soil (Madigan and Martinko, 2005). A member of the genus *Bacillus*, *B. subtilis* is rod-shaped, and has the ability to form a tough, protective endospore, allowing the organism to tolerate extreme environmental conditions. Unlike several other well-known species, *B. subtilis* has historically been classified as an obligate aerobe, though recent research has demonstrated that this is not strictly correct (Nakano and Zuber, 1998).

B. subtilis is not considered a human pathogen; it may contaminate food but rarely caused food poisoning. *B. subtilis* produces the proteolytic enzyme subtilisin. *B. subtilis* spores can survive the extreme heating that is often used to cook food, and it is responsible or causing ropiness (a sticky, string

consistency caused by bacterial production of long-chain polysaccharides) in spoiled bread dough (Ryan and Ray, 2004).

B. subtilis has also been used in several research articles. Adams, *et al.*, (2006) investigated the potential eco-toxicity of nanosized TiO_2, SiO_2, and ZnO water suspensions by using Gram-positive *B. subtilis* and Gram-negative *Escherichia coli* as test organisms. Wolfrum, *et al.*, (2002) reported carbon mass balance and kinetics data for the total oxidation of cell, spores (using both cells and spores of *B. subtilis*), and biomolecules deposited on illuminated titanium dioxide surfaces in contact with air. Lin and Li (2003) evaluated the titanium dioxide filter media in controlling bioaerosols in a laboratory test chamber by using *E. coli*, *B. subtilis* endospores, yeast cells of *Candida famata* var. *flarri*, and spores of *Penicillium citrinum* as a model pollutant.

(d) *Staphylococcus aureus*

Staphylococci (staph) are Gram-positive spherical bacteria that occur in microscopic clusters resembling grapes. Bacteriological culture of the nose and skin of normal humans invariably yields staphylococci. *Staphylococcus aureus* (*S. aureus*), literally the "golden cluster seed" or "the seed gold" and also known as *golden staph* and Oro staphira, is the most common cause of staph infections. *S. aureus* was discovered in Aberdeen, Scotland in 1880 by the surgeon Sir Alexander Ogston in pus from surgical abscesses (Ogston, 1984).

S. aureus is a spherical bacterium, frequently part of the skin flora found in the nose and on skin. About 20% of the population are long-term carriers of *S. aueus*. *S. aureus* can cause a range of illness from minor skin infections, such as pimples, impetigo (may also be caused by *Streptococcus pyogenes*), boils (furuncles), cellulitis folliculitis, carbuncles, scalded skin syndrome and abscesses, to life-threatening disease such as pneumonia, meningitis, osteomyelitis, endocarditis, toxic shock syndrome (TSS), bacteremia and septicemia. Its incidence is from skin, soft tissue, respiratory, bone, joint, endovascular to wound infections. It is still one of the five most common causes of nosocomial infections, often causing postsurgical

wound infections. Abbreviated to *S. aureus* or *Staph aureus* in medical literature, *S. aureus* should not be confused with the similarly named and similarly dangerous (and also medically relevant) species of the genus *Streptococcus* (Kluytmans, *et al.*, 1997).

S. aureus is catalase positive, meaning that it can produce the enzyme "catalase") and able to convert hydrogen peroxide (H_2O_2) to water and oxygen, which makes the catalase test useful to distinguish staphylococci from enterococci and streptococci (Ryan and Ray, 2004).

S. aureus has also been used in several research articles. Seven, *et al.*, (2004) studied photocatalytic disinfection of two-groups of microorganisms which are known as bacteria and fungus in pathogenic-organisms (*E.coli, P. aeruginosa, S aureus, S. cerevisiae,* and *C. albicans, A. niger*) in aqueous suspension by irradiated TiO_2, ZnO and Sahara desert dust with a 400 W sodium lamp for various time periods in order to simulate solar radiation. Asahara, *et al.*, (2009) investigated the bactericidal effects of low-concentration TiO_2 particle mixture (19 ppm) against *S. aureus* under UV light, which hope to ultimately apply a mixture of this type as part of a clinical treatment regimen. Shiraishi, *et al.*, (2008) evaluated the photocatalytic bactericidal effects of anatase TiO_2 films on *S. aureus* associated with surgical site infections after exposed to UVA illumination from black light. Cheng, *et al.*, (2009) reported the significantly enhanced in antimicrobial activity of anatase/rutile mixed-phase carbon-containing TiO_2 under visible-light on tested pathogen: *S. aureus, S. flexneri* and *A. baumannii.*

(e) Methicillin-resistant *Staphylococcus aureus*

Methicillin-resistant *Staphylococcus aureus* (MRSA) is a bacterium responsible for several difficult-to-treat infections in humans. It may also be referred to as multidrug-resistant *Staphylococcus aureus* oxacillin-resistant *Staphylococcus aureus* (ORSA). MRSA is by definition any strain of *S. aureus* bacteria that is resistant to a large group of antibiotics called the beta-lactams, which include the penicillins and the cephalosporins. MRSA has adapted to survive treatment with beta-lactam antibiotics, including methicillin, dicloxacillin, nafcillin,

and oxacillin. MRSA is especially troublesome in hospital-associated (nosocomial) infections. In hospitals, patients with open wounds, invasive devices, and weakended immune systems are at greater risk for infection than the general public. Hospital staff who do not follow proper sanitary procedures may transfer bacteria from patient to patient. Visitors to patients with MRSA infections or MRSA colonization are advised to follow hospital isolation protocol by using gloves, gowns, and masks when indicated. Visitors, including health care providers, who do not follow such protocols are capable of spreading the bacteria to areas such as cafeterias, bathrooms, elevators, or various other surfaces (Jernigan, *et al.,* 2006).

MRSA was discovered in 1961 in the United Kingdom. It made its first major appearance in the United States in 1981 among intravenous drug users. MRSA is often referred to in the press as a "superbug". In 1997, four fatal cases were reported involving children from Minnesota and North Dakota (Raygada and Levine, 2009). Over the several years, it became clear that CA-MRSA (community-acquired MRSA) infections were caused by strains of MRSA that differed from the older and better studied health care-associated strains (Okuma, *et al.*, 2002).

MRSA is often sub-categorized as community-acquired MRSA (CA-MRSA) or health care-associated MRSA (HA-MRSA) although this distinction is complex. Some have defined CA-MRSA by characteristics of patients who develop an MRSA infection while other authors have defined CA-MRSA by genetic characteristics of the bacteria themselves. The first reported cases of community-acquired MRSA began to appear in the mid-1990s from Australia, New Zealand, the United States, the United Kingdom, France, Finland, Canada, and Somoa, notable because they involved people who had not been exposed to a health-care setting (Raygada and Levine, 2009). The new CA-MRSA strains have rapidly become the most common cause of cultured skin infections among individuals seeking emergency medical care in urban areas of the United States. These strains also commonly cause skin infections in athletes, prisoner and soldiers. However, in a 2002 report about CA-MRSA, many cases were children who required hospitalization (Jernigan, *et al.,* 2006).

Few researches have been done on MRSA, for example; Pelizetti and Minero, (1993) reported the utilization of TiO_2-coated tiles for sterilization and resolution of *E. coli* and MRSA.

The images of 5 bacteria used in this research are illustrated in Fig. 6 below.

(a) *E. coli* (-)
(www.astrographics.com)

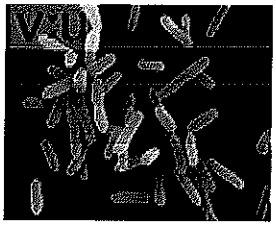

(b) *P. aeruginosa* (-)
(www.randstarteam.blogspot.com)

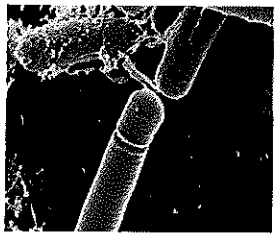

(c) *B. subtilis* (+)
(www.dailytech.com)

(d) *S. aureus* (+)
(www.swampie.wordpress.com)

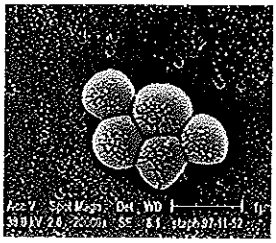

(e) MRSA (+)
(http://en.wikipedia.org/wiki/MRSA)

Figure 6. Morphology of (a) *E. coli*, (b) *P. aeruginosa*, (c) *B. subtilis*, (d) *S. aureus*, and (e) MRSA.

1.2.2.1.2 Yeast

Yeasts are eukaryotic microorganisms classified in the kingdom Fungi, with about 1,500 species currently described; they dominate fungal diversity in the oceans. Most reproduce asexually by budding, although a few do so by binary fission. Yeasts are unicellular, although some species with yeast forms may become multicellular through the formation of a string of connected budding cells known as *pseudohyphae*, or *false hyphae* as seen in most molds (Kutzman and Fell, 2005) Yeast size can vary greatly depending on the species, typically measuring 3-4 μm in diameter, although some yeasts can reach over 40 μm. The yeast species *Saccharomyces cerevisiae* has been used in baking and fermenting alcoholic beverges for thousands of years (Legras, *et al.* 2007). It is also extremely important as a model organism in modern cell biology research, and is one of the most thoroughly researched eukaryotic microorganisms. Researchers have used it to gather information about the biology of the eukaryotic cell and ultimately human biology (Ostergaard, *et al.* 2000). Other species of yeast, such as *Candida albicans*, are opportunistic pathogens and can cause infections in humans. Yeasts have recently been used to generate electricity in microbial fuel cells, and produce ethanol for the biofuel industry. Yeasts do not form an exact taxonomic or phylogenetic grouping. At present it is estimated that only 1% of all yeast species have been described (Kurtzman and Piškur, 2006).

(a) *Candida albicans*

The terms "yeast" and "fungus" and "mold" are often used interchangeably. For simplification, all species of yeast and fungus which grow in the human body may be lumped together for this discussion and simply called "yeast". *Candida* is a genus of yeast having a number of species that are human pathogens. The most common species is *Candida albicans*, also referred to scientifically as *C. albicans* (http://www.fungusfocus.com/html/candida_info.htm).

C. albicans is a diploid fungus (a form of yeast) and a causal agent of opportunistic oral and genital infections in humans. Systemic fungal infections (fungemia) have emerged as important causes of morbidity and mortality in immunocompromised patients (e.g., AIDS, cancer chemotherapy, organ or bone marrow transplantation). In addition, hospital-related infections in patients not previously considered at risk (e.g., patients in an intensive care unit) have become a cause of major health concern (http://en.wikipedia.org/wiki/Candida_albicans).

C. albicans is commensal and is among the gut flora, the many organisms that live in the human mouth and gastrointestinal tract. Under normal circumstances, *C. albicans* lives in 80% of the human population with no harmful effects, although overgrowth results in candidiasis. Candidiasis is often observed in immunocompromised individuals such as HIV-positive patients. Candidiasis also may occur in the blood and in the genital tract. Candidiasis, also known as "thrush", is a common condition, usually easily cured in people who are not immunocompromised. To infect host tissue, the usual unicellular yeast-like form of *C. albicans* reacts to environmental cues and switches into an invasive, multicellular filamentous forms (Ryan and Ray, 2004).

C. albicans has also been used in several research articles. Seven, *et al.*, (2004) studied photocatalytic disinfection of two-groups of microorganisms which are known as bacteria and fungus in pathogenic-organisms (*E.coli, P. aeruginosa, S aureus, S. cerevisiae,* and *C. albicans, A. niger*) in aqueous suspension by irradiated TiO_2, ZnO and Sahara desert dust with a 400 W sodium lamp for various time periods in order to simulate solar radiation. Sahara desert dust showed no microbicidal effect, while efficient disinfection effects of TiO_2 and ZnO were detected under soldium light irradiation, except for *A. niger*.

Akiba, *et al.* (2005) evaluated the photocatalytic antifungal effect on *C. albicans* biofilms and photodegradation effects of adsorbed protein by colorimetric assays measuring. The results suggest that coating agents with TiO_2 photocatalyst can be effective for the maintenance of tissue conditioners when dentures are removed during sleep.

Shibata, *et al.* (2007) developed an acrylic resin with antifungal properties by leveraging the photocatalytic activity of apatite-coated titanium dioxide (Ap-TiO_2). *C. albicans* was used for antifungal activity assay of the specimen plates under ultraviolet A (UVA) with a black light source. The result showed that acrylic resin containing 5 wt% Ap-TiO_2 could exert antifungal effects on *C albicans*.

Shi, *et al.* (2008) prepared a novel chitosan/nano-TiO_2 composite emulsion (CTCE) by inverse suspension technology and the gauze treated with chitosan/nano-TiO_2 composite emulsion showed excellent antimicrobial activities against *E. coli, A. niger* and *C. albicans* that the microbicidal ratios could reach 99.96%, 100% and 78.3% after 24 hrs, respectively.

(b) *Cryptococcus neoformans*

C. neoformans is an encapsulated yeast-like fungus that can live in both plants and animals. *C. neoformans* is composed of three variants (v.): *C. neoformans v. gattii, v. grubii,* and *v. neoformans*. *C. neoformans v. gattii* is found mostly in the tropics, but has also been confirmed on southern Vancouver Island on the southwestern coast of Canada. *Cryptococcus gattii* has recently been shown to be different enough from other subspecies to be elevated to its own species level. *C. neoformans v. grubii* and *v. neoformans* have a worldwide distribution and are often found in soil which has been contaminated by bird excrement (http://en.wikipedia.org/wiki/Cryptococcus_neoformans).

C. neoformans is a basidiomycetous yeast ubiquitous in the environment, a model for fungal pathogenesis, and an opportunistic human pathogen of global importance, the genome sequence of *C. neoformans v. neoformans* was published in 2005 (Loftus, *et al* 2005.) Recent studies suggested that colonies of *C. neoformans* and related fungi growing on the ruins of the melted down reactor of the Chernobyl Nuclear Power Plant may be able to utilize the energy of radiation (primary beta radiation) for "radiotrophic" growth (Dadachova, *et al.* 2007).

Far fewer drugs are available to combat infections caused by eukaryotic microbial pathogens (protozoa and fungi) versus those produced by bacteria. Pathogenic fungi are a significant clinical problem because of immunosuppression (due to HIV infection or immunosuppressive drugs) and antibiotic use. Infection with *C. neoformans* is termed cryptococcosis. Most infections with *C. neoformans* consist of a lung infection. Infections with this fungus are rare in those with fully functioning immune systems. For this reason, *C. neoformans* is sometimes referred to as an opportunistic fungus. The opportunistic pathogenic yeast *C. neoformans* is the most common cause of fungal meningitis, especially as a secondary infection for AIDS patients. This single species is estimated to cause 15-40% of 3.1 M annual deaths from HIV/AIDS worldwide (Bicanic and Harrison, 2004).

Less studies have been done on TiO_2 and *C. neoformans*, for example; Martinez-Gutierrez, *et al.*, (2010) reported the synthesis, characterization and evaluation of antimicrobial activity and cytotoxic effect of silver and titanium nanoparticles against a panel of selected pathogenic and opportunistic micro-organisms, *C. neoformans* and *C. albicans* were used in this article. The results showed that silver-coated nanoparticles having a size of 20-25 nm were the most effective aid all the nanoparticles assayed against the tested microorganisms. In addition, these nanoparticles showed no significant cytotoxicity, suggesting their use as antimicrobial additives in the process of fabrication of ambulatory and non-ambulatory medical devidces.

The images of 2 yeasts are demonstrated in Fig. 7. Some fungi can alternate between a yeast phase and a hyphal phase, depending on environmental conditions. Such fungi are termed dimorphic (with two shapes) and they included several that cause disease of humans, the most prominent being *C. albicans.* The dimorphic nature of *C. albicans* can be seen in Fig. 7a, on the right beginning its hyphal form. The morphology of *C. neoformans* is also shown in Fig. 7b.

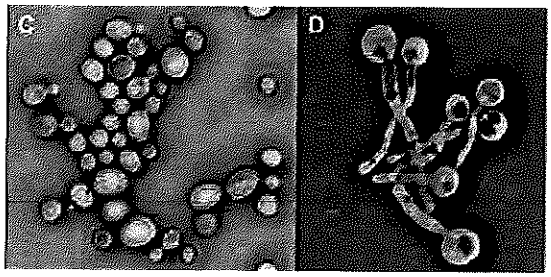

(a) *C. albicans*

(http://www.fungusfocus.com/)

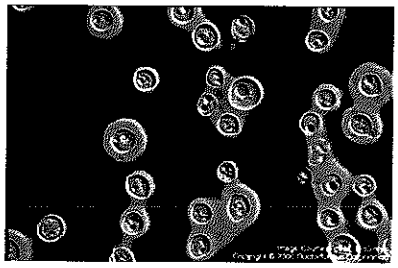

(b) *C. neoformans*

(http://www.advancedenviro.net/fungi.htm)

Figure 7. Morphology of (a) *C. albicans* and (b) *C. neoformans*.

1.2.3 Principles of heterogeneous photocatalysis

The basic principles of heterogeneous photocatalysis can be summarized as follows. In a semiconductor exists an occupied series of levels of highest energy, call valence band (VB), followed by a finite energy gap between this level and a corresponding series of unoccupied levels, known as the conduction band (CB). The magnitude of this energy gap (band gap, E_g) for a bulk solid is analogous to the HOMO-LUMO separation for a small molecule (Chandler, *et al.*, 1993).

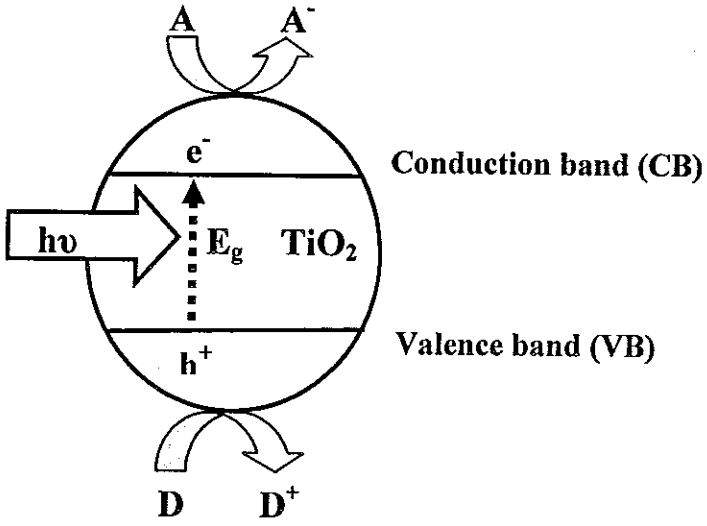

Figure 8. Schematic representation of the semiconductor showing the electron/hole pair formed in the conduction band and the valence band, respectively. (A = acceptor and D = donor).

When a photon with energy of hν higher or equal to the band gap energy, E_g, is absorbed by a semiconductor particle, an electron (e^-_{CB}), is promoted from the valence band, VB, into the conduction band, CB, leaving a hole, h^+_{VB} behind. The e^-_{CB} and the h^+_{VB} can recombine on the surface or in the bulk of the particle in a few nanoseconds (and the energy dissipated as heat) or can be trapped in surface states where they can react with donor (D) or acceptor (A) species adsorbed or close to the surface of the particle. Thereby, subsequent anodic and cathodic redox reactions can be initiated (Fig. 8). The energy level at the bottom of the CB is actually the reduction potential of photoelectrons and the energy level at the top of the VB determines the oxidizing ability of photoholes, each value reflecting the ability of the system to promote reduction and oxidations (Litter, 1999).

Some oxide and chalcogenides have enough bandgap energies to be excited by UV or visible light, and the redox potentials of the edges of the valence band and conduction band can promote a series of oxidative or reductive reactions. From the available semiconductors, ZnO is generally unstable in illuminated aqueous

solutions, especially at low pH values, and WO_3, although useful in the visible range, is generally less photocatalytically active than TiO_2. Among others, CdS, ZnS and iron oxides have been also tested. However, and without any doubt, TiO_2 is extensively used as photocatalyst due to its optical and electronic properties, chemical stability, non-toxicity, and low cost (Djebbar and Sehili, 1998).

The first step in heterogeneous photocatalytic process consists of the generation of the hole-electron pair through the irradiation of the TiO_2 particles with photonic energy equal to, or greater than, its band gap energy (≈ 3.2 eV). The electron is then extracted from the valence band (VB) to the conduction band (CB). This process results in a positive region in the VB (Hole h^+) and a free electron (e^-) in the CB (Benabbou, *et al.*, 2007) as in Eq. (1):

$$TiO_2 + h\nu \longrightarrow TiO_2(e^-_{CB} + h^+_{VB}) \qquad (1)$$

The hole, at the catalyst surface, reacts with hydroxyl ions (OH^-) and adsorbs water to form free radicals ($HO^\bullet$) as in Eqs. (2) and (3):

$$TiO_2(h^+_{VB}) + OH^- \longrightarrow TiO_2 + HO^\bullet \qquad (2)$$

$$TiO_2(h^+_{VB}) + H_2O_{ads} \longrightarrow TiO_2 + HO^\bullet + H^+ \qquad (3)$$

The CB electron reduces oxygen to the superoxide ion: $O_2^{\bullet-}$ (Eq.(4)). This reaction prevents the e^-/h^+ recombination, in the absence of other electron acceptors.

$$(O_2)_{ads} + e^-_{CB} \rightarrow O_2^{\bullet-} \qquad (4)$$

The further reduction of $O_2^{\bullet-}$ produce H_2O_2, as described in Eq. (5) (Min, *et al.*, 2004):

$$O_2^{\bullet-} + e^-_{CB} + 2H^+ \rightarrow H_2O_2 \qquad (5)$$

The superoxide ion and its protonated form subsequently dismute to yield hydrogen peroxide or a peroxide anion (Rincon and Pulgarin, 2003) as in Eqs. (6) - (8):

$$O_2^{\bullet -} + H^+ \rightarrow HO_2^{\bullet} \quad (6)$$

$$O_2^{\bullet -} + 4HO_2^{\bullet} \rightarrow 2OH^{\bullet} + 3O_2 + H_2O_2 \quad (7)$$

$$2HO_2^{\bullet} \rightarrow H_2O_2 + O_2 \quad (8)$$

It has also been shown that the addition of hydrogen peroxide can increase the photodegradable rate under certain conditions (Pichat, *et al.*, 1995), probably by the formation of $^{\bullet}OH$ radicals via the Harber-Weiss reaction (Eq. (9)) or through the reduction of H_2O_2 by the CB e^- as in Eq. (10) (Pichat, *et al.*, 1995; Rincon and Pulgarin, 2003):

$$O_2^{\bullet -} + H_2O_2 \rightarrow OH^{\bullet} + OH^- + O_2 \quad (9)$$

$$H_2O_2 + e_{CB}^- \rightarrow HO^{\bullet} + HO^- \quad (10)$$

On the other hand, recombination of $^{\bullet}OH$ radicals can lead again to the production of hydrogen peroxide as in Eq. (11):

$$HO^{\bullet} + HO^{\bullet} \rightarrow H_2O_2 \quad (11)$$

Among all the ROS (reactive oxygen species) that are generated, according to the reaction described above, the $^{\bullet}OH$ radical would be the most important oxidant species that is responsible for bacteria inactivation (Rincon and Pulgarin 2003).

Many studied have shown that heterogeneous photocatalytic oxidation processes can be used for microbial disinfection. In 1985, Matsunaga and co-workers reported for the first time that a TiO_2 photocatalyst could kill bacterial cells in water. They investigated the effectiveness of photocatalytic oxidation of several microorganisms such as *Lactobacillus acidophilus* (gram positive bacteria), *Saccharomyces ceerevisiae* (yeast), *Escherichia coli* (gram negative bacteria) and *Chlorella vulgaris* (green algae) in water. Their results show killing of the microbial

cells in 60-120 min using a TiO_2-Pt photocatalyst. They determined that the mode of action of the process was the photooxidation of Coenzyme A (CoA) leading to inhibition of cell respiration and thus cell death. The process was not entirely effective against *Chlorella vulgaris* though, because of its thicker cell wall (Matsunaga, *et al.*, 1985). Since then, numerous studies related to the bacterial effect of TiO_2 photocatalysts have been reported. This led to an extensive research in the field of photocatalytic oxidation for destruction of various microorganisms including bacteria, viruses, fungi, algae, and protozoa. TiO_2 photocatalytic killing studies (Matsunaga, *et al.*, 1985; Saito, *et al.*, 1992; Sjogren and Sierka, 1994; Lee, *et al.*, 1997; Otaki, *et al.*, 2000; Cho, *et al.*, 2005; Robertson, *et al.*, 2005).

1.3 Objectives

The objectives of this research are as follows:

Part 1: Evaluation of antimicrobial activity of several TiO_2 powders. This part consists of the following steps.

(1) Comparing products prepared from several methods for their physical properties and photocatalytic activities, the TiO_2 powders will be prepared by the sol-gel method using different acids as hydrolysis catalyst and $TiCl_4$ as precursor. The acids to be used are hydrochloric acid and sulfuric acid. The amount of water, refluxing temperature, and refluxing time are to be varied. TiO_2 powder with Al^{3+} and B^{3+}-dopant will also be synthesized.

(2) Samples obtained in (1) will be investigated by relevant physical methods, such as, XRD, BET, electron microscopy, and spectrophotometric methods.

(3) Samples obtained in (1) will be evaluated for the antimicrobial activities and compare the results with commercial TiO_2 samples (P25, anatase and rutile). Five strains of bacteria: *Escherichia coli* ATCC25922, *Pseudomonas aeruginosa* ATCC28753, *Bacillus subtilis* BGA, *Staphylococcus aureus* ATCC25923, and Methicillin-resistant *Staphylococcus aureus* DMST2054; and two species of yeasts: *Candida albicans* ATCC90028 and *Cryptococcus neoformans* ATCC90112 will be used for this study.

CHAPTER 2

EXPERIMENTAL

2.1 Synthesis of nanocrystalline TiO_2 powders

2.1.1 Materials

(1) Ammonium hydroxide (Ammonia solution) 28.0-30.0%, NH_4OH, A.R., code no. 9721-03, J.T. Baker, U.S.A.

(2) Aluminium sulfate, $Al_2(SO_4)_3$, A.R., Carlo Erba, Italy.

(3) Boron oxide, B_2O_3, A.R., Merck, Germany.

(4) Hydrochloric acid, HCl, A.R., code no. 1.00317.2500, Merck, Germany.

(5) Silver nitrate, $AgNO_3$, A.R., code no. 102333J, BDH, England.

(6) Sulfuric acid, H_2SO_4, A.R., code no.9681-03, J.T. Baker.

(7) Titanium tetrachloride, $TiCl_4$, A.R., code no. 8.12382.1000, Merck, Germany.

(8) Titanium dioxide (Anatase), A.R., code no.488257, Carlo Erba, Italy.

(9) Titanium dioxide (P25), code no. D-60287, Degussa AG, Frankfurt, Germany.

(10) Titanium dioxide (Rutile: R706), Dupont, U.S.A.

2.1.2 Methods

2.1.2.1 Preparation of nanosized TiO_2

Titanium dioxide powders were prepared from 3 different procedures corresponding to the synthesized conditions (refluxing temperature, refluxing time and acid catalyst). The syntheses can be shown as a flow chart in Fig. 9.

(1) TiO_2-200w-80HCl (amorphous + anatase + rutile) and

TiO_2-200w-80H_2SO_4 (amorphous + anatase)

Titanium tetrachloride (20 mL) was added slowly to 200 mL of cold deionized water (2 °C), which had been placed in an ice-water bath at least 10 minutes prior to the addition. The solution was then mixed with 2 mL of conc. acid (HCl or H_2SO_4) and was heated at 80 °C for 1 h under vigorous stirring. The solution was then treated with ammonia solution until pH ≈ 7 and maintained at the same temperature for 24 hrs. The white precipitate formed was filtered and then washed with deionized water until no chloride ion ($AgNO_3$ solution test). The product was dried overnight at 105 °C and ground to fine powder, until a final white powder was obtained. The products were designated as TiO_2-200w-80HCl and TiO_2-200w-80H_2SO_4, corresponding to the work by Kanna and Wongnawa (2008).

(2) TiO_2-200w-95HCl (amorphous + rutile + anatase) and

TiO_2-100w-95HCl (amorphous + rutile)

Titanium tetrachloride (20 mL) was added slowly to cold deionized water (2°C), 100 or 200 mL, which had been cooled in an ice-water bath at least 10 minutes prior to the addition. The solution was then left over night. The clear solution was then mixed with small amount of conc. HCl (acts as hydrolysis catalyst) in a three necked round bottom flask and the mixture was heated at 95°C for 13 hour under vigorous stirring. The solution was then treated with ammonia solution until

pH ≈ 7 and maintained at the same temperature for 13 hours. The white precipitate that formed was filtered and then washed with distilled water until free of chloride ion ($AgNO_3$ test). The product was dried overnight and ground to fine powder. The products were designated as TiO_2-200w-95HCl and TiO_2-100w-95HCl, corresponding to the preparation method of each by adding 200 and 100 mL of deionized water, respectively (Choychangtong, 2004).

(3) TiO_2-am (amorphous)

Titanium tetrachloride, 30 mL in a three-neck round bottom flask, was placed in an ice-bath along the reaction process. The diluted NH_4OH solution (50% v/v) 240 mL was slowly added with vigorous stirring. The milky mixture was then filtered and washed several time with distilled water until the filtered was free of Cl^- ($AgNO_3$ test). After that, the white powder product was collected and dried over night. The dried product was then ground to fine powder. The product was designated as Ti-am (Randorn, 2004).

2.1.2.2 Preparation of Al(III)- and B(III)-doped TiO_2

TiO_2-Al-150w (amorphous + anatase + Al),

TiO_2-Al-50w (amorphous + anatase + rutile + Al),

TiO_2-B-150w (amorphous + anatase + rutile + B), and

TiO_2-B-50w (amorphous + rutile + B)

$TiCl_4$ was slowly added to deionized water ($TiCl_4$:H_2O volume ratios was 1:7.5 and 1:2.5) at room temperature. For the Al(III)-doped titania, $Al_2(SO_4)_3.18H_2O$ (0.04 mol% Al) and 2 mL of conc. HCl were added into the solution then the mixture was kept overnight without stirring. After that the resulting clear solution was heated at 95 °C for 13 hrs. The solution was treated with ammonia solution to adjust the pH to 7 and continually refluxed for 13 hrs. This treatment produced a milky white TiO_2 suspension. Afterwards the suspension was filtered,

washed, and dried to obtain the final product as white powder. In the case of B(III)-doped titania, B_2O_3 (0.08 mol% B) was used instead of $Al_2(SO_4)_3.18H_2O$. These samples were designated as: TiO_2-Al-150w, TiO_2-Al-50w, TiO_2-B-150w, and TiO_2-B-50w (Suwanchawalit, 2005). The suffixes 150w and 50w correspond to high and low ratio of water used.

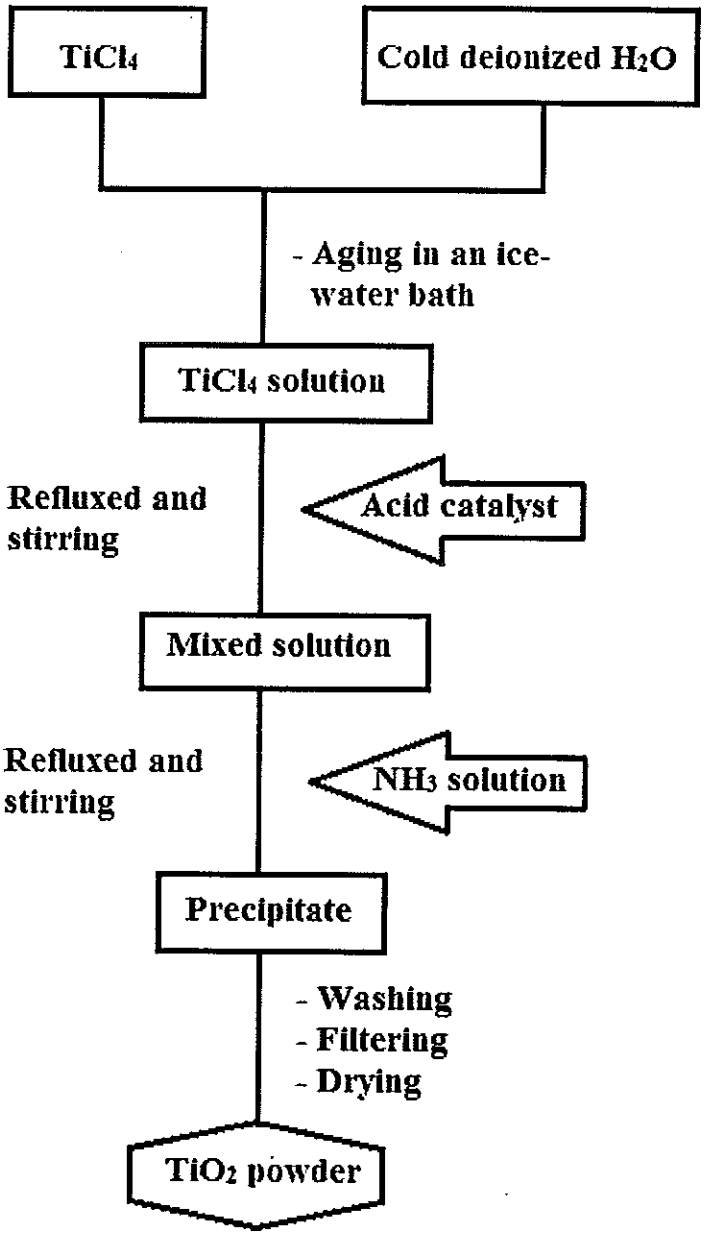

Figure 9. Flow chart of the syntheses of titanium dioxide powders.

2.2 Products characterization

2.2.1 X-ray powder diffractometry (XRD)

Powder X-ray diffraction (XRD, PHILIPS X' Pert MPD with Ni-filtered and Cu Kα radiation) was used for crystal phase identification. From the line broadening of the corresponding X-ray diffraction peaks and using the Scherrer's formula, the crystallite size was estimated by

$$L = \frac{K\lambda}{\beta_{hkl}\cos\theta} \qquad (1)$$

where L is the average crystallite size in nm, K is a constant usually taken as 0.9, λ is the wavelength of the X-ray radiation (using CuK_α = 0.154056 nm), β_{hkl} is the line width at half-maximum height in radians, and θ is the diffracting angle (Zielinska et al., 2001; Sivalingam et al., 2003). The XRD spectra were acquired at the Scientific Equipment Center, Prince of Songkla University, Hat Yai, Songkhla.

2.2.2 BET Surface area

The Brunauer-Emmett-Teller (BET) surface area of TiO_2 powders were determined with the Coulter, model SA3100 (U.S.A) using nitrogen adsorption at -196°C. All data were acquired at the Department of Chemical Engineering, Faculty of Engineering, Prince of Songkla University, Hat Yai, Songkhla.

2.2.3 Fourier-transformed infrared spectrophotometry (FTIR)

The infrared spectra were recorded using Fourier-transformed infrared (FT-IR) spectrophotometer (EQUINOX55, Bruker, Germany) in diffused reflectance mode covering the range 400-4000 cm^{-1} with KBr as blank.

2.2.4 Ultraviolet-visible spectrophotometer (UV-VIS)

The diffuse reflectance spectra of the solid catalysts were performed on a Shimadzu UV-2401PC spectrophotometer (Japan). The spectra were recorded in diffused reflectance mode with $BaSO_4$ as a reference in the range of 200 – 600 nm. The band gap energies (E_g) of the catalyst were calculated by the Planck's equation:

$$E_g = \frac{hc}{\lambda} = \frac{1240}{\lambda} \qquad (2)$$

where E_g is the bandgap energy (eV), h is the Planck's constant, c is the light velocity (3×10^8 m/s), and λ is the wavelength of the absorption edge (nm).

2.2.5 Scanning electron microscopy (SEM)

The SEM micrographs were performed on gold-coated samples using a Jeol apparatus (JSM-5800 LV) equipped with a Link analyzer (iSIS 300) for X-ray energy-dispersive analysis (EDX). All data were acquired by the Scientific Equipment Center, Prince of Songkla University, Hat Yai, Songkhla.

2.3 Evaluation of antimicrobial activity of TiO_2 powder.

2.3.1 Materials

(1) Mueller Hinton broth (MHB), Difco, U.S.A.

(2) Mueller Hinton agar (MHA), Difco, U.S.A.

(3) Nutrient agar (NA), Difco, U.S.A.

(4) Nutrient broth (NB), Difco, U.S.A.

(5) Sabouraud dextrose agar (SDA), Difco, U.S.A.

(6) Sabouraud dextrose broth (SDB), Difco, U.S.A.

(7) Sodium Chloride (NaCl), Merck, Germany.

(8) Deionized water, Department of Microbiology, Faculty of Science, Prince of Songkla University.

(9) All microorganisms in this research were obtained from the laboratory stock of the Department of Microbiology, Faculty of Science, Prince of Songkla University.

(9.1) *Escherichia coli* ATCC25922

(9.2) *Pseudomonas aeruginosa* ATCC27853

(9.3) *Bacillus subtilis* BGA

(9.4) *Staphylococcus aureus* ATCC25923

(9.5) Methicillin-resistant *Staphylococcus aureus* DMST2054

(9.6) *Candida albicans* ATCC90028

(9.7) *Cryptococcus neoformans* ATCC90112

2.3.2 Procedures

2.3.2.1 Culture of microorganisms

(a) Bacteria

The bacteria, *E. coli* ATCC25922, *P. aeruginosa* ATCC27853, *B. subtilis* BGA, *S. aureus* ATCC25923, and MRSA DMST2054, were used for the antibacterial activity test for the photocatalyst. All bacteria were cultured overnight at 37 °C in nutrient agar (NA). The density of final inocula contained 10^4 CFU/spot on the titanium dioxide amended agar. A bacterial inoculum was prepared by picking couple colonies of overnight growth culture into 1 mL nutrient broth and incubated them with agitation under aerobic condition at 35 °C for 3 hrs. A 0.5 McFarland standard was used for visual comparison to adjust the suspension to a density

equivalent to approximately 10^8 CFU/mL by using 0.85% saline solution. Then the suspension of organisms was diluted in 0.85% saline solution to give 10^7 CFU/mL. Plates have been inoculated using multipoint inoculator within 30 min to avoid any changes in the inoculum density.

(b) Yeast

The photocatalytic disinfection of *C. albicans* ATCC90028 and *C. neoformans* ATCC90112 by titanium dioxide were also studied in this work. The inocula should be an actively growing culture diluted in saline to 10^4 to 10^5 CFU/mL. For *C. albicans*, the colonies were cultured overnight at 35 °C in Sabouraud dextrose agar (SDA). Couple colonies of overnight growth culture were picked into 1 mL of Sabouraud dextrose broth (SDB) and incubated at 35 °C with agitation under aerobic condition for 3 hrs. The suspension was then diluted with 1 mL of normal saline and the opacity adjusted to McFarland 2. A 1/20 dilution of this suspension was made and within 30 minutes of dilution the test plates should be inoculated with micropipette to deliver 0.001 mL.

2.3.2.2 Photocatalytic disinfection test

Commercial anatase, rutile, Degussa P25, and the synthesized TiO_2 samples were used for all experiments. The method for testing the antibacterial activity is the agar dilution method to determine the minimal inhibitory concentration (MIC) of antimicrobial agents. The MIC is the lowest concentration of the agent that completely inhibits visible growth as judged by the naked eyes, disregarding a single colony or a thin haze within the area of the inoculated spot. The procedure, based on the recommendations from the Clinical and Laboratory Standards Institute (CLSI) for this method using a suspension of TiO_2 photocatalyst, was adapted to the agar dilution susceptibility test in this work (Approved standard M7-A4, 2002).

In each antibacterial test experiment, titanium dioxide agar plates were prepared in four concentrations 100, 50, 25, and 12.5 mg/mL in Mueller-Hinton

agar (MHA). The weighed titanium dioxide powders were incorporated in 10 mL of melted MHA and poured into 100 mm x 15 mm Petri dishes. The pH of each batch of the medium was about 6.9. By using inoculum-replicating apparatus, the final inocula contained 10^4 CFU/spot, three spots/bacterial strain as shown in Fig. 10. After inoculation, test plates were allowed to dry at room temperature before irradiation under UV light for a predetermined time was carried out.

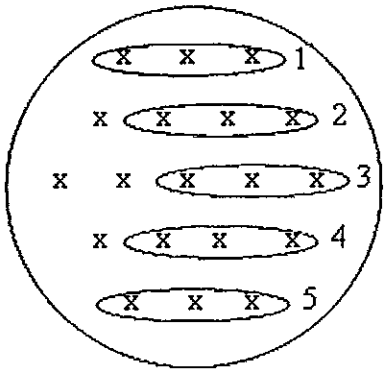

1 = *P.aeruginosa* ATCC28753

2 = *E.coli* ATCC25922

3 = *B.subtilis* BGA

4 = *S.aureus* ATCC25923

5 = MRSA DMST2054

Figure 10. Titanium dioxide agar plate inoculated with various types of bacteria.

In the case of yeast, *C. albicans* and *C. neoformans*, the screen test of photocatalytic disinfection of titanium dioxide samples were carried out. TiO_2 agar plates were prepared in 50 mm x 12 mm polypropylene Petri dish by using SDA with the highest concentration as of bacteria (100 mg/mL). The pH of each batch of the medium was about 6.9. The inocula should be applied as a spot that covers a circle about 5-8 mm in diameter. A micropipette to deliver 0.001 mL of the inoculums was used to spot inoculate the cultures. Inoculated plates were left undisturbed until the spots of inocula have dried.

The synthesized titanium dioxide agar plates were irradiated in an UV box, equipped with five fluorescent blacklight tubes, 20 W each, with λ_{max} 366 nm (Randorn, *et al.*, 2004) as shown in Fig. 11 and 12. The sample plates were collected immediately after the titanium dioxide agar plates were exposed to UV light and subsequently every 30 min. The bacterial test plates were incubated at 35 °C for

18 hrs. For yeast, after the sample plates were exposed to UV light for 120 min, the plates were then incubated at 35 °C for 24 hrs and at room temperature (30 °C) for 48 hrs in the case of *C. albicans* and *C. neoformans*, respectively. The results then were inspected visually and the minimum inhibitory concentration (MIC) values were recorded. The MIC represents the lowest concentration of a compound that will inhibit the visible growth of a test microorganism after overnight incubation (Islam, *et al.*, 2008). All tests and inoculation on each plate were run in duplicate.

A control plate was carried out under the same conditions with antimicrobial activity test but without TiO_2 powders. Photographs of typical agar plates are shown in Fig. 13 and 14 for bacteria and yeast, respectively.

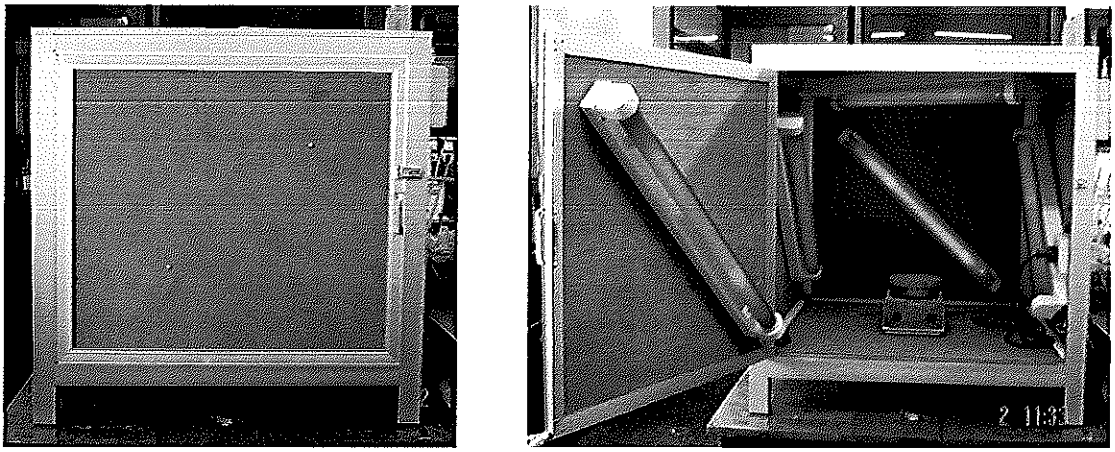

(a) Outer compartment **(b)** Inner compartment

Figure 11. The wooden compartment for photocatalytic experiment (a) outer and (b) inner views.

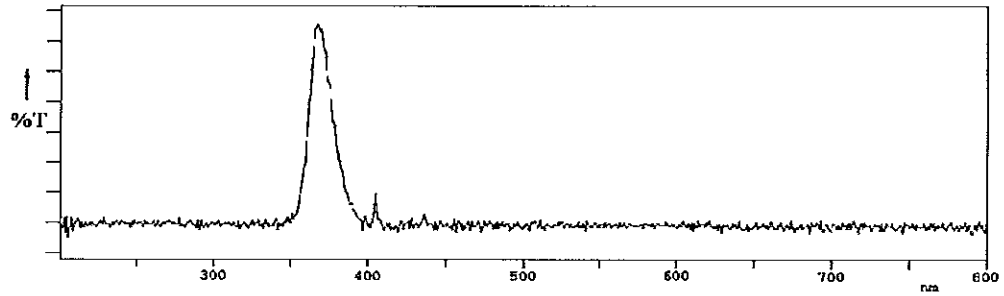

Figure 12. Spectrum of UV-light source used in this work (Randorn, *et al.*, 2004).

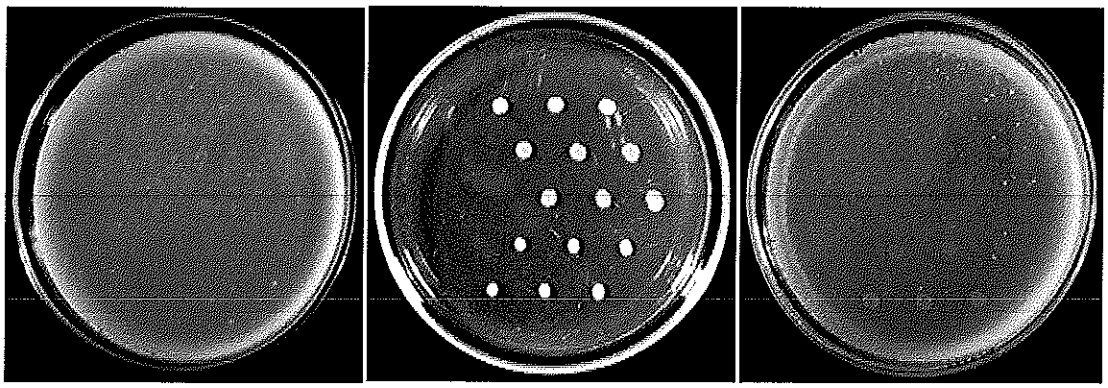

(a) (b) (c)

Figure 13. Images of bacteria tested agar plates: a) agar plate with 25 mg/mL of TiO_2-200w-80H_2SO_4 irradiated under UV light for 30 min, b) control plate without TiO_2, and c) agar plate with 12.5 mg/mL of TiO_2-200w-80H_2SO_4 irradiated under UV light for 30 min.

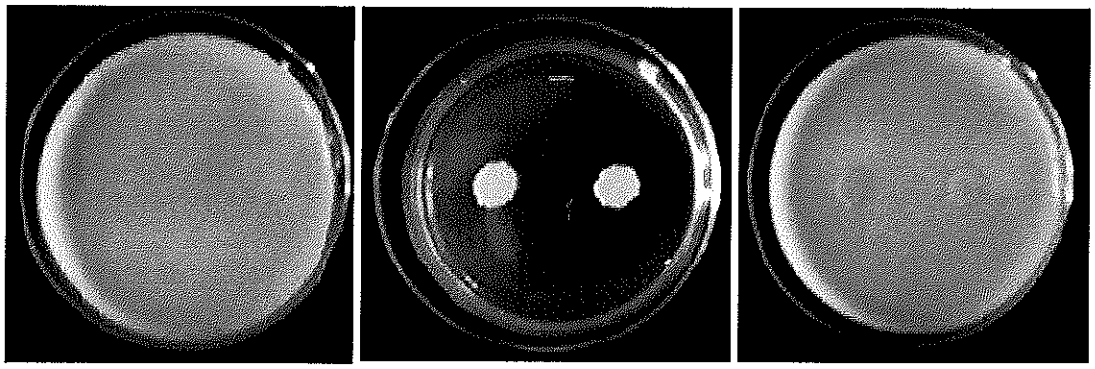

(a) (b) (c)

Figure 14. Images of yeast tested agar plates: (a) agar plate with 100 mg/mL of TiO_2-200w-80H_2SO_4 irradiated under UV light for 120 min, (b) control plate without TiO_2, and (c) agar plate with 100 mg/mL of TiO_2-Al-50w irradiated under UV light for 120 min.

CHAPTER 3

RESULTS AND DISCUSSION

3.1 Synthesis and Characterization of nanocrystalline TiO_2 powders

Sol-gel method was used to synthesize the acid catalysed nanosized TiO_2 with two different acids, HCl and H_2SO_4, as catalysts in the hydrolysis process, by varying the refluxing temperature, refluxing time, and volume of water used. Samples of Al(III) - and B(III)-doped TiO_2 are also prepared in this work.

3.1.1 Physical properties of nanosized TiO_2 and Al(III)- , B(III)-doped TiO_2

3.1.1.1 X-ray powder diffractometry (XRD) and BET surface area

The XRD results, Fig. 15, show that varying the synthesis parameters affected the growth of anatase and rutile to some extent. When using H_2SO_4 acid prepared with large amount of water the products were mainly amorphous TiO_2 with small amount of anatase phase, however, with HCl acid prepared with small amount of water, the mixture of mainly amorphous titania with small amount of both anatase and rutile phases were obtained. The presence of sulfate has been known to accelerate the growth of TiO_2 cluster in the anatase phase. In this study, when H_2SO_4 was added as acid catalyst in the hydrolysis process also resulted in the formation of anatase since the SO_4^{2-} ion induced the growth of anatase phase (Zhang, *et al.*, 1999; Zhang, *et al.*, 2000; Kanna and Wongnawa, 2008).

In the case of TiO_2-200w-95HCl, the composition was mainly amorphous TiO_2 with small amount of both anatase and rutile phase, whereas TiO_2-100w-95HCl sample was mainly amorphous TiO_2 with small amout of only rutile phase. The different in crystalline phase may be due to the volume of water in the preparation step. As seen in this study that only rutile phase appears in TiO_2-100w-95HCl sample, this could be attributed to only the TiO_2-100w-95HCl sample which

result from the low volume of water in the reaction stabilized the equilibrium between hydrolysis and condensation reactions. For TiO_2-200w-95HCl sample, it consists not only rutile phase but also anatase phase. This could be explained that the equilibrium between hydrolysis and condensation reaction is broken from the larger amount of water which result in faster condensation and slower hydrolysis. As a result, the possibility to form structure unit of anatase phase is obtained. Therefore, the high volume of water in the reaction catalyzed the reaarangement of TiO_6 octahedral in amorphous titanium dioxide, promoting the formation of anatase structure (Zhang, *et al.*, 2000; Tang, *et al.*, 2002). This result indicated that low volume of water affected in the growing of rutile phase. This could be also used to describe the phase component of TiO_2-Al-150w, TiO_2-Al-50w, TiO_2-B-150w, and TiO_2-B-50w.

Summary of results obtained from the X-ray diffraction patterns are shown in Table 3

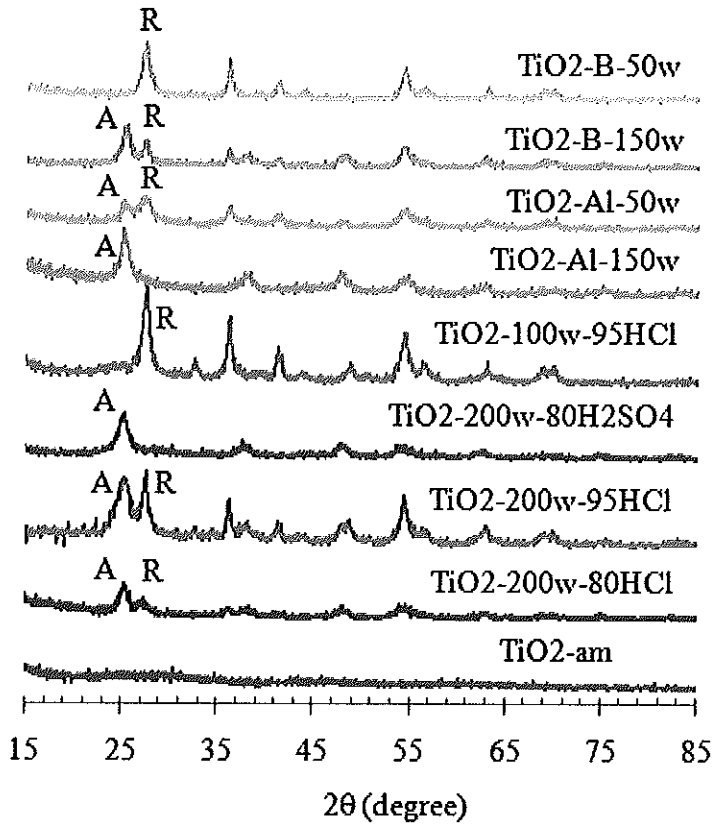

Figure 15. XRD patterns of the synthesized TiO_2 powders (A denotes anatase and R denotes rutile).

In Table 3 shown below, The degrees of crystallinity (the 2nd column) of the samples were determined from the XRD intensities by using the standard addition method. The commercial titanium dioxide (anatase (Carlo Erba) and rutile (Dupont R706)) were mixed with the original synthesized titanium dioxide samples in different percent weight; 0, 10, 20, 40, and 60%, and then measured the peak intensities. A calibration curve was made by plotting the total XRD-peak-intensity against the percentage of the added standard. The original percentage of anatase (or rutile) was obtained by the interception point on the percent weight axis (Kanna and Wongnawa, 2008).

Table 3. Physical properties of commercial and synthesized TiO_2 samples.

Samples	Crystallinity [a] (%)	Crystallite size [b] (nm)		BET (m^2/g)	
		Anatase	Rutile	This work	Literatures
Anatase (Carlo Erba)	100 (A)	13.4	-	11.3	5.9 [g]
Rutile (Dupont R706)	100 (R)	-	11.6	13.1	-
P25 (Degussa)	80 (A), 20 (R) [c]	10.1	11.6	65.9	50 [h]
TiO_2-am	-	-	-	505.4	-
TiO_2-200w-80HCl	13 (A), 6 (R) [d]	6.7	6.7	250.2	-
TiO_2-200w-95HCl	15 (A), 30 (R) [e]	4.7	8.1	93.9	-
TiO_2-200w-80H_2SO_4	15 (A) [d]	5.4	-	320.1	-
TiO_2-100w-95HCl	30 (R) [e]	-	8.1	150.5	-
TiO_2-Al-150w	23.4 (A) [f]	6.7	-	277.1	-
TiO_2-Al-50w	9.1 (A), 11.5 (R) [f]	5.4	4.5	244.9	-
TiO_2-B-150w	6.3 (A), 6.8 (R) [f]	6.7	10.1	234.8	-
TiO_2-B-50w	48.3 (R) [f]	-	6.4	106.6	-

[a] Determined by XRD using standard addition method, the rest is amorphous phase. A denotes anatase and R denotes rutile.

[b] Calculated from XRD data using Scherrer's formula.

[c] Stylidi, *et al.*, 2004

[d] Kanna and Wongnawa, 2008

[e] Choychangtong, 2004.

[f] Suwanchawalit, 2005.

[g] Sclafani, *et al.*, 1990

[h] Neppolian, *et al.*, 2002

The crystallite sizes of the samples were calculated using the peak at $2\theta = 25.4^{\circ}$ and 27.5° for anatase and rutile phase, respectively, and are also shown in Table 3. The crystallite sizes of all the samples can be classified as nanocrystalline TiO_2 powders and are smaller than those of the commercial ones.

The specific surface areas of samples are also shown in Table 3. The data were compared between the synthesized TiO_2 and the commercial TiO_2. All the synthesized titanium dioxide samples exhibited higher surface area than the commercial ones due to lower crystallinity of the synthesized samples without calcination in this work. Among the synthesized samples, both TiO_2-200w-80H_2SO_4, TiO_2-Al-150w and TiO_2-Al-50w exhibited higher surface area than the rest of samples, except for TiO_2-am. This result agrees with those in the reports that the surface area of sulfated-titania was higher than that of pure TiO_2 (Gómaz, *et al.*, 2003) and the nanosized TiO_2 prepared in the presence of sulfate ion had higher BET surface than those prepared in the absence of sulfate ion (Zhang, *et al.*, 2000). The values of surface area of all these commercial TiO_2 came out similar to those given in literatures.

3.1.1.2 Fourier-transformed infrared spectrophotometry (FT-IR)

The infrared spectra of all the synthesized titanium dioxide powders in the range 4000-400 cm^{-1} are shown in Fig. 16. Table 4 lists the assigned modes of the functional groups that are responsible for the vibration bands in Fig. 16.

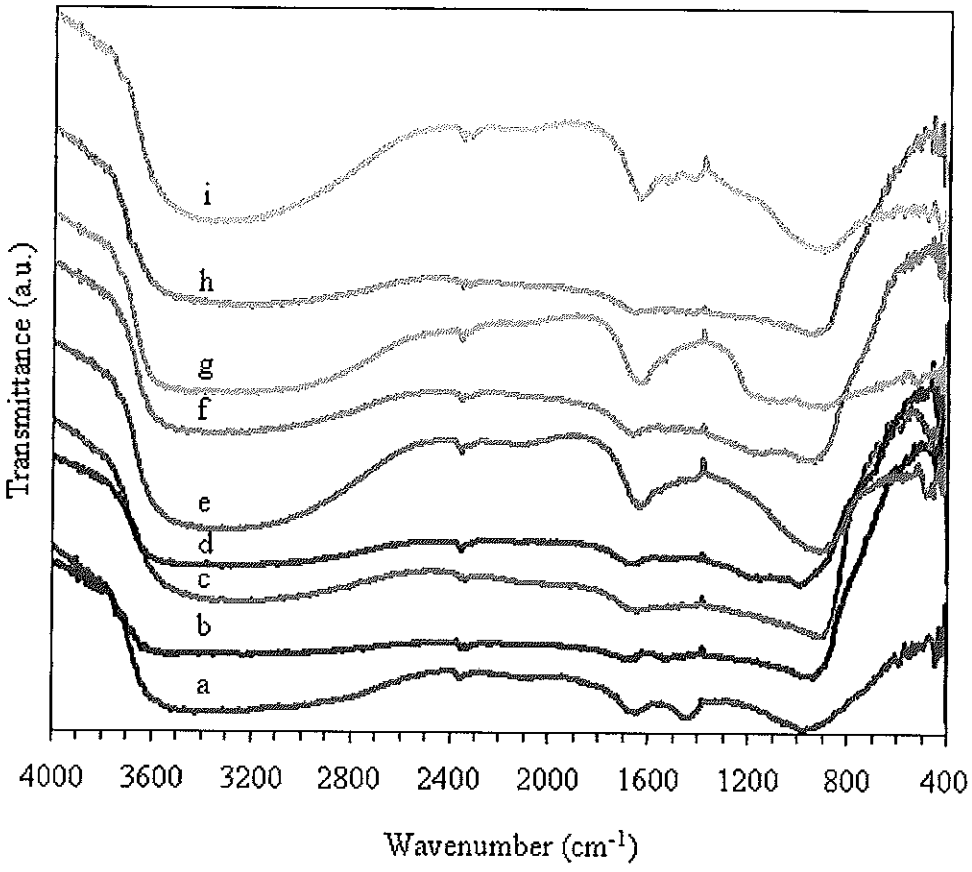

Figure 16. FT-IR spectra of the synthesized TiO_2 powders: (a) TiO_2-am, (b) TiO_2-200w-80HCl, (c) TiO_2-200w-95HCl, (d) TiO_2-200w-80H_2SO_4, (e) TiO_2-100w-95HCl, (f) TiO_2-Al-150w, (g) TiO_2-Al-50w, (h) TiO_2-B-150w, and (i) TiO_2-B-50w.

All the FTIR spectra show a large broad band at 3600-3100 cm^{-1} which can be assigned to mixed ν_{OH} and ν_{NH} modes (stretching modes). These bands are in the hydroxyl stretching region and correspond to O-H vibration of the Ti-OH groups and H_2O molecules. The band around 3500 cm^{-1} can be assigned to O-H vibration of the Ti-OH groups (Velasco, *et al.*, 1999). The stretching vibration of O-H in Ti-OH bonding could not be removed easily and must be heated until relatively high temperature (Wang, *et al.*, 2000). Near the band around 3500 cm^{-1}, a shoulder was generated by an asymmetric vibration mode of the residual ammonium ions. The rather narrow bands around 1600 and 1400 cm^{-1} can be assigned to δ_{OH} and δ_{NH} modes (bending modes) of hydroxyl (OH) and ammonium (NH_4^+) groups,

respectively (Khalil and Zaki, 1997; Youn, *et al.*, 1999). All of these bands indicated that H_2O and NH_4^+ are present in the products. In the low energy region (below 800 cm^{-1}), the band due to stretching mode of Ti-O (ν_{Ti-O}) which was the envelope of the phonon bands of a Ti-O-Ti bond of a titanium oxide network could be assigned (Velasco, *et al.*, 1999). The absence of any bands in this spectral region may then suggest that the precipitate is amorphous.

Table 4. Assignment of the FT-IR bands of titanium dioxide samples (Fig. 16).

Samples	Wavenumber (cm^{-1})	Assignment	Functional groups /molecule	Literatures
a-i	3600 - 3100	ν_{OH} and ν_{NH}	H_2O and NH_4^+	Khalil and Zaki, 1997 Youn, *et al.*, 1999
a-i	~1600	δ_{OH}	OH groups	Khalil and Zaki, 1997 Youn, *et al.*, 1999
a, b, c, e, h and i	~1400	δ_{NH}	NH_4^+ groups	Khalil and Zaki, 1997 Youn, *et al.*, 1999
d, f, and g	1200-1100	ν_{S-O}	SO_4^{2-}	Samnantaray, *et al.*, 2003
a-i	Below 800	ν_{Ti-O}	Ti-O bond	Velasco, *et al.*, 1999

(a) TiO_2-am, (b) TiO_2-200w-80HCl, (c) TiO_2-200w-95HCl, (d) TiO_2-200w-80H_2SO_4, (e) TiO_2-100w-95HCl, (f) TiO_2-Al-150w, (g) TiO_2-Al-50w, (h) TiO_2-B-150w, and (i) TiO_2-B-50w

In addition, the spectra of TiO_2-200w-80H_2SO_4, TiO_2-Al-150w, and TiO_2-Al-50w in Fig. 16d, f, and g, respectively, show broad band at 1250-1100 cm^{-1} which is the characteristic frequencies of SO_4^{2-} group. In TiO_2-Al-150w and TiO_2-Al-50w samples, the SO_4^{2-} came from Al(III)-dopant starting material, $Al_2(SO_4)_3$. The broad band in this region resulted from the lowering of the symmetry in the free SO_4^{2-}

(Td point group) to either C_{2v} (Fig. 17b) or C_{3v} (Fig. 17a and 17c) when SO_4^{2-} is bound to the titania surface (Samantaray, *et al.*, 2003; Nakamoto, 1986). The results from XRD and FT-IR led to the conclusion that samples were a hydrated amorphous titanium dioxide with minute amount of impurities, such as NH_4^+ and SO_4^{2-}.

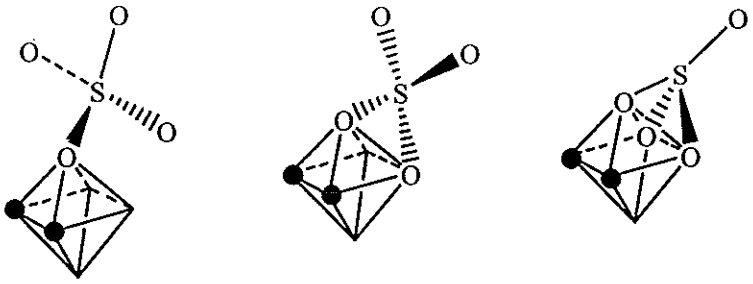

Figure 17. Bonding mode of SO_4^{2-} anion as, (a) monodentate, (b) bidentate, and (c) tridentate ligand (● indicates OH position) (Kanna and Wongnawa, 2008).

In the case of adding H_2SO_4 acids, the product was mainly amorphous and only small amount of the anatase phase existed as a minor component. The rutile phase was completely absence in this case. The rather high negative charge (-2) of sulfate should attract strongly with Ti^{4+} ion in the Ti basic unit. The EDX spectra (Fig. 24b) with the characteristic peak of S and FT-IR spectra (Fig. 16) with the characteristic vibration of the sulfate group on TiO_2 are evidenced for the presence of sulfate anion. The sulfate anion has tetrahedral geometry with the negative end at the oxygen atoms where they can bond to Ti octahedral in three ways as shown in Fig. 17. Due to the *chelate effect*, the bonding mode of bidentate (Fig. 17b) and tridentate (Fig. 17c) are favored. The bonding of SO_4^{2-} in these multidentate modes occupy one full face of octahedral and inhibit the growing of chain along this edge and hence inhibit the formation of rutile. This result is in agreement with other researchers who reported the presence of SO_4^{2-} ion helped promote formation of anatase phase (Samantaray, *et al.*, 2003; Zhang, *et al.*, 1999; Kanna and Wongnawa, 2008).

3.1.1.3 Ultraviolet-visible spectrophotometer (UV-VIS)

The diffuse reflectance spectra of acid-catalyst TiO_2, Al(III)/B(III) dopant-TiO_2 and commercial titanium dioxide are shown in Fig. 18, 19 and 20, respectively. The absorption edge can be approximated by the intersection of two straight lines: a straight line extrapolated from the baseline, and a line drawn through the ascending slope of the onset of absorption (Chandler, *et al.*, 1993). The band gap energies of the titanium dioxide calculated from Plank's equation are shown in Table 5.

In the case of commercial TiO_2, Fig. 18, the absorption edge of rutile (R706) appears at longer wavelength than that of anatase (Carlo Erba). The absorption edge wavelengths of commercial titanium dioxide are in order of rutile (R706) > Degussa P25 > anatase (Carlo Erba). The bandgap energies, calculated using Planck's equation, of rutile (R706), Degussa P25, and anatase (Carlo Erba) are 3.00, 3.14, and 3.22 eV, respectively, which are identical to the literature values of 3.00, 3.14, and 3.20 eV (Miao, *et al.*, 2003; Zielińska, *et al.*, 2003).

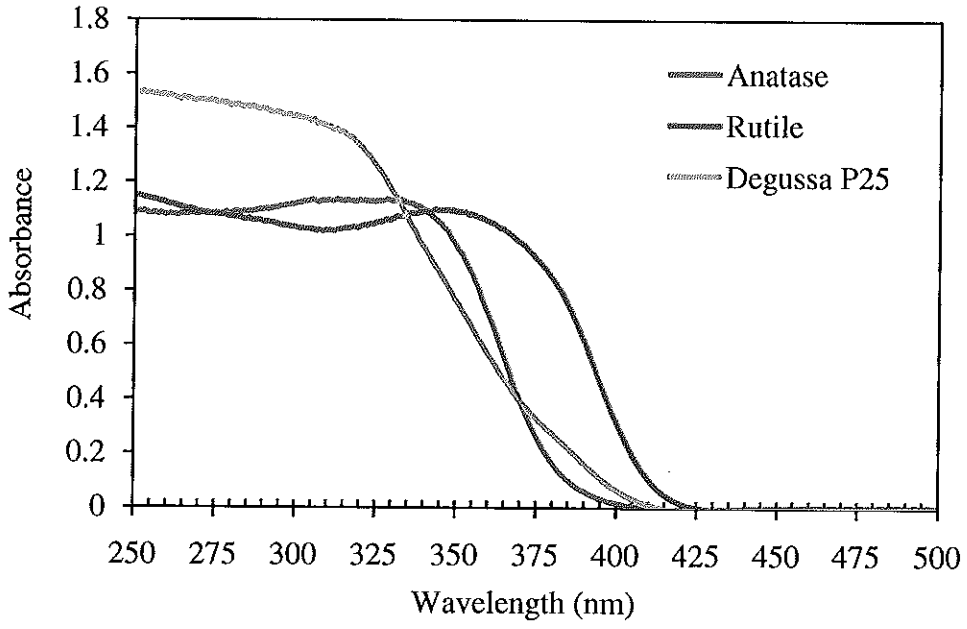

Figure 18. Diffuse reflectance spectra of the commercial TiO_2 powders.

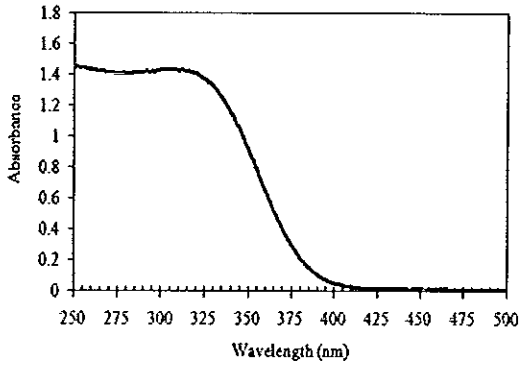

(a) TiO_2-am

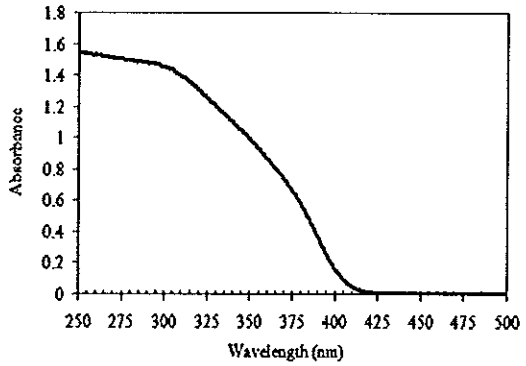

(b) TiO_2-200w-80HCl

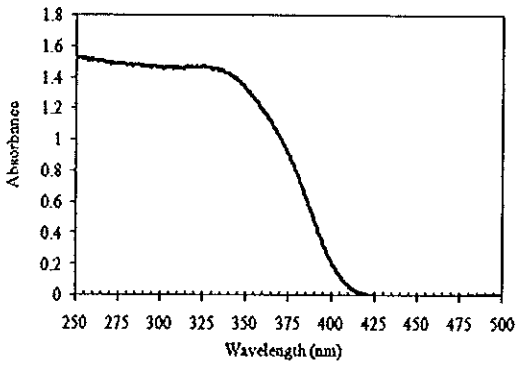

(c) TiO_2-200w-95HCl

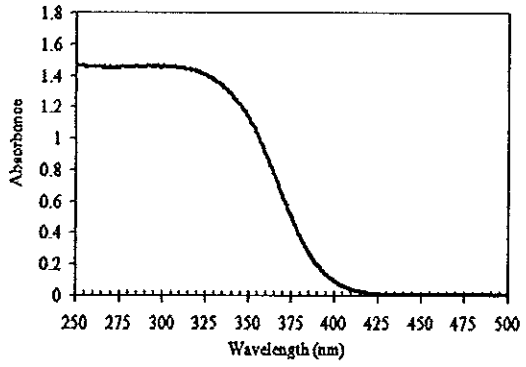

(d) TiO_2-200w-80H_2SO_4

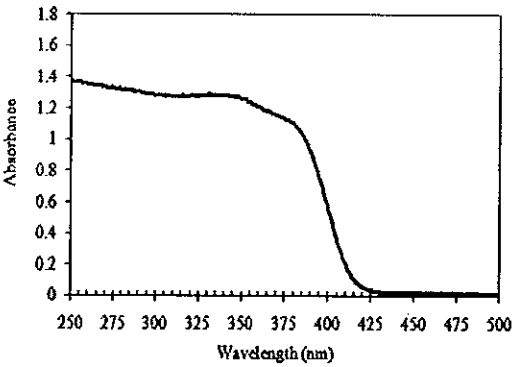

(e) TiO_2-100w-95HCl

Figure 19. Diffuse reflectance spectra of the synthesized TiO_2 powders: (a) TiO_2-am, (b) TiO_2-200w-80HCl, (c) TiO_2-200w-95HCl, (d) TiO_2-200w-80H_2SO_4, and (e) TiO_2-100w-95HCl.

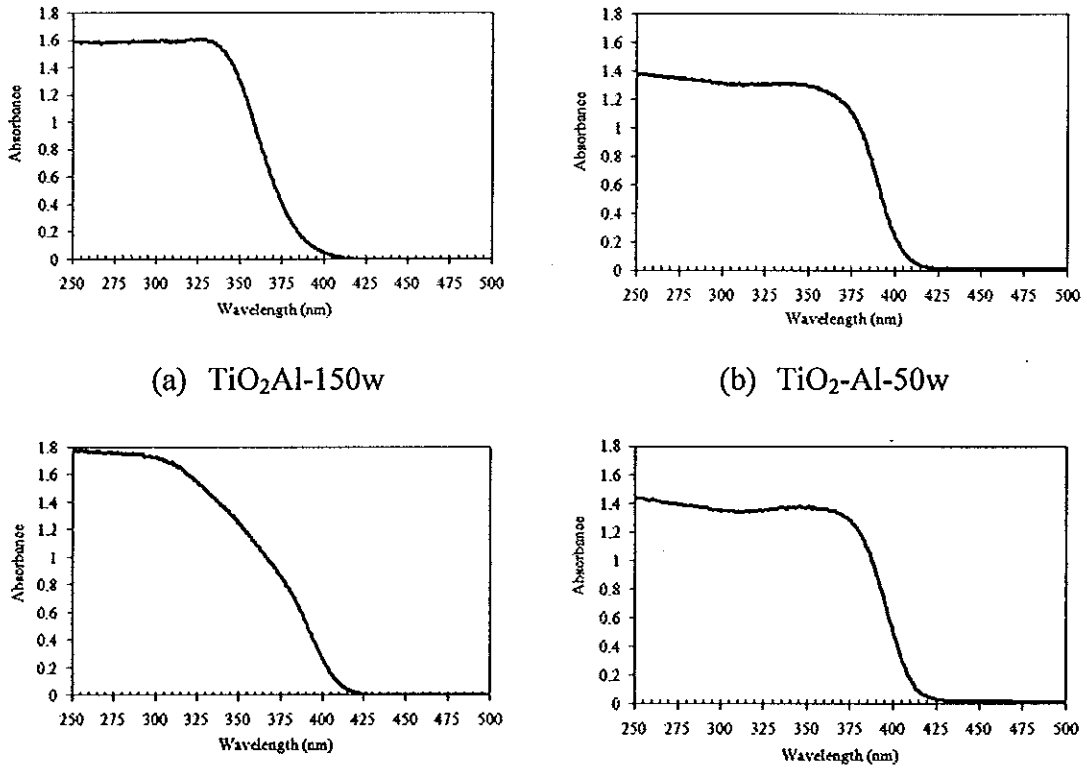

Figure 20. Diffuse reflectance spectra of the synthesized dopant-TiO_2 powders: (a) TiO2-Al-150w, (b) TiO_2-Al-50w, (c) TiO_2-B-150w, and (d) TiO_2-B-50w.

The absorption edges of TiO_2-200w-80HCl, TiO_2-200w-95HCl, TiO_2-100w-95HCl, TiO_2-Al-50w, TiO_2-Al-150w, TiO_2-B-150w, and TiO_2-B-50w appear at longer wavelength than that of TiO_2-200w-80H_2SO_4, TiO_2-Al-150w and Ti-am.

The bandgap energies of TiO_2-200w-80HCl, TiO_2-200w-95HCl, TiO_2-100w-95HCl, TiO_2-Al-50w, TiO_2-Al-150w, TiO_2-B-150w, and TiO_2-B-50w are in the same range of rutile (R706). Both TiO_2-Al-150w and TiO_2-am have larger bandgap energy and are in the same range of anatase (Carlo Erba). The last, TiO_2-200w-80H_2SO_4 bandgap energy is in the same range of P25 (Degussa).

Table 5. The absorption edges and band gap energies of titanium dioxide powders.

Sample	Absorption edge (nm)	Band gap energy (eV)	
		This work	Literatures
Anatase (Carlo Erba)	383	3.24	3.20 [a]
Rutile (R706, Dupont)	411	3.02	3.00 [a]
Degussa P25	395	3.14	3.14 [b]
TiO_2-am	386	3.21	-
TiO_2-200w-80HCl	406	3.05	-
TiO_2-200w-95HCl	406	3.05	-
TiO_2-200w-80H_2SO_4	394	3.15	-
TiO_2-100w-95HCl	414	3.00	-
TiO_2-Al-150w	385	3.22	-
TiO_2-Al-50w	405	3.06	-
TiO_2-B-150w	410	3.02	-
TiO_2-B-50w	411	3.02	-

[a] Sclafani, *et al.*, 1990; Miao, *et al.*, 2003

[b] Zielińska, *et al.*, 2003

3.1.1.4 Scanning electron microscopy (SEM)

The SEM micrographs were performed on gold-coated samples using a Jeol apparatus (JSM-5800 LV) equipped with a Link analyzer (ISIS 300) for X-ray energy-dispersive analysis (EDX).

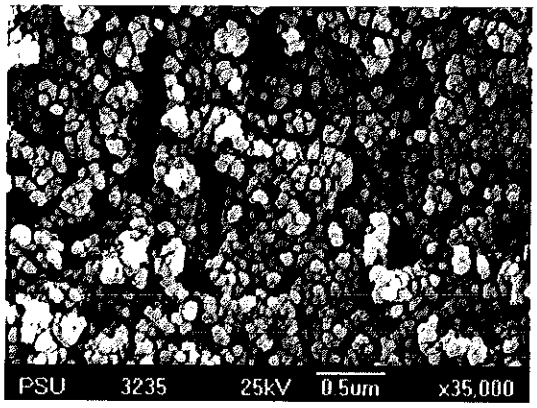

(a) Degussa P25

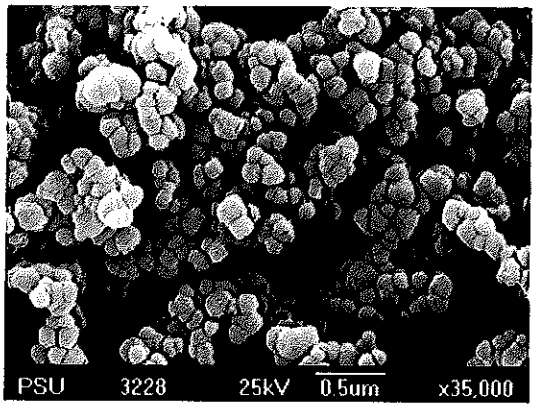

(b) Anatase (Carlo Erba)

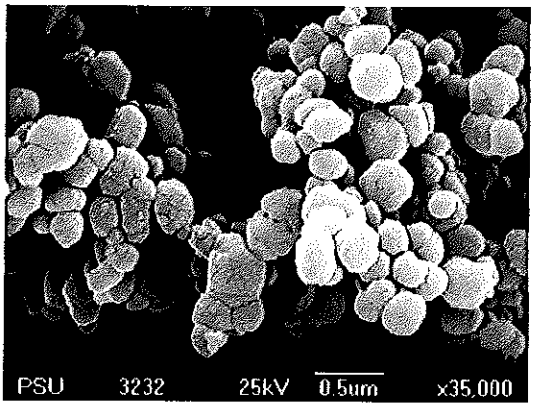

(c) Rutile (Dupont R706)

Figure 21. SEM images of the commercial TiO_2 powders: (a) Degussa P25, (b) Anatase (Carlo Erba), and (c) Rutile (Dupont R706).

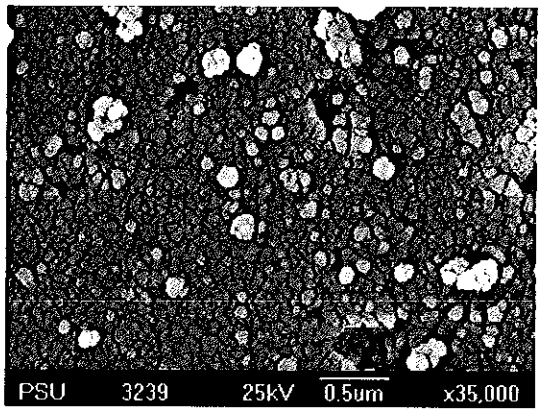

(a) TiO_2-am

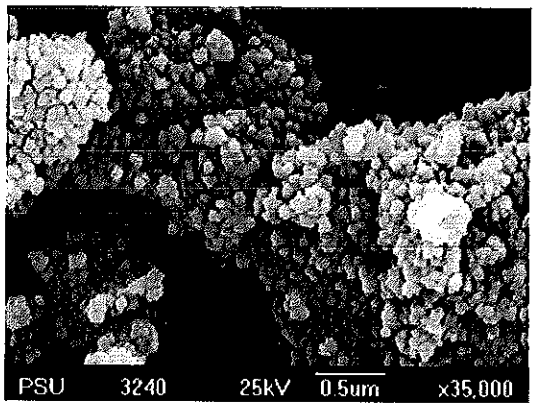

(b) TiO_2-200w-80HCl

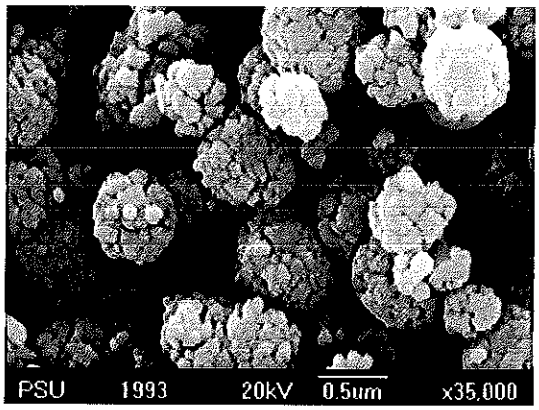

(c) TiO_2-200w-95HCl

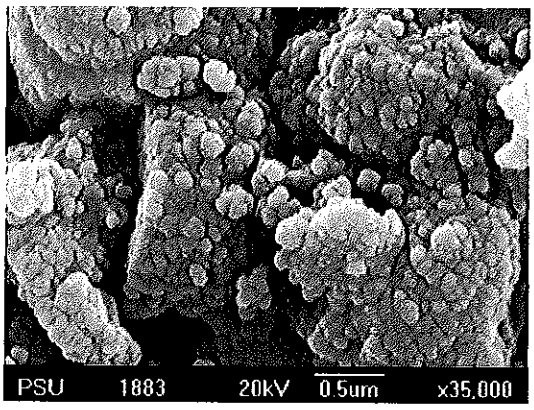

(d) TiO_2-200w-80H_2SO_4

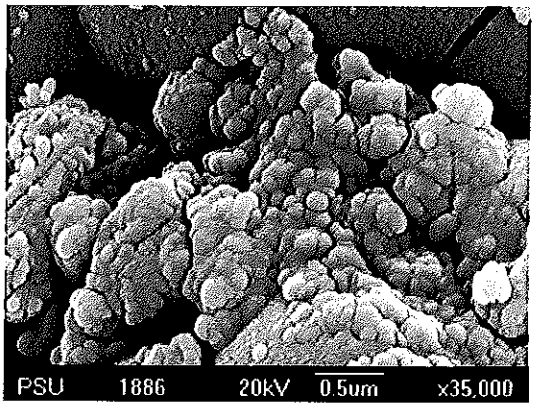

(e) TiO_2-100w-95HCl

Figure 22. SEM images of the synthesized TiO_2 powders: (a) TiO_2-am, (b) TiO_2-200w-80HCl, (c) TiO_2-200w-95HCl, (d) TiO_2-200w-80H_2SO_4, and (e) TiO_2-100w-95HCl.

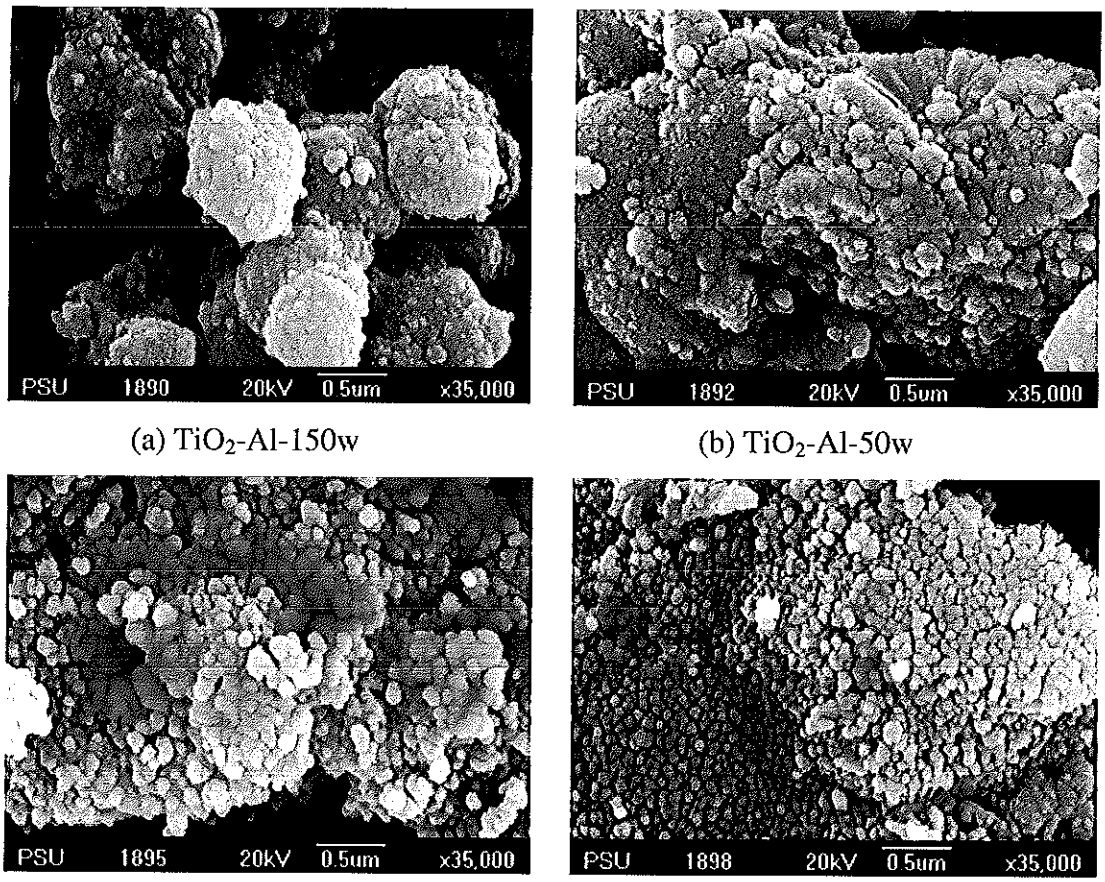

(a) TiO_2-Al-150w (b) TiO_2-Al-50w

(c) TiO_2-B-150w (d) TiO_2-B-50w

Figure 23. SEM images of the synthesized dopant-TiO_2 powders: (a) TiO_2-Al-150w, (b) TiO_2-Al-50w, (c) TiO_2-B-150w, and (d) TiO_2-B-50w.

Fig. 21, 22, and 23 show SEM images of commercial TiO_2 powders and synthesized TiO_2 powders, respectively. From the SEM images, magnified by 35,000×, the images show delicate structures of spherical building units. The synthesized samples, which exist mostly in amorphous phase show higher aggregation forming bigger chunk than the commercial samples. This could be the result from no calcinations at high temperature was applied.

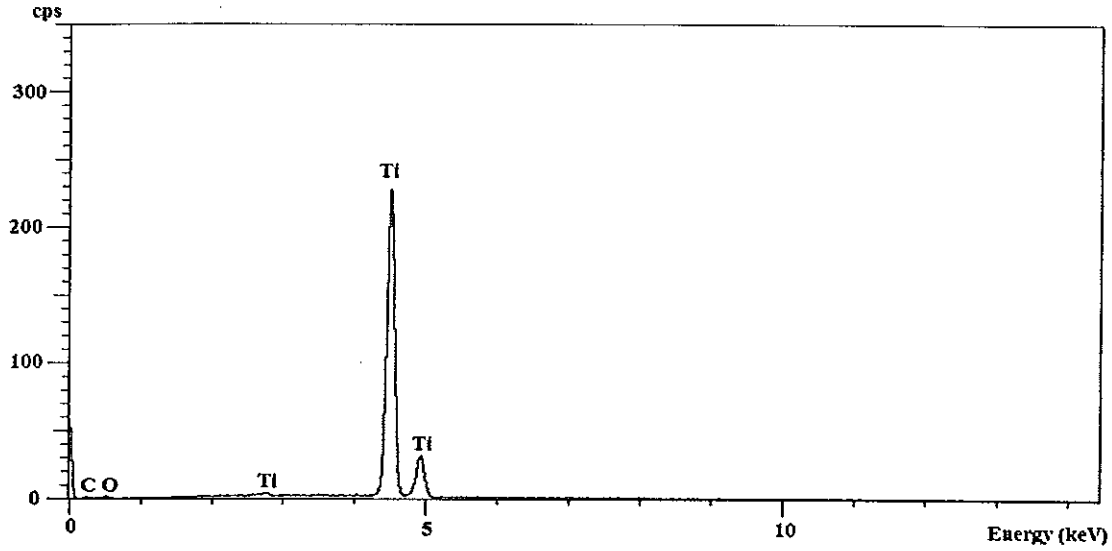

(a) TiO_2-am, TiO_2-200w-80HCl, TiO_2-200w-95HCl, TiO_2-100w-95HCl, TiO_2-B-150w, and TiO_2-B-50w

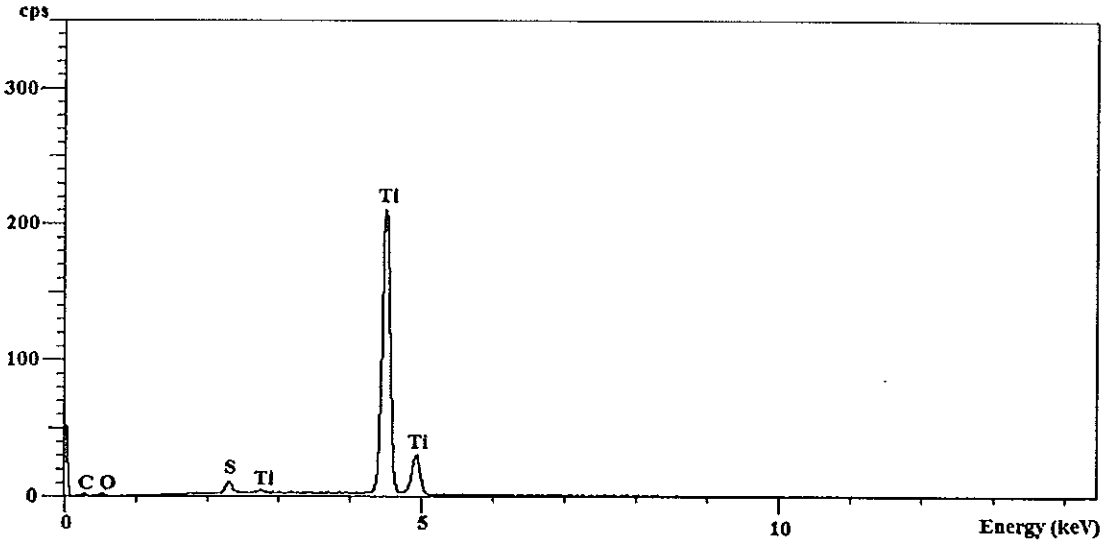

(b) TiO_2-200w-80H_2SO_4

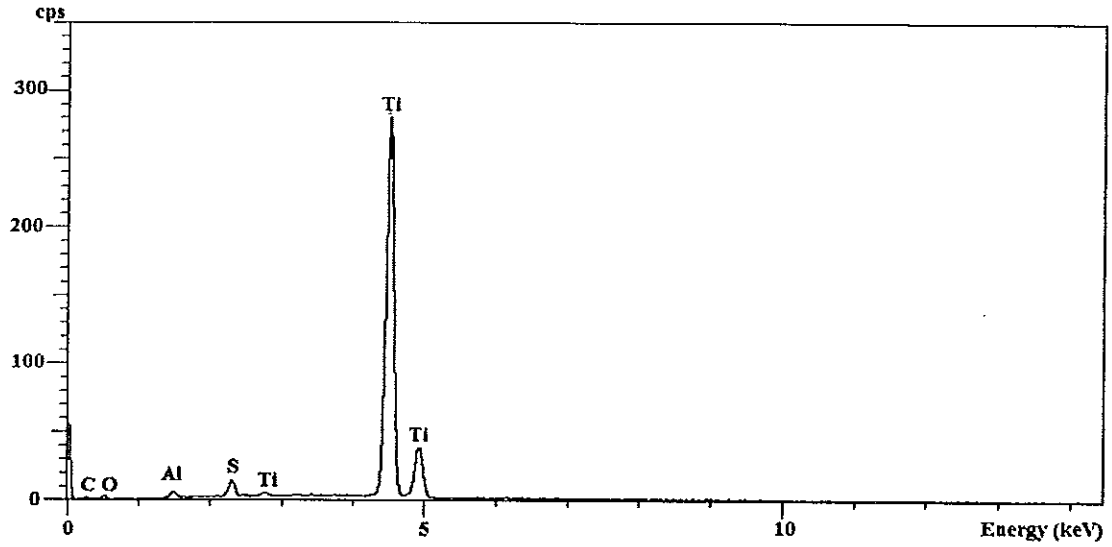

(c) TiO_2-Al-150w and TiO_2-Al-50w

Figure 24. EDX spectra of the synthesized TiO_2 powders: (a) TiO_2-am, TiO_2-200w-80HCl, TiO_2-200w-95HCl, TiO_2-100w-95HCl, TiO_2-B-150w, TiO_2-B-50w, (b) TiO_2-200w-80H_2SO_4, and (c) TiO_2-Al-150w, TiO_2-Al-50w.

Fig. 24 shows EDX patterns of as-synthesized TiO_2 powders. The EDX results revealed that, with the exception of three samples, all powder samples did not contain chloride anion which indicated that it was washed out completely at the washing stage. However, the samples obtained from using sulfuric showed the presence of S indicating the SO_4^{2-} ions still adhered to the titanium dioxide surfaces which agreed with the FT-IR results. In addition, the Al(III)-doped titania sample indicated the presence of Al and S, which results from the source of Al(III)-dopant (aluminium sulfate), showing that traces the Al^{3+} and SO_4^{2-} ions are left on the TiO_2 surfaces.

3.2 Photocatalytic disinfection study

3.2.1 Evaluation of antimicrobial activity

Five strains of bacteria (*E. coli* ATCC25922, *P. aeruginosa* ATCC27853, *B. subtilis* BGA, *S. aureus* ATCC25923, and MRSA DMST2054, and two species of yeast (*C. albicans* ATCC90028 and *C. neoformans* ATCC90112) were used in the study of the photocatalytic disinfection of titanium dioxide. The experiment was divided into 2 groups: bacteria and yeast. The antimicrobial study of both bacteria and yeast were performed in the presence of fixed-TiO_2 photocatalyst in agar media and irradiated with UV light. A blank experiment was done by irradiating agar plate in the absence of titanium dioxide in order to observe the growth of microbial in each batch experiment.

(a) Antibacterial activity

The bactericidal acvitity of synthesized and commercial TiO_2 nanoparticles were evaluated by growth inhibition of *P. aeruginosa*, *E. coli* (the Gram-negative bacteria), and *B. subtilis*, *S. aureus*, MRSA (the Gram-positive bacteria). The results were listed in Table 6. The Gram-positive bacteria have a relatively thick wall composed of many layers of peptidoglycan polymer and only one layer of membrane. The Gram-negative bacteria have only a thin layer of peptidoglycan and a more complex cell wall with two cell membranes, an outer membrane, and a plasma membrane. Under certain conditions, the Gram-negative bacteria are more resistant to many chemical agents than Gram-positive cells (Tortora, *et al.*, 2001).

Table 6. The MIC value of titanium dioxide powders with various bacteria.

TiO_2 sample	Irradiation time (min)	MIC (mg/mL)				
		P.aeruginosa	*E.coli*	*B.subtilis*	*S.aureus*	MRSA
Anatase (Carlo Erba)	30	-	-	-	-	-
	60	12.5	-	-	-	-
	90	12.5	100	-	-	-
	120	12.5	12.5	100	-	-
Rutile (R706)	30	-	-	-	-	-
	60	-	-	-	-	-
	90	-	-	-	-	-
	120	-	-	-	-	-
Degussa P25	30	-	-	100	-	-
	60	100	100	50	100	100
	90	100	100	25	100	100
	120	100	100	25	100	100
TiO_2-am	30	-	-	100	25	-
	60	-	-	100	25	100
	90	-	-	100	12.5	100
	120	100	100	100	12.5	50
TiO_2-200w-80HCl	30	-	-	-	-	-
	60	-	-	-	-	-
	90	-	-	-	-	-
	120	100	100	100	100	100
TiO_2-200w-95HCl	30	100	-	100	-	-
	60	50	100	25	100	100
	90	25	100	25	25	100
	120	25	100	25	25	25
TiO_2-200w-80H_2SO_4	30	25	50	25	25	25
	60	25	25	25	25	25
	90	25	25	25	25	25
	120	25	25	25	25	25
TiO_2-100w-95HCl	30	-	-	100	-	-
	60	-	-	50	-	-
	90	-	-	50	-	-
	120	100	100	50	100	100

Table 6. (Cont.) The MIC value of titanium dioxide powders with various bacteria.

TiO_2 sample	Irradiation time (min)	MIC (mg/mL)				
		P.aeruginosa	*E.coli*	*B.subtilis*	*S.aureus*	MRSA
TiO_2-Al-150w	30	50	100	50	50	50
	60	25	50	50	50	50
	90	25	50	25	25	25
	120	25	25	25	25	25
TiO_2-Al-50w	30	100	-	-	-	-
	60	100	100	100	-	-
	90	100	100	100	-	-
	120	50	50	50	100	100
TiO_2-B-150w	30	100	-	-	-	-
	60	100	100	100	-	-
	90	100	100	100	-	-
	120	50	50	50	100	100
TiO_2-B-50w	30	100	-	12.5	25	100
	60	100	-	12.5	25	50
	90	50	-	12.5	25	50
	120	50	100	12.5	25	50

* (-) represent the bacterial growth equal to the control (no inhibition)

MIC = minimum inhibitory concentration (mg/mL)

As shown in Table 6, two of the synthesized samples, TiO_2-200w-80H_2SO_4 and TiO_2-Al-150w, showed the best results in inhibiting the cell growth of all tested bacteria with lowest amount of titania and irradiation time. Another two of samples, TiO_2-200w-95HCl and TiO_2-B-50w, eventhough slightly inferior to the first two samples but also showed better result than P25. The commercial P25 TiO_2 which has been used in many reports with good results also showed good performance in this test by being able to cause inactivation of all five bacteria but with higher MIC values than the first four samples. The commercial anatase TiO_2, usually showing slightly lower photocatalytic activity than P25 in the dye degradation study, fails to inactivate *S. aureus* and MRSA bacteria in this test. The commercial rutile did not show any activity at all for all the five bacteria which is consistent with its poor performance found in the dye degradation study (Kanna and Wongnawa, 2008). The amorphous form titania, TiO_2-am, exhibited good results in inactivation of Gram-

positive bacteria but it required long irradiation time and high MIC value to inactivate Gram-negative bacteria. Another two of the synthesized samples, TiO_2-A1-50w and TiO_2-B-150w, showed respectable results with all five bacteria. The last two, TiO_2-200w-80HCl and TiO_2-100w-95HCl, eventhough they could inactivate all five bacteria but needed long irradiation time with high MIC values compared with all the synthesized samples in this study. In summary, it is interesting to see that all of the nine synthesized samples could inactivate all five bacteria in this screening test albeit with varying MIC values. In comparison with P25, four samples showed better antibacterial activity than P25. The order of performance can be arranged as follows:

TiO_2-200w-80H_2SO_4 > TiO_2-Al-150w > TiO_2-B-50w > TiO_2-200w-95HCl > P25 > TiO_2-Al-50w ≈ TiO_2-B-150w > TiO_2-am > TiO_2-100w-95HCl ≈ TiO_2-200w-80HCl > anatase > rutile.

(b) Anti-yeast activity

The screening test of antimicrobial activity against yeast by titanium dioxide samples was investigated by inspecting the inhibition growth of yeast at highest condition (100 mg/mL of TiO_2 concentration with irradiation time 120 min). The result demonstrated that all titanium dioxide samples could not kill both types of yeasts in this experiment but they retarded the growth of yeast which could be observed visually as shown in Table 7. As shown in Fig. 14, the culture spots of blank plates looked wet and greasy (Fig. 14b) while the culture spots of as-prepared TiO_2 agar plates (Fig. 14a and 14c) were drier and paler than the control. In this result, all prepared-TiO_2 samples could impede the growth of yeast, *C. albicans,* equally well compared with Degussa P25. For inhibitory test of *C. neoformans*, all synthesized-TiO_2 powders could retard *C. neoformans* growing as good as Degussa P25, except for TiO_2-am, TiO_2-100w-95HCl, and TiO_2-B-50w.

Table 7. The antimicrobial screen test of titanium dioxide powders with two species of yeasts, *C. albicans* and *C. neoformans* (TiO_2 concentration 100 mg/mL, irradiation time 120 min).

Sample (100 mg/mL)	*C. albicans*	*C. neoformans*
Control	++	++
Anatase (Carlo Erba)	++	++
Rutile (R706, Dupont)	++	++
Degussa P25	+	+
TiO_2-am	+	++
TiO_2-200w-80HCl	+	+
TiO_2-200w-95HCl	+	+
TiO_2-200w-80H_2SO_4	+	+
TiO_2-100w-95HCl	+	++
TiO_2-Al-150w	+	+
TiO_2-Al-50w	+	+
TiO_2-B-150w	+	+
TiO_2-B-50w	+	++

* (++) represent the microbial cell growth which equal to the control (no inhibition).

(+) represent the microbial cell growth which were smaller and drier than the control.

With regard to the photocatalytic activity, there have been many reports that anatase shows higher activity than rutile in many photocatalytic reactions in air and water (Mills and Sawunyama, 1994; Sclafani and Herrmann, 1996; Lucarelli, *et al.*, 2000; Sato and Taya, 2006) except in some cases (Ohno, *et al.*, 1997). The effect of crystalline structures on biocidal activity of TiO_2 particles has been

clarified by investigating the photocatalytic deactivation of phage MS2 in suspensions of anatase TiO_2 and rutile TiO_2 as well as their mixtures. The results showed that the contact between both types of TiO_2 particles in aggregations caused the enhancement of quantum yield of TiO_2 suspension, thereby reactive oxygen species generation from photocatalytic reaction, which leads to the enhancement of biocidal activity of the photocatalytic particles (Sato and Taya, 2006). In another study, the photocatalytic process of anatase has been shown to produce highly reactive species such as hydroxyl radical, hydrogen peroxide, and superoxide which, in principle, can cause fatal damage to microorganisms by injury of the cell membranes when bacteria come into contact with TiO_2 surface (Sunada, *et al.*, 1998; Sunada, *et al.*, 2003).

Most of the recent researches on the inhibition of bacterial cell growth (Gumy, *et al.*, 2006a; Gumy, *et al.*, 2006b; Verran, *et al.*, 2007) have been studied by using the suspended-TiO_2 in solution. In suspension, TiO_2 nanoparticles were trapped onto the bacterial surface resulting in the adsorption of TiO_2 particles on the bacteria surface which could lead to inactivation of bacteria in couple with the photocatalytic oxidation reaction described above. In this study, the agar dilution method was chosen to eliminate the possibility of inactivation by surface adsorption, hence the inactivation results could be said to come solely from the photocatalytic property of the photocatalysts. In this method the TiO_2 nanoparticles were fixed in agar and would not be adsorbed onto the bacterial surface. The disadvantage of this method is that, due to the fixed TiO_2 particles in the agar matrix, higher concentration of photocatalyst is required and, hence, the MIC values from this method would be higher than that from the suspension method.

3.2.2 Microorganism inactivation by TiO_2 photocatalysis mechanism.

The first work on this topic was by Matsunaga, *et al.*, (1985), who demonstrated the photooxidation of Coenzyme A (CoA) in *Lactobacillus acidophilus* (bacteria), *Saccharomyces cerevisiae* (yeast), and *Escherichia coli* (bacteria) in suspensions of irradiated TiO_2. Decreased CoA in those cells caused their metabolic activity to diminish, leading to cell death, which they reported was inversely

proportional to the thickness and complexity of the cell wall. Other studies have also confirmed this finding. The study by Saito and co-workers (Saito, *et al.*, 1992) demonstrated that photo-activated TiO_2 provoked rupture of the cell membrane in *Streptococcus sobrinus*, as shown by electron microscopy and demonstrated by intracellular leakage of K^+ ions that paralleled cell death. Further evidence of this mechanism was found by Sunada, *et al.* (1998) who proved that TiO_2 mediated photocatalytic destruction of endotoxin, an integral component of the outer membrane of *E. coli*. Maness, *et al.* (1999) showed that lipid peroxidation is the underlying mechanism of *E. coli* K-12 cells in the presence of irradiated TiO_2. They demonstrated that the occurrence of lipid peroxidation and the simultaneous loss of both membrane-dependent respiratory activity and cell viability strictly depended on the presence of both light and TiO_2.

In further research to better understand bactericidal activity of photo-excited titanium dioxide, Huang, *et al.* (2000) investigated the sites of cellular damage and their contribution to cell death in *E. coli*. These authors propose that oxidative damage first takes place on the cell wall, where the TiO_2 photocatalytic surface first makes contact with whole cells. Cells suffering from cell-wall damage were proven to still be viable. Photocatalytic action progressively increased cell permeability and, thereafter, the open flow of intracellular components, allowing TiO_2 particles easier access and photo-oxidation of intracellular elements, accelerating cell death. Recent work published by Sunada and co-worker (2003a) has contributed similar results to those reported by Huang, *et al.* (2000). They propose the photokilling mechanism of titanium dioxide which can be schematically illustrated as in Fig. 25. The initial reaction is a partial decomposition of the outer membrane by the reactive species produced by TiO_2 photocatalysis (Fig. 25b). During this process, cell validity is not lost very efficiently. The partial decomposition of the membrane, however, changes the permeability to reactive species. Correspondingly, the permeability change of the outer membrane enables reactive species to easily reach the cytoplasmic membrane. Thus, the cytoplasmic membrane is attacked by reactive species, leading to the peroxidation of membrane lipid (Fig. 25c). Work by Nadtochenko, *et al.* (2004) demonstrated the events leading to *Escherichia coli* photokilling with viability data

and ATR-FTIR spectroscopy of the organized structure of intact and viable cell membranes. In work by the same group (Kiwi, *et al.*, 2005), the formation of peroxidation products such as aldehydes, ketones, and carboxylic acids were detected in parallel to the disappearance of cell wall membrane component and oxidation products due to TiO_2 photocatalysis on sugar rings, lipid chains, and polypeptide.

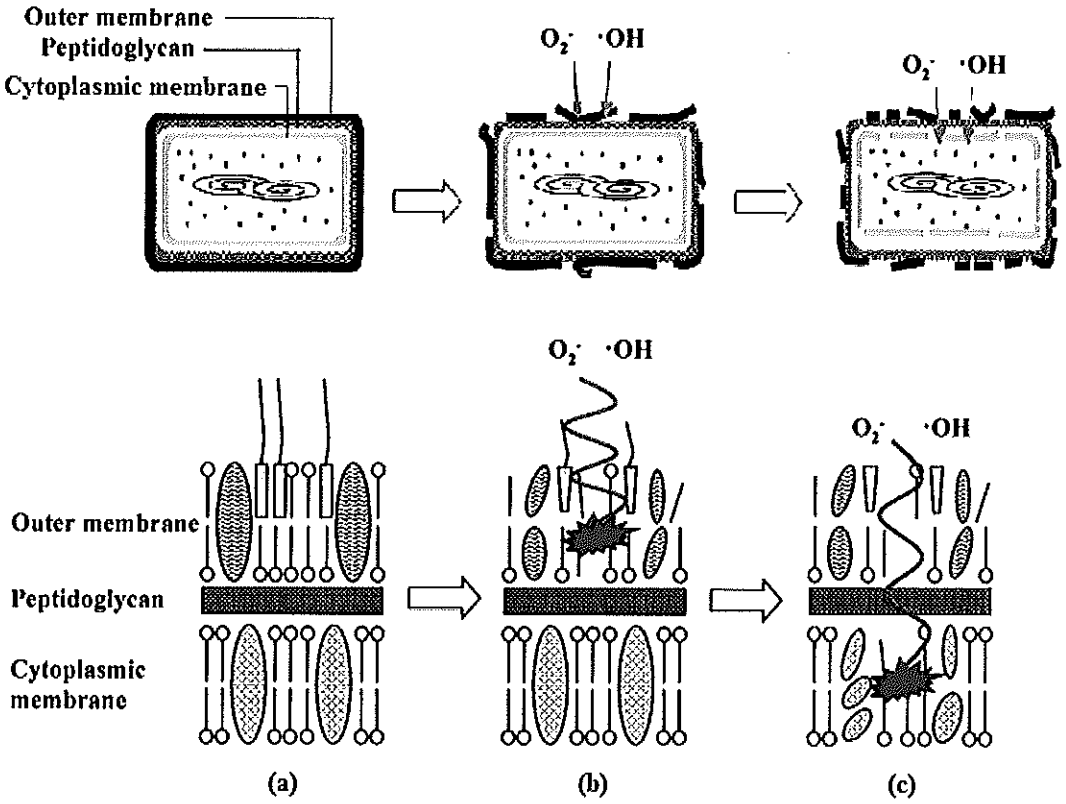

Figure 25. Schematic illustration of the process of bacteria photokilling on TiO_2. In lower row, the part of cell envelope is magnified (adapted from Sunada, *et al.*, 2003).

It is well known that UV irradiation induces DNA damage, e.g., pyrimidine dimmers. Moreover, once cell wall damage is caused by the photo-oxidative action of titanium dioxide, the photocatalyst can also produce detrimental effects to the intracellular components. Of the experimental evidence in this regard (Huang, *et al.*, 1997; Kim, *et al.*, 2004), it is important to mention work by Hidaka, *et al.* (1997), who performed *in vitro* experiments monitoring the fate of DNA, RNA, and their

pyrimidine and purine bases once irradiated by UVA and UVB in the presence of titanium dioxide particles. They verified the detrimental effect on DNA and RNA by scanning electron microscopy and gel permeation chromatography.

At the present time, the photochemical mechanism of the TiO_2 biocidal action remains largely unclear. It is uncertain what reactive oxygen species are directly involved in the photokilling process (Blake, *et al.*, 1999), especially the identities of the main reactive oxygen species (ROS), which not only include the $^{\bullet}OH$ radical, but also $O_2^{\bullet-}$, and H_2O_2. The recent contribution of Cho, *et al.* (2002) demonstrates the important role of the $^{\bullet}OH$, acting either independently or in collaboration with other ROS, in the inactivation of *Escherichia coli* in presence of UV-illuminated TiO_2 particles with excellent linear correlation between steady-state concentration of $^{\bullet}OH$ and the rate of *E. coli* inactivation.

These experiments demonstrated that both UV-light and a photocatalyst, such as TiO_2, were needed for the effective disinfection of microbe. This is due to the fact that when TiO_2 is illuminated with the light of energy equal or higher than the band gap energy the electron-hole pairs are produced. The photokilling behavior may be explained as follows: UV illumination of TiO_2 produces various reactive species (e.g., $^{\bullet}OH$, $HO_2^{\bullet}$, H_2O_2) in the presence of water and air by the following reaction (Hoffman, *et al.*, 1995; Mills and Hunte, 1997).

$$TiO_2 + h\nu \longrightarrow e^- + h^+ \qquad (1)$$

[Reduction site]

$$O_2 + e^- \longrightarrow O_2^- \qquad (2)$$

$$O_2^- + H^+ \longrightarrow HO_2^{\bullet} \qquad (3)$$

$$HO_2^{\bullet} + HO_2^{\bullet} \longrightarrow H_2O_2 + O_2 \qquad (4)$$

$$H_2O_2 + e^- \longrightarrow OH^- + {}^{\bullet}OH \qquad (5)$$

[Oxidation site]

$$H_2O + h^+ \longrightarrow {}^{\bullet}OH \quad (6)$$

$${}^{\bullet}OH + {}^{\bullet}OH \longrightarrow H_2O_2 \quad (7)$$

$$H_2O_2 + 2h^+ \longrightarrow 2H^+ + O_2 \quad (8)$$

These reactive oxygen species can decompose organic compounds and extinguish cellular activity.

CHAPTER 4

CONCLUSIONS

In this part, photocatalyst TiO_2 powders in anatase or rutile or a mixture of anatase and rutile phases have been synthesized from an aqueous solution of $TiCl_4$ by the sol-gel process. The Al^{3+} or B^{3+}-doped titania were also prepared via the same process. No calcination at high temperature was applied to these syntheses. The product TiO_2 composed of mainly amorphous phase with a small amount of anatase or rutile or a mixture of both. All samples were characterized by powder XRD, BET, SEM, EDX, FT-IR, and UV-Vis techniques. The powder XRD evidence showed that the synthesized parameters (acid catalyst, volume of water used, refluxed temperature and refluxed time) results in changing of TiO_2 phase component. In conclusion, low volume of water content affects the growing of TiO_2 cluster in the rutile phase, and the presence of sulfate accelerates the growth of TiO_2 cluster in the anatase phase. The low volume of water and high refluxing temperature tend to favor the rutile phase titania (Ding, *et al.*, 1997).

These samples were tested for antimicrobial activity (bacteria and yeast) in comparison with the commercial products, anatase, rutile, and Degussa P25. All the nine synthesized samples showed inactivation activity towards bacteria, two of them (TiO_2-200w-80H_2SO_4 and TiO_2-Al-150w) showed a higher activity than Degussa P25. This activity could be the combined results of the high surface area and the suitable width of the band gap energy of the synthesized samples.

In the studied of photocatalytic disinfection of TiO_2 powders of yeasts, the results indicated that the synthesized titania retarded the growth of yeasts within 120 min irradiation time. For those with good performances, these products can be regarded as an inexpensive alternative to the presently available commercial ones due to simple synthesis without the need for calcination.

Part II

Nanosized TiO_2 Particles Decorated on SiO_2 Spheres (TiO_2/SiO_2): Synthesis and Photocatalytic Activities

CHAPTER 1

INTRODUCTION

1.1 Introduction

Titania (TiO_2, titanium dioxide) has received significant attention because of its numerous applications, such as photocatalysis and catalyst support, white pigments for paints, cosmetics, fillers, and battery electrodes (Fujishima, *et al.*,2000). However, titania powders having high surface areas are not thermally stable and lose their surface area readily at elevated temperature through phase transformation and crystallite growth. Therefore, many research groups have investigated coating titania on silica spheres which can serve as high surface area support (Fujishima, *et al.*, 2000; Li, *et al.*, 2003).

Over the last decades, applications and uses of supported metal oxides on silica have driven research towards the production of catalysts characterized by the presence of high percentage of the metal oxide in a dispersed state (two dimensional surface metal oxide overlayers) (Bond, *et al.*, 1991; Roark, *et al.*, 1992; Castillo, *et al.*, 1996). An interesting example is given by silica-supported titania TiO_2/SiO_2 catalysts that have been considered as advanced support materials substituting pure TiO_2. The higher mechanical strength, thermal stability and specific surface area of the supported titania oxides, compared to pure TiO_2, have recently attracted much attention and driven interest towards the use of these materials not only as catalytic supports, but also as catalysts through the generation of new catalytic active sites (Deo, *et al.*, 1993; Iengo, *et al.*, 1999).

Moreover, TiO_2/SiO_2 particles exhibit novel properties that are not found in either single oxide. Recently, it was reported that TiO_2/SiO_2 particles show better catalytic properties and improved photoactivity than do the classical single oxides, such as titania and silica (Fu, *et al.*, 2001; Cheng, *et al.*, 2003). This was partially explained in terms of interaction between TiO_2 and SiO_2, as well as the

different structure from bulk TiO_2. It is well known that silica surface is fairly inert, however, the silica surface hydroxyls generally act as adsorptive/reactive sites because of their hydrophilic character. Thus, the preparation of highly dispersed metal oxides on silica often involves highly reactive precursors, such as titanium alkoxides or $TiCl_4$, which readily react with the surface hydroxyls of the silica support (Deo, *et al.*, 1993; Castillo, *et al.*, 1996). In report of Anderson and Bard, the effect of incorporation of silica on the behavior of titania-based photocatalysts prepared by a sol-gel technique showed that in the decomposition of rhodamine-6G by the titania/silica mixed oxide with a ratio 30/70 produced the highest activity, about three times higher than the Degussa P25 titania (Anderson and Bard, 1995).

In this research, nanosized pure TiO_2 and nanosized TiO_2 grafted on SiO_2 sphere (TiO_2/SiO_2) were prepared by the sol-gel method using titanium tetraisopropoxide (TTIP) and methyl-trimethoxysilane (MTMS) as precursors. The physical properties of TiO_2/SiO_2 particles were investigated by FT-IR, XRD, and XPS. We also determined the effect that the amount of TiO_2 grafted on SiO_2 had on the physical properties of nanosized TiO_2/SiO_2 particles. In addition, their photocatalytic activities on the decomposition of methylene blue were also investigated. In this work, the effect of this particular decoration of titanium metal oxide onto the silicon metal oxide will be discussed with respect to the observed enhanced photocatalytic activity as a means for increasing adsorption and photoreaction rates.

1.2 Review of literatures

1.2.1 The sol-gel process

The sol-gel process allows synthesizing ceramic materials of high purity and homogeneity by means of preparation techniques different from the traditional process of fusion of oxides. This process involves the evolution of inorganic networks through the formation of a colloidal suspension (sol) and gelation of the sol to form a network in a continuous liquid phase (gel). The precursors for synthesizing these colloids consist usually of a metal or metalloid element surrounded by various

reactive ligands. The starting material is processed to form a dispersible oxide and forms a sol in contact with water or dilute acid. Removal of the liquid from the sol yields the gel, and the sol/gel transition controls the particle size and shape. Calcination of the gel produces the oxide.

Sol-gel process occurs in liquid solution of organometallic precursors such as $Si(OEt)_4$ (tetraethyl orthosilicate, or TEOS), Ti(IV)-butoxide, which, by means of hydrolysis and condensation reactions, lead to the formation of a new phase (sol). The reactions involved in the sol-gel chemistry based on the hydrolysis and condensation of metal alkoxides $M(OR)_z$ can be described as follows (Brinker and Scherer, 1990; Hench and West, 1990):

$$\text{M-O-R} + H_2O \rightarrow \text{M-OH} + \text{R-OH} \qquad \text{(hydrolysis)}$$

$$\text{M-OH} + \text{HO-M} \rightarrow \text{M-O-M} + H_2O \qquad \text{(water condensation)}$$

$$\text{M-O-R} + \text{HO-M} \rightarrow \text{M-O-M} + \text{R-OH} \qquad \text{(alcohol condensation)}$$

Sol-gel method of synthesizing nanomaterials is very popular amongst chemists and is widely employed to prepare oxide materials.

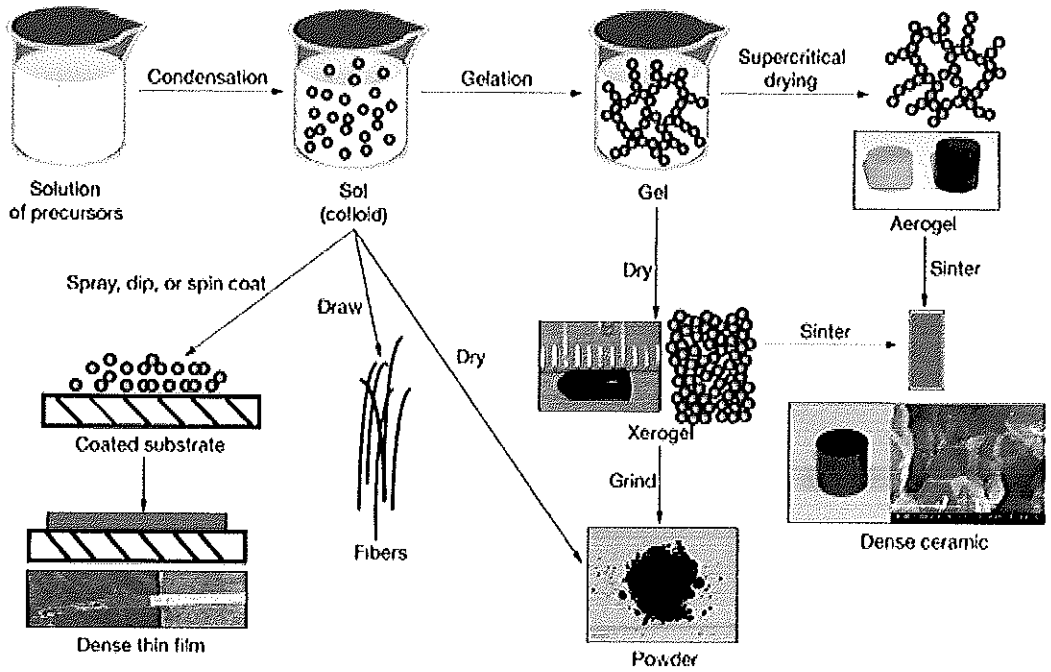

Figure 26. Schematic representation of sol-gel process of synthesis of nanomaterials (https://www.llnl.gov/str/May05/Satcher.html).

The interest in this synthesis method arises due to the possibility of synthesizing nonmetallic inorganic materials like glasses, glass ceramics or ceramic materials at very low temperatures compared to the high temperature process required by melting glass or firing ceramics. The most attractive features of the sol-gel process include the production of compositions not possible with conventional ceramic preparation methods, along with the retention of the mixing level of the solution in the final product, often on the molecular scale (Hu, *et al.*, 1992; Lenza, *et al.*, 2000). By controlling the synthesis conditions carefully, these reactions may lead to a variety of structure, and to different final states for the materials (Brunet and Cabane, 1993).

In recent years, an improvement in the photocatalytic behavior of particulate titanium dioxide (TiO_2) by the intimate incorporation of SiO_2 have been investigated (Arai, *et al.*,2006; Yu, *et al.*,2006; Qi *et al.*, 2007). It was reported that TiO_2 in SiO_2/TiO_2 composite materials exhibited better photoactive than pure TiO_2

powders due to smaller grain size and improved adsorption (Yu, *et al.*, 2001; Cheng, *et al.*, 2003; Hong, *et al.*, 2003). Furthermore, it was found that TiO_2/ SiO_2 composite microspheres are good candidate materials for photonic crystals with complete band gap in the near-infrared and visible regions (Han and Kumacheva, 2001; Kimura, *et al.*,2003). Usually, TiO_2/SiO_2 composite microspheres could be prepared by many methods including impregnation, grafting, precipitation, reverse suspension, sol-gel technology and so on (Dutoit, *et. al.*, 1995; Holgado, *et al.*, 2000; Retuert, *et al.*, 2000; Han and Kumacheva, 2001; Khalil, *et al.*, 2002; Kimura, *et al.*, 2003). However, the composite microspheres prepared by the above method showed low surface areas due to using non-porous silica as substrates. This limited their further potential applications in many fields, such as catalysis and molecular separations.

In this work, the method to synthesized TiO_2 decorated on SiO_2 sphere is consisted of 2 steps as follow. First, the sol-gel method was used to prepare nanosized TiO_2, SiO_2 sphere, and nano-anatase TiO_2 sols for decorated on SiO_2 spherical core shells. Afterward, the deposition of titania colloid particles on the surface of monodispersed silica microsphere which was done by using a simple electrostatic attraction strategy, and then calcined at 500 °C for 3 h.

1.2.2 Dye and treatment of dye pollutant

1.2.2.1 Dye

A dye can generally be described as a colored substance that has an affinity to the substrate to which it is being applied. The dye is generally applied in an aqueous solution, and may require a mordant to improve the fastness of the dye on the fiber.

The first human-made (synthetic) organic dye, mauveine, was discovered by William Henry Perkin in 1856. Many thousands of synthetic dyes have since been prepared. Synthetic dyes quickly replaced the traditional natural dyes. They cost less, they offered a vast range of new colors, and they imparted better properties upon the dyed materials.

In this research, methylene blue (MB) was used as a model of dye pollutant. Methylene blue, MB, is a brightly colored, blue cationic thiazine dye. The structural formula of MB (3,7-bis(dimethylamino)phenothiazin-5-ium chloride, $C_{16}H_{18}ClN_3S$) are shown below (Epling and Lin, 2002). The uses of MB include being an antidote for cyanide poisoning in humans, antiseptic in veterinary medicine and, most commonly, in vitro diagnostic in biology, cytology, hematology and histology (Mills and Wang, 1999). At room temperature it appears as a solid, odorless, dark green powder that yields a blue solution when dissolved in water.

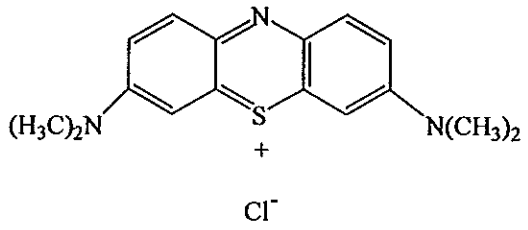

Methylene blue has been used in several research articles. Mills and Wang (1999) studied the photobleaching of MB in an aqueous solution in the absence and presence of oxygen. Xu, *et al.*, (1999) reported the influence of particles size of TiO_2 on the photocatalytic degradation of MB in a suspended aqueous solution. Houas, *et al.*, (2001) investigated the TiO_2/UV photocatalytic degradation of methylene blue (MB) in water. Epling and Lin (2002) studied the photoassisted bleaching of MB utilizing TiO_2 and visible light. Awati, *et al.*, (2003) studied the photocatalytic decomposition of MB using nanocrystalline anatase titania prepared by ultrasonic technique. Randorn, *et al.*, (2004) reported the bleaching of methylene blue by hydrated titanium dioxide. Kanna and Wongnawa (2008) determined the photocatalytic decolorization of MB using mixed amorphous and nanocrystalline TiO_2 powders, which prepared by acid-catalyzed sol-gel method at 80 °C without calcinations.

1.2.2.2 Methods for the treatment of dye pollutants

Many dyes pose environmental hazards because their degradations may produce toxic intermediates. For example, those dyes with substructures of nitrobenzene, benzidine and quaternary amines have carcinogenicity and toxicity. With increasing awareness of water-resource protection to ensure a safe drinking supply, dye-containing wastewater originated from dye manufacturing industries and dyeing industries needs to be treated before being discharged (Epling and Lin, 2002).

Over the last two decades photocatalytic process has been shown to be potentially advantageous and useful for the treatment of wastewater pollutants. This process has several advantages over competing processes such as: (1) complete mineralization, (2) no waste-solids disposal problem, and (3) only mild temperature and pressure conditions are necessary (Mahmoodi, *et al.*, 2005).

The usefulness of metal oxide for water purification lies in the ability of the photogenerated electrons and holes to participate in reactions with the pollutants that have been mineralized to harmless products. Most organic pollutants can be removed by oxidation reactions. As shown in Fig. 27, either the photogenerated hole directly reacts with the pollutant or the hole reacts with water forming hydroxyl species, which oxidize the pollutants. The photocatalytic mechanism of TiO_2 has been well documented and can be summarized as follows (Houas, *et al.*, 2001; Anpo and Takeuchi, 2003).

$$TiO_2 + h\nu \rightarrow e_{cb} + h_{vb} \quad (1)$$

$$O_{2\,ads} + e_{cb} \rightarrow O_2^- \quad (2)$$

$$O_2^- + H^+ \rightarrow {}^{\bullet}OOH \quad (3)$$

$$2\,{}^{\bullet}OOH \rightarrow H_2O_2 + O_2 \quad (4)$$

$$H_2O_2 + e^- \rightarrow OH^{\bullet} + OH^- \quad (5)$$

$$H_2O_{ads} + h_{vb} \rightarrow H^+ + OH^{\bullet} \quad (6)$$

$$\text{Organic pollutants} + OH^{\bullet} \rightarrow \text{degradation products} \quad (7)$$

$$\text{Organic pollutants} + h_{vb} \rightarrow \text{degradation products} \quad (8)$$

The reaction begins with TiO_2 particles being excited with UV light resulting in the formation of electron-hole pair, as displayed in eq. (1). The electron in the conduction band, e_{cb}, and the hole in the valence band, h_{vb}, may recombine and nullify further reactions. The $e_{cb} - h_{vb}$ pair, if they survive from the recombination process, will eventually diffuse to the bulk surface and react with other molecules nearby. The e_{cb} can react with molecular O_2 adsorbed at the bulk surface and after few more steps will lead to the formation of $OH^{\bullet}$ radical, eq. (2)-(5), which plays a major role in photocatalytic reaction. The h_{vb} can react with H_2O at the bulk surface leading to formation of $OH^{\bullet}$ radical as well, eq. (6). The very reactive $OH^{\bullet}$ radical can go on by attacking the dye molecules to completely mineralize them, eq. (7). In addition, the h_{vb} itself can also attack and mineralize dye molecules, eq. (8). This cycle continues when light is available. Note for Fig. 27 that the desired oxidation-reduction reaction to occur for organic compounds, the redox potential needs to be smaller than the bandgap, and the reduction potential below in absolute position with respect the conduction band potential, and above for the oxidation and the valence band.

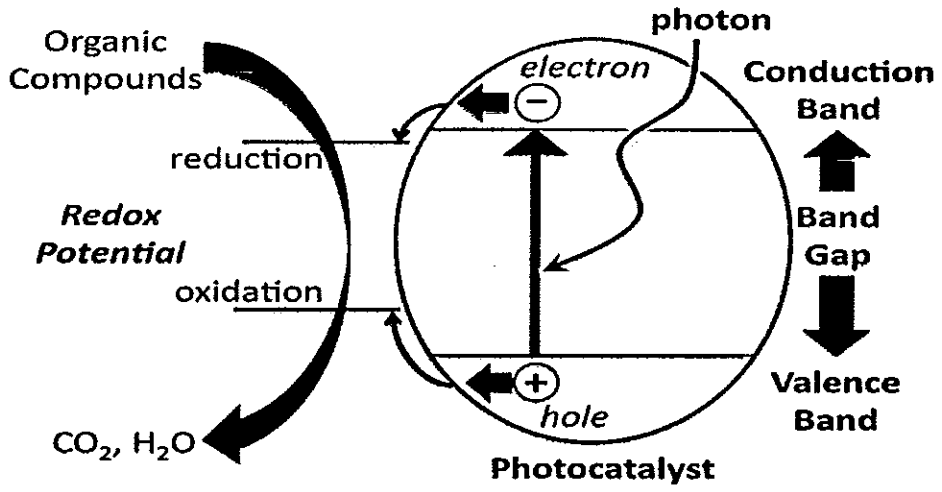

Figure 27. Schematic representation of the photocatalytic oxidation mechanism of semiconductor materials (VB: valence band and CB: conduction band).

The relative positions of the redox potentials for the formation of hydroxyl species and the valence band for some common semiconductors are shown in Fig. 28. A semiconductor such as Si with a valence band above the redox potential required for hydroxyl radical formation is not useful for photocatalytic oxidation. Conversely, titanium dioxide which has valence bands below the redox potential required for hydroxyl radical formation is suitable for photocatalytic oxidation. Furthermore, the difference between the redox potential for the desired reaction and the valence and conduction bands acts as the driving potential for the desired reaction; the higher this driving potential is, the faster the oxidation (valence) and reduction (conduction) reactions. Note that too in Fig. 28, the redox couple is generally asymmetric with respect to the band gap, and that if either the reduction or oxidation potential is above or below the conduction and valence band of the photocatalyst, the reaction will not go forward. For example, in the case of anatase TiO_2, the conduction band is about -0.1 eV and the valence band is about +3.0 eV. At pH = 0, the redox couple of $OH^{\cdot}/H_2O$ equals to +2.73 eV which is between the conduction band and the valence band of anatase titania, then this reaction could go forward.

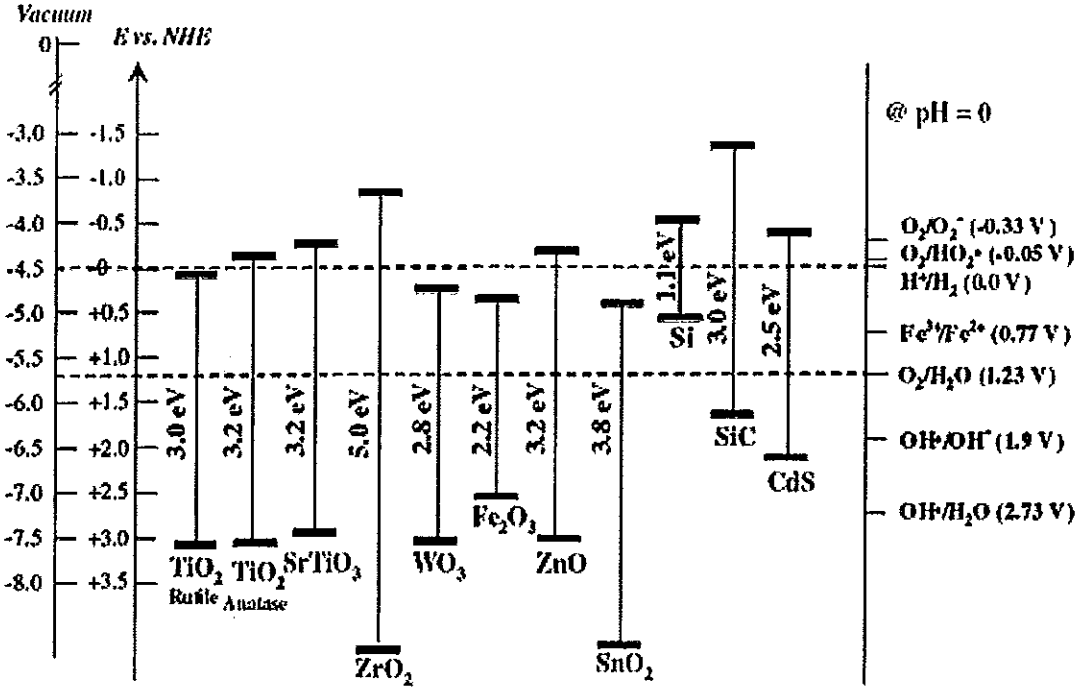

Figure 28. Conduction band and valence band energy positions for common semiconductors at pH = 0. The values noted on the right axes are the redox potentials for certain common redox couples of interest in water purification (Chandrasekharan, 2008).

However, the limitations of photocatalysts for water purification is the low photoefficiency of photocatalysts and the high energy required for the photon (near UV or UV) to generate electrons and holes. Previous literatures have explored multiple ways to improve the photoefficiency of the decontamination and disinfection process for titanium dioxide and other semiconductors. Methods to reduce the energy bandgap and hence the required energy of the photon have also been investigated. Some of the proposed methods to increase photoefficiency focus on increasing the charge separation between the electrons and holes; thus reducing the recombination rates and increasing availability of the electrons and holes to participate in the redox reactions. These methods include the deposition of tiny metal particles on the photocatalyst surfaces that act as electron receptors or supporting of the photocatalysts on substrates as a means for increasing adsorption and photoreaction rates (Wachs, 1996). In this work, to enhance the photocatalytic activity of photocatalyst, the deposition of titania colloid particles on the surface of monodispersed silica microsphere was done by using a simple electrostatic attraction strategy.

Many studies have shown that heterogeneous photocatalytic oxidation processes can be used for removing coloring material from dye effluent. Zhang, *et al.*, (1998) demonstrated the TiO_2-assisted photodegradation of dye pollutants under illumination by visible light. Kiriakidou, *et al.*, (1999) reported the effect of operational parameters and TiO_2-doping on the photocatalytic degradation of Acid Orange 7 (AO7). Zhu, et al., (2000) studied the photocatalytic degradation of azo dyes by supported TiO_2 + UV in aqueous solution. Epling and Lin (2002) demonstrated the photoassisted bleaching of dyes utilizing TiO_2 and visible light. Daneshvar, *et al.*, (2003) studied the photocatalytic degradation of azo dye acid red 14 in water and investigated the effect of operational parameters. Xie and Yuan (2003)

reported the photocatalytic activity and recycle application of titanium dioxide sol for X-3B photodegradation. Qumar, *et al.*, (2005) reported the photocatalytic degradation of two selected dye derivatives, chromotrope 2B and amido black 10B, in aqueous suspensions of titanium dioxide.

1.3 Objectives

The objectives of this research is to improve photocatalytic activity of nanosized TiO_2 by grafting it on SiO_2 sphere core shell (TiO_2/SiO_2). The work comprises of;

(1) Nanosized TiO_2 grafted on SiO_2 sphere core shell (TiO_2/SiO_2) will be prepared by the sol-gel method. Pure TiO_2 and SiO_2 will also be synthesized.

(2) Samples obtained in (1) will be studied further for the photocatalytic activities using methylene blue as a model pollutant.

CHAPTER 2

EXPERIMENTAL

2.1 Synthesis of nano-anatase TiO_2 decorated on SiO_2 spherical core shells

2.1.1 Materials

(1) Acetic acid, CH_3COOH, A. R., Sigma-aldrich, U.S.A.

(2) Ammonium hydroxide (Ammonia solution) 28.0-30.0%, NH_4OH, A.R., J.T. Baker, U.S.A.

(3) Ethanol, CH_2CH_3OH, A.R., Sigma-aldrich, U.S.A.

(4) Methyltrimethoxysilane 98%, $C_4H_{12}O_3Si$ (MTMS), A.R., code no. 246174, Sigma-aldrich, U.S.A.

(5) Nitric acid, HNO_3, A.R., Sigma-aldrich, U.S.A.

(6) Titanium(IV) isopropoxide 99.999%, $Ti[OCH(CH_3)_2]_4$ (TTIP), A.R., code no. 377996, Sigma-aldrich, U.S.A.

2.1.2 Methods

2.1.2.1 Catalysts preparation

(a) Preparation of TiO_2 sols

TiO_2 sols were prepared according to the method previously reported (Qi, *et al.*, 2007). Titanium tetraisopropoxide (TTIP, Aldrich, 99.99%) 5 mL, was added dropwise into 100 mL acidic ethanol solution containing 1 mL nitric acid and 10 mL acetic acid under vigorous stirring. Then the mixture was heated at 60°C

while stirring for 20 h. In addition, pure TiO_2 was synthesized by this method and the titania powder was obtained by filtration and was calcined in air at 500 °C for 3 h.

(b) Preparation of SiO_2 spheres

Silica spherical core-shell structure with particle size around 400 nm was prepared as follows. Adding 2.5 mL of methyl-trimethoxysilane (MTMS, Sigma 98%) into 100 mL of 1 x 10^{-4} M nitric acid aqueous solution that was heated to 60°C while vigorous stirring was maintained. Then 2.5 mL ammonia was added to the solution. A milky silica solution was attained. SiO_2 powder was extracted by centrifuging the milky suspension of silica, and the supernatant removed.

(c) Synthesis of TiO_2 decorated on SiO_2 particles

The as-synthesized SiO_2 powder was added to different relative weight percentage of TiO_2 sols (30%, 50%, and 75% of TiO_2 on SiO_2). Then the mixture was dispersed in an ultrasonic bath for 15 min. The TiO_2/SiO_2 mixture was kept for 24 h to form TiO_2 grafted on SiO_2 spherical core-shell structure. The formation mechanism of TiO_2 grafted on SiO_2 sphere was shown in Scheme 1. The suspension mixture then was filtered and calcined in air at 500°C for 3 h. Different amounts of titania decorated on SiO_2 sphere formed different grafted patterns related to spacing and clumping of TiO_2 particles on SiO_2 surface.

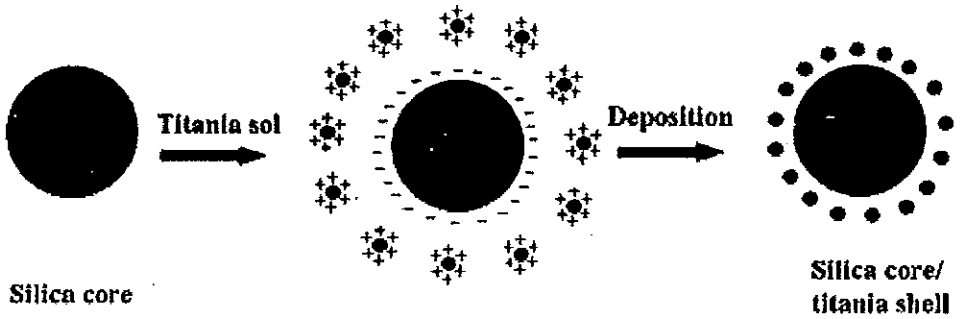

Scheme 1. The formation mechanism of TiO_2 grafted on SiO_2 sphere (Qi, *et al.*, 2007).

2.1.2.2 Products characterization

The crystal structure of pure TiO_2, SiO_2, and TiO_2/SiO_2 powder were analyzed by X-ray diffraction (XRD). XRD study was made on a Rigaku D-Max X-ray powder diffractometer (Rigaku Corporation, Tokyo, Japan) with Ni-filtered CuKα (0.15418 nm) radiation at 45 kV and 20 mA. The crystallite size was calculated by using the Scherrer's formula,

$$L = \frac{K\lambda}{\beta_{hkl}\cos\theta}, \qquad (1)$$

where L is the average crystallite size in nm, K is a constant usually taken as 0.9, λ is the wavelength of the X-ray radiation (using CuK_α = 0.154056 nm), β_{hkl} is the line width at half-maximum height in radians, and θ is the diffracting angle (Zielińska, *et al.*, 2001; Sivalingam, *et al.*, 2003).

The Brunauer-Emmett-Teller (BET) surface area of all powders were determined using Coulter, model SA3100. The infrared spectra were investigated by a Bruker EQUINOX 55, in the range 4000-400 cm^{-1}.

The composition of the powder was determined by X-ray photoelectron spectroscopy (XPS). XPS measurements were performed on a Physical Electronics PHI 5400 X-ray Photoelectron Spectrometer (Perkin-Elmer Corporation, Eden Prairie, MN) with an Mg K anode (1253.6 eV photon energy, 15 kV, 300 W) at a take-off angle of 45°. Multiplex XPS spectra of O 1s, Ti 2p, Si 2p were recorded using a band-pass energy of 178.95 eV corresponding to an energy resolution of 1.0 eV. The atomic concentrations of these elements were obtained by comparing the peak areas of their spectra.

The morphology of the powder was investigated by scanning electron microscopy (SEM) and transmission electron microscopy (TEM). A SEM sample was made by applying powder sample on the a conductive carbon tape, the sample was sputtered with gold for 25 s (Emitech K575 Sputter Coater, Emitech Ltd.,

Ashford, U.K.) before imaging. The SEM image was performed on a Hitachi S-4700 scanning electron microscope (Hitachi Ltd., Tokyo, Japan). A TEM sample was made by dispersing a thin film of powder sample on a Cu grid. The TEM observation was performed on a JEOL 2010LaB6 transmission electron microscope (JEOL Ltd., Tokyo, Japan) operated at 200 kV, with a point-to-point resolution of 0.28 nm.

2.2 Photocatalytic study

2.2.1 Materials

(1) Methylene blue, $C_{16}H_{18}N_3ClS_2.2H_2O$; Laboratory Reagent, UNILAB, Australia.

2.2.2 Procedures

Photodegradation of methylene blue

In order to quantify the effectiveness of a photocatalyst for water decontamination and also to explore techniques to increase photoefficiency, it is necessary to come up with methodologies to quantify the photochemical and photoelectrical properties of photocatalysts. Usually, photocatalyst decontamination performance is evaluated by quantifying the photochemical degradation rate for either an actual pollutant or a model pollutant such as a dye with a specific absorption peak in the visible region, e.g. methylene blue. The photoreactions were carried out by shining UV light on a slurry of the photocatalyst powder and measuring the degradation rate of the pollutant. The limitation of such a system lies in the difficulty of quantifying transport of light and the reactants and products to and from the surface of the photocatalysts. The actual amount of light that reaches each individual photocatalyst particle is hard to quantify given the scattering of UV off the photocatalyst powder particles and absorption by the water and the pollutant in them.

Similarly, the reactive-diffusion of pollutants and products is hard to quantify given the lack of knowledge of light intensity at the particle and also the distribution of the particles in the slurry. Given this limitation in correctly quantifying transport properties, accurately comparing photocatalysts that are different from each other in particle size and optical (scattering) characteristics is not possible. In this work, we used a fixed bed reactor in order to be able to compare photocatalysts undergoing the same photon flux and attenuation within the fixed bed, instead of having large variations in flux that occurs with slurry. The fixed bed makes it possible to maintain similar light and species transport conditions across samples thus enabling more direct comparison in photocatalytic activity.

A schematic of the experimental system is shown in Fig. 29. A packed bed of ~1-2 mm of the photocatalyst is spread on top of a nanoporous filter and an aqueous solution of the target pollutant is circulated through this bed. The light source used was a 254 nm UV lamp.

The initial concentration of the methylene blue was 10^{-7} M. The aqueous solution of the organic molecules was re-circulated through the photocatalyst bed using a peristaltic pump. Prior to illumination using UV light, the aqueous solutions were circulated through the samples for at least 2 hours in the dark. This dark adsorption helps to differentiate between the photodegradation and the adsorption of the pollutant onto the samples. Subsequent to irradiation by UV light, samples were collected once every 10 minutes and the concentration of the methylene blue was determined using a Cary 5G UV-Vis spectrometer. The 660 nm methylene blue peak along with Beer Lambert's law was used to quantify the methylene blue concentration.

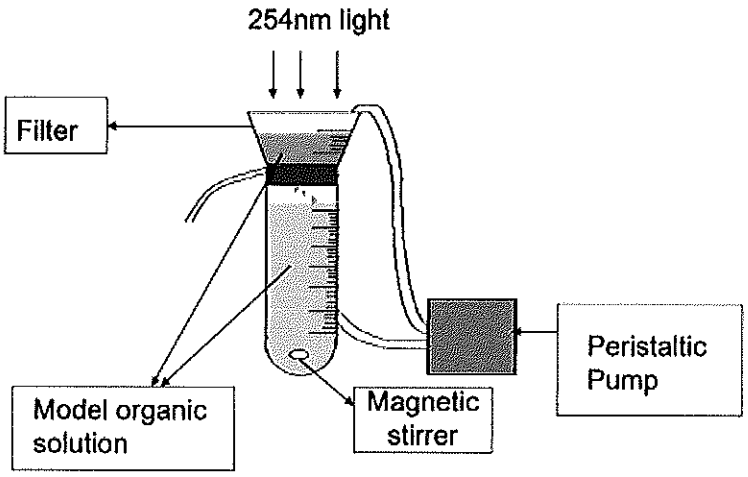

Figure 29. Experimental setup to measure photochemical degradation of methylene blue (Chandrasekharan, 2008).

CHAPTER 3

RESULTS AND DISCUSSION

3.1 Synthesis of nano-anatase TiO_2 decorated on SiO_2 spherical core shells

Pure TiO_2, SiO_2 and TiO_2 decorated on SiO_2 (TiO_2/SiO_2) powders were prepared by a sol-gel method and simple electrostatic attraction. The physical properties of all synthesized powders were investigated as follows.

3.1.1 Physical properties of the synthesized powders

3.1.1.1 X-ray powder diffractometry (XRD) and BET surface area

The X-ray diffraction patterns of SiO_2, TiO_2, and nanosized TiO_2/SiO_2 (with varying weight percentage of TiO_2; 30, 50, and 75% of TiO_2 on SiO_2) samples are illustrated in Fig. 30. All were calcinated under the same condition in air at 500 °C for 3 h. TiO_2 and nanosized TiO_2/SiO_2 showed a clear anatase-type crystal structure. The sharp peaks and strong intensity indicated that crystallization was present, and the higher the percentage of TiO_2 gave higher intensity of peaks. The peak associated with SiO_2 show that it is an amorphous form of silica. The crystallite size of titania and TiO_2/SiO_2 are listed in Table 8.

Table 8. The crystallite size and BET surface area of TiO_2, SiO_2, and TiO_2 grafted on SiO_2.

Catalysts	Phase	Crystallite size (nm)	BET surface area (m^2/g)
100% SiO_2	Amorphous	-	11.57
30% TiO_2/SiO_2	Anatase	6.8	367.58
50% TiO_2/SiO_2	Anatase	6.0	211.87
75% TiO_2/SiO_2	Anatase	8.5	148.47
100% TiO_2	Anatase	16.2	54.401

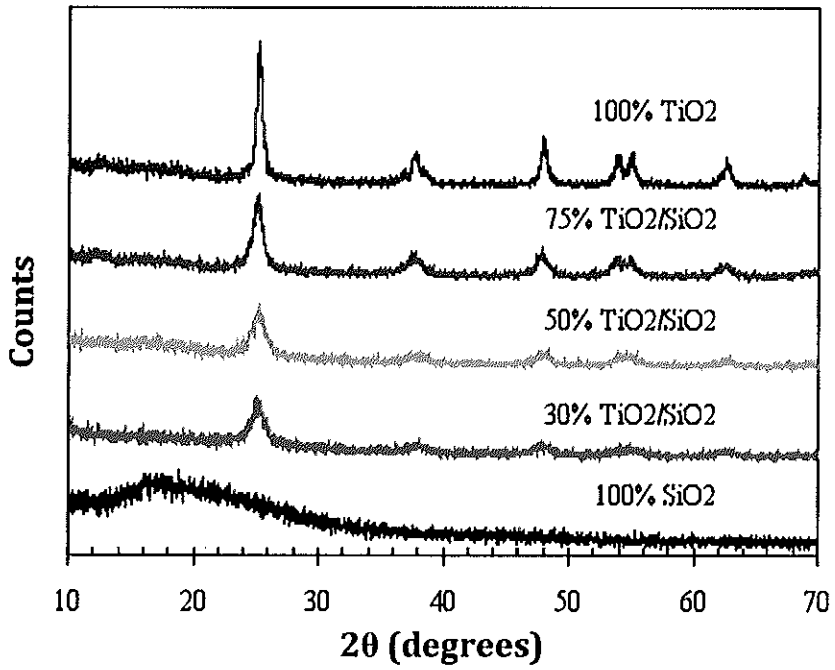

Figure 30. X-ray diffraction patterns of TiO_2, SiO_2, and TiO_2/SiO_2, (with various relative weight percent of TiO_2 on SiO_2) obtained by calcinating powder samples in air for 3 h at 500°C.

The crystallite sizes of the samples were calculated using the peak at $2\theta = 25.4^{\circ}$ for anatase TiO_2. From the crystallite size and BET surface area data in Table 8, it appears that the amount of SiO_2 sphere has an effect on the crystallite size of grafted nanosized TiO_2, with higher amount of SiO_2 resulting in smaller crystallite size, and larger surface area of TiO_2 particles. This effect may be due to the SiO_2 limiting the agglomeration of TiO_2 particles.

The slightly anomalous order crystallite size of 50% TiO_2/SiO_2 (6.0 nm) and that of 30% TiO_2/SiO_2 (6.8 nm) was observed. This could come from the appropriate percentage of titania which disperse on SiO_2 sphere. If this small difference was not caused by the experiment inaccuracy, at this point, we would like to concluded that 50% TiO_2/SiO_2 is an optimum quantity of TiO_2 that could be spread onto SiO_2 sphere.

3.1.1.2 Fourier-transformed infrared spectrophotometry (FTIR)

In Fig. 31, the transmittance spectra of nanosized TiO_2 and TiO_2 grafted on SiO_2 sphere with various relative weight percent of TiO_2 are presented. The band centered near 3740 cm^{-1} which shows up in the case of pure SiO_2 and 75% TiO_2/SiO_2 has been assigned to silanols (single Si-OH groups and geminal $Si(OH)_2$ group) that are completely unassociated or very weakly associated sites. The feature near 3670 cm^{-1} is due to vicinal silanols that undergo mutual hydrogen bonding. The broad band centered near 3500 cm^{-1} has been assigned to sites that interact with residual physisorbed water (Bergna and Roberts, 2006). The band at 1630 cm^{-1} observed in all spectra are attributed to stretching mode of hydroxyl (Dutoit, *et al.*, 1995; Rubio, *et al.*, 1997). In pure SiO_2, the bands at 820 cm^{-1} and 1120 cm^{-1} are ascribed to the symmetric vibration of Si-O-Si and the asymmetric stretching vibration of Si-O-Si, respectively (Duran, *et al.*, 1986; Dutoit, *et al.*, 1995). In the nanosized TiO_2/SiO_2 samples, the peaks of Si-O-Si asymmetric stretching mode are splitted into 2 peaks (1140, 1040 cm^{-1}) when disorder of the structure is introduced (Gaskell and Johnson, 1976). The band at 940-960 cm^{-1} indicates the presence of Ti-O-Si, while the vibration Si-O-Si stretching are in the range 1050-1120 cm^{-1} (Jung,

et al., 2007). The spectrum of 75% TiO_2/SiO_2 sample observed was similar to pure TiO_2. Table 9 lists the assigned modes of the functional groups that are responsible for the vibration bands in Fig. 31.

Table 9. Assignment of the FT-IR bands of TiO_2, SiO_2 and TiO_2 grafted on SiO_2 samples (Fig. 31).

Samples	Wavenumber (cm^{-1})	Assignment	Functional groups /molecule	Literatures
b, e	3740	ν_{OH}	Silanol (Si-OH)	Dutoit, *et al.*, 1995
a-e	3500	ν_{OH} and ν_{NH}	H_2O and NH_4^+	Bergna and Robert, 2006
a-e	1630	δ_{OH}	OH groups	Dutoit, *et al.*, 1995 Rubio, *et al.*, 1997
b	820, 1120	$\nu_{Si\text{-}O\text{-}Si}$ $\nu_{Si\text{-}O\text{-}Si}$	Si-O-Si (sym.) Si-O-Si (asym.)	Duran, *et al.*, 1986 Dutoit, *et al.*, 1995
c, d, and e	1140,1040	$\nu_{Si\text{-}O\text{-}Si}$	Si-O-Si (asym.)	Gaskell and Johnson, 1976
c and d	940 - 960	$\nu_{Ti\text{-}O\text{-}Si}$	Ti-O-Si	Jung, *et al.*, 2007.
a	Below 800	$\nu_{Ti\text{-}O}$	Ti-O bond	Velasco, *et al.*, 1999

(a) pure TiO_2, (b) pure SiO_2, (c) 30% TiO_2/SiO_2, (d) 50% TiO_2/SiO_2, (e) 75% TiO_2

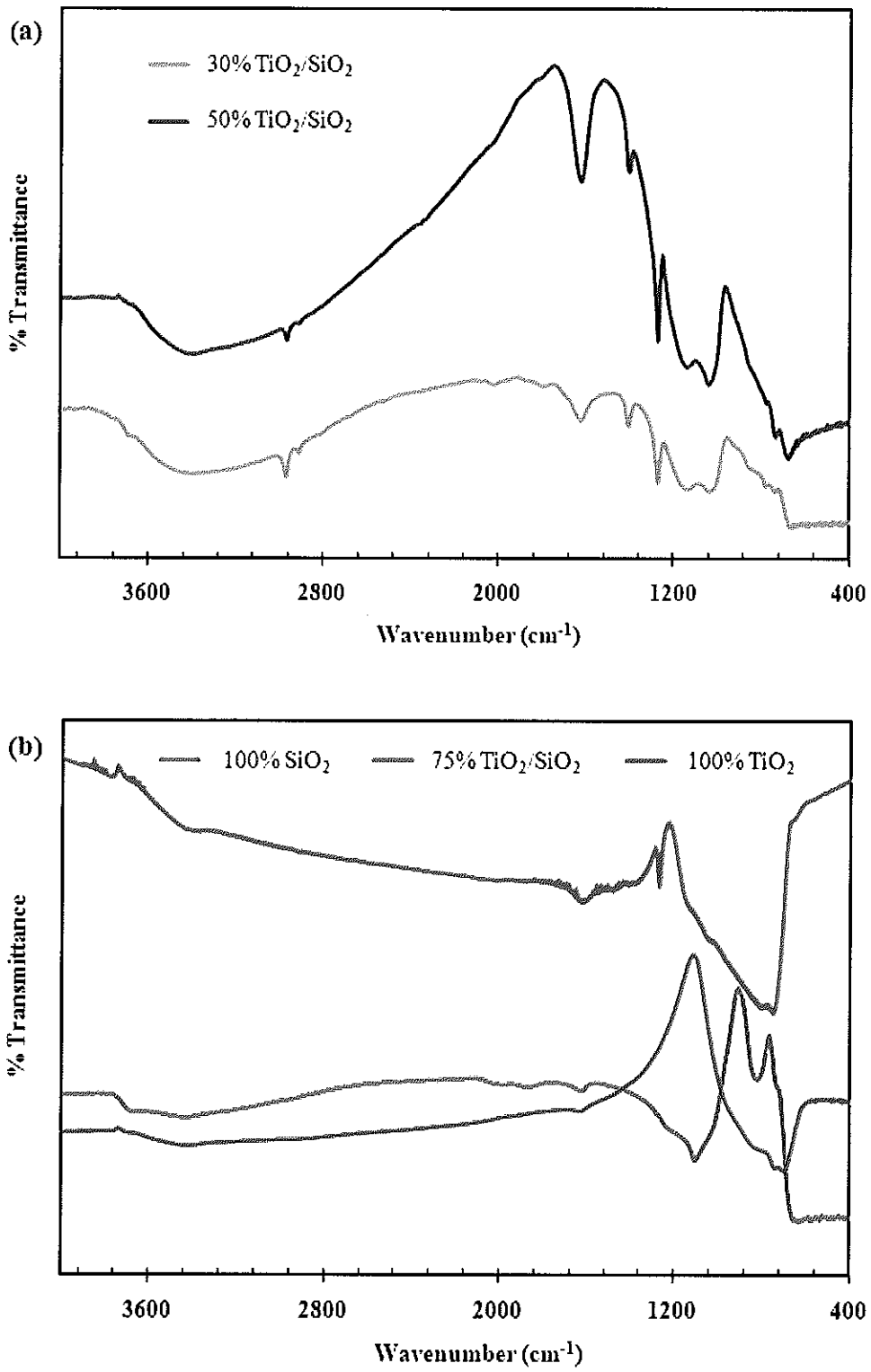

Figure 31. The FTIR spectra of as-synthesized TiO_2, SiO_2 and samples with different ratio of TiO_2/SiO_2; (a) 30% and 50% TiO_2/SiO_2 and (b) 75% TiO_2/SiO_2, 100% TiO_2, and 100% SiO_2.

3.1.1.3 Transmission electron microscopy (TEM)

Morphology and size of the silica and titania particles were examined using TEM. Fig. 32 shows the TEM images of calcined 30%, 50% and 75% of TiO_2 grafted on SiO_2 spheres. This result shows that the particle size of silica is about 100 times bigger than TiO_2 particles, the average particle size of the titania particles is around 3 nm while the SiO_2 sphere core shell averages around 350 nm. TiO_2 particles deposited on the surface of SiO_2 sphere only partially, without complete coverage (Fig. 32a). On a closer inspection, TiO_2 particles agglomeration can be seen in Fig. 32b, while in Fig. 32c, with the highest percentage of TiO_2, deposition of particles became denser leading to higher order of crystallinity as evidenced by the smoother surface on the TiO_2.

The intensities of XRD peaks varied directly with the increasing amount of TiO_2 deposited on SiO_2 sphere. It is interesting to note that the specific surface area decreased as the percentage of TiO_2 increased. As TEM results show that the complete coverage of SiO_2 sphere was not observed (Fig. 32a). The result for this could be that as the amount of TiO_2 increases, it selectively deposits on the TiO_2 already present. Furthermore, at 75% TiO_2 the deposited chunk of TiO_2 became more crystalline (as mentioned above) resulting in lower surface area and also slightly larger crystallite size (Table 8).

(a) 30% TiO_2/SiO_2

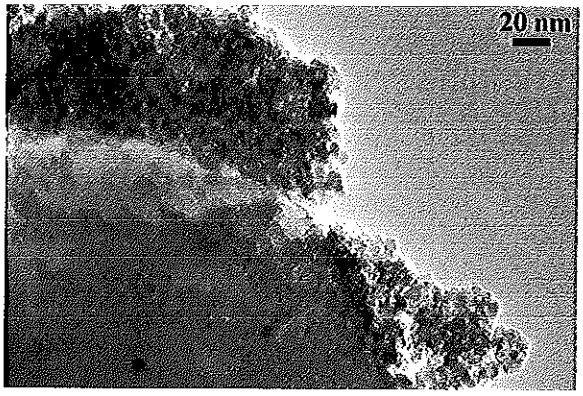

(b) 50% TiO_2/SiO_2

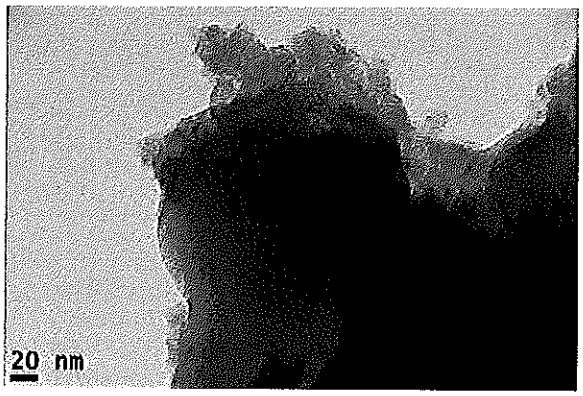

(c) 75% TiO_2/SiO_2

Figure 32. TEM images for nanosized (a) 30%, (b) 50%, and (c) 75% of TiO_2 on SiO_2 sphere core shell.

3.1.1.4 X-ray photoelectron spectrosocopy (XPS)

The wide XPS spectra of the as-prepared TiO_2/SiO_2, TiO_2, and SiO_2 samples are illustrated in Fig. 33. Si(2p), Ti(2p) and O(1s) photoelectron peaks of nanosized TiO_2 grafted on SiO_2 sphere annealed at 500°C for 3 h are presented in Fig. 34. The surface atomic concentration of the powders was also calculated as listed in Table 9. The binding energy (BE) of Si(2p) peak was at 108.9 eV for pure SiO_2 sphere. The BE of Si(2p) are shifted towards lower values as the amount of TiO_2 increased in the grafting. The BE of the $Ti(2p_{3/2})$ for the pure TiO_2 was 460.7 eV, which shifted upwards as increasing the amount of SiO_2. The major O(1s) peak was at 531.9 eV and 538.4 eV for the pure TiO_2 and pure SiO_2, respectively. Both peaks are shown in TiO_2 grafted on SiO_2. The intensity of O(1s) peak, which belongs to SiO_2 decreased with increasing the percentage of TiO_2 grafted on SiO_2 as expected.

Table 10. Calculated surface atomic concentration of synthesized TiO_2/SiO_2, TiO_2, and SiO_2.

Sample	Surface atomic concentration (%)		
	O1s	Ti2p	Si2p
100% SiO_2	60.7	-	27.8
30% TiO_2/SiO_2	51.7	6.8	17.9
50% TiO_2/SiO_2	60.5	13.4	12.0
75% TiO_2/SiO_2	58.3	17.6	4.6
100% TiO_2	55.6	21.0	-

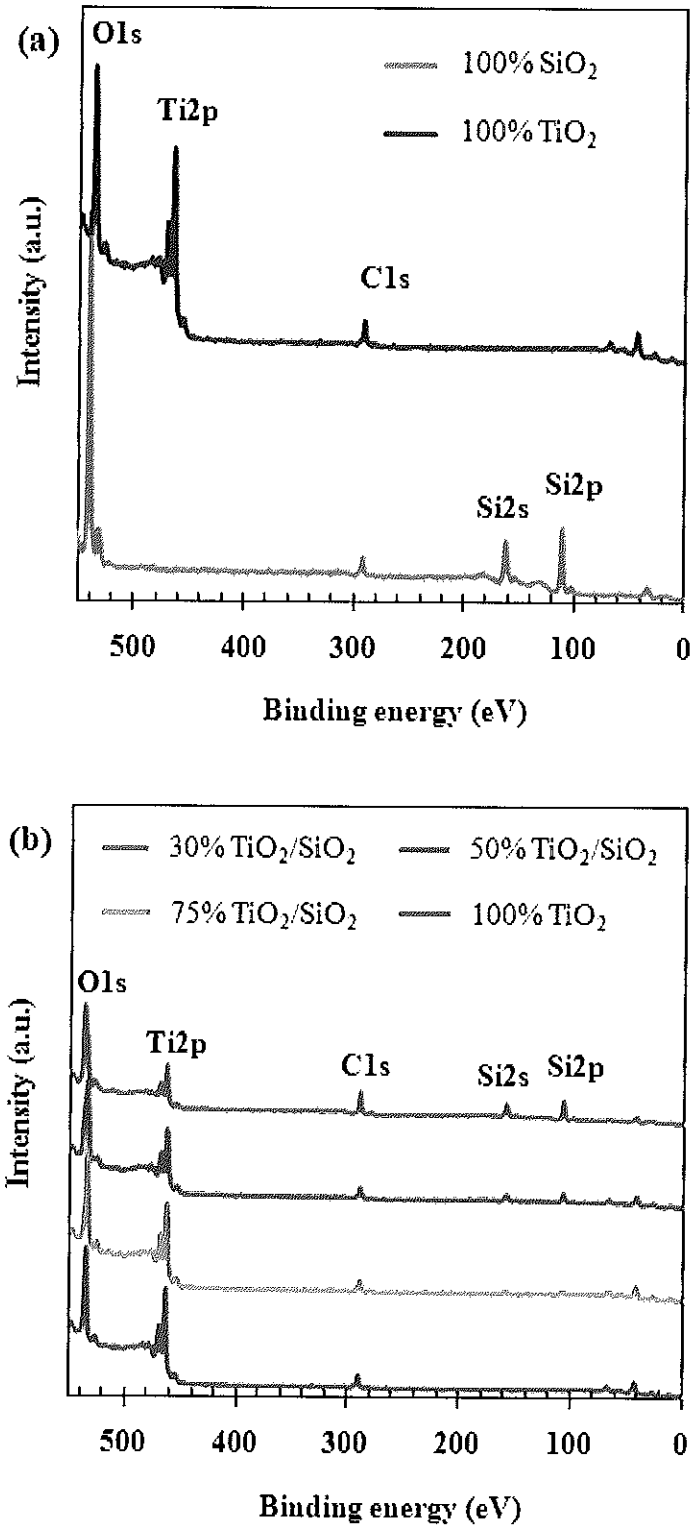

Figure 33. Wide XPS spectra of: (a) pure TiO_2 and SiO_2, (b) pure TiO_2 and nanosized TiO_2 grafted on SiO_2 sphere.

Atmospheric contaminants are indirectly confirmed by the presence of typical carbon contaminant peak C 1s at 285 eV in binding energy scale that was observed for all sample (see Fig. 33). In addition, this typical carbon contaminant peak was also considered to be the organic residuals of the gel, which could be confirmed by DTA/TG analysis (Andrulevicius, *et al.*, 2008).

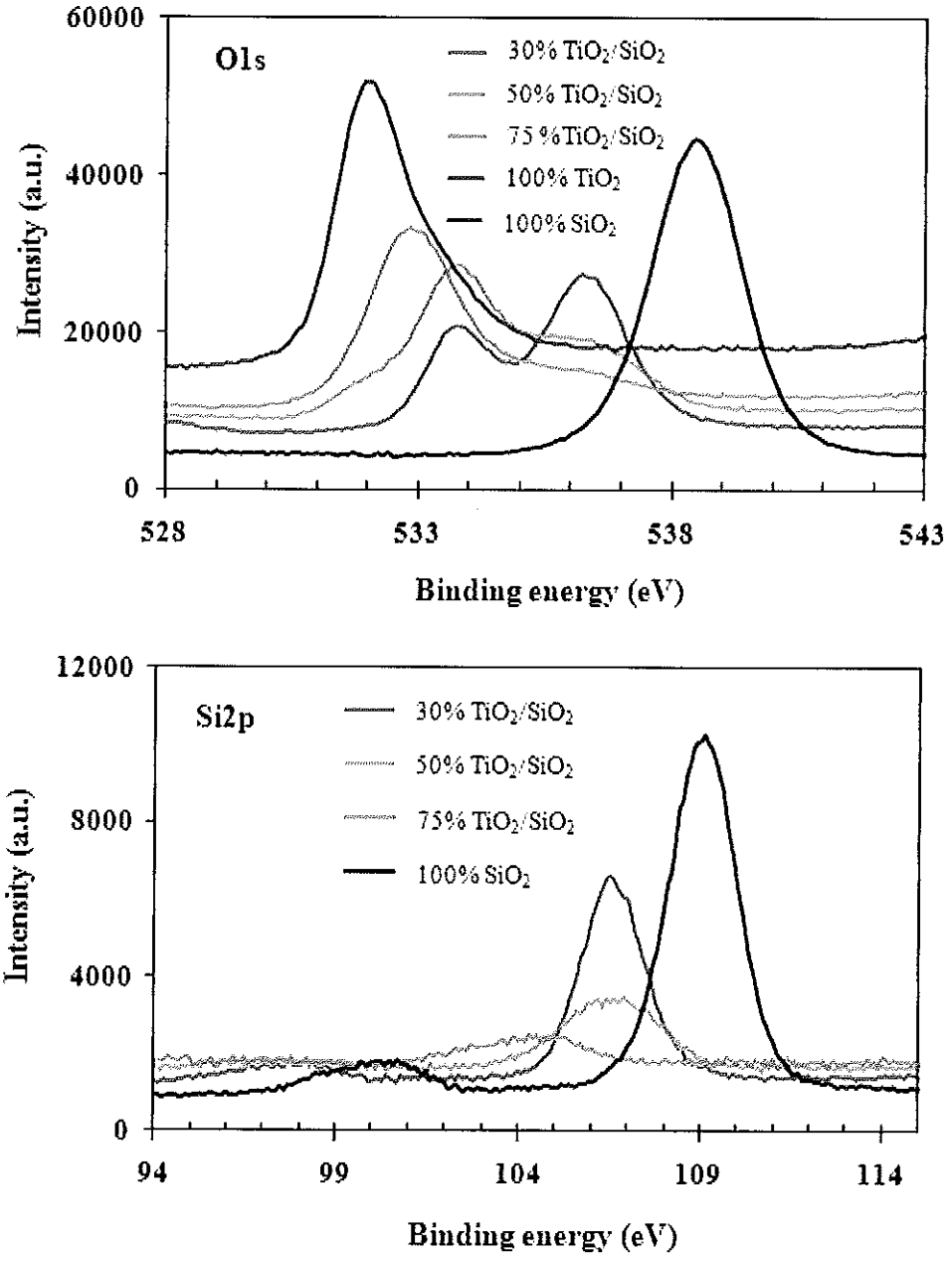

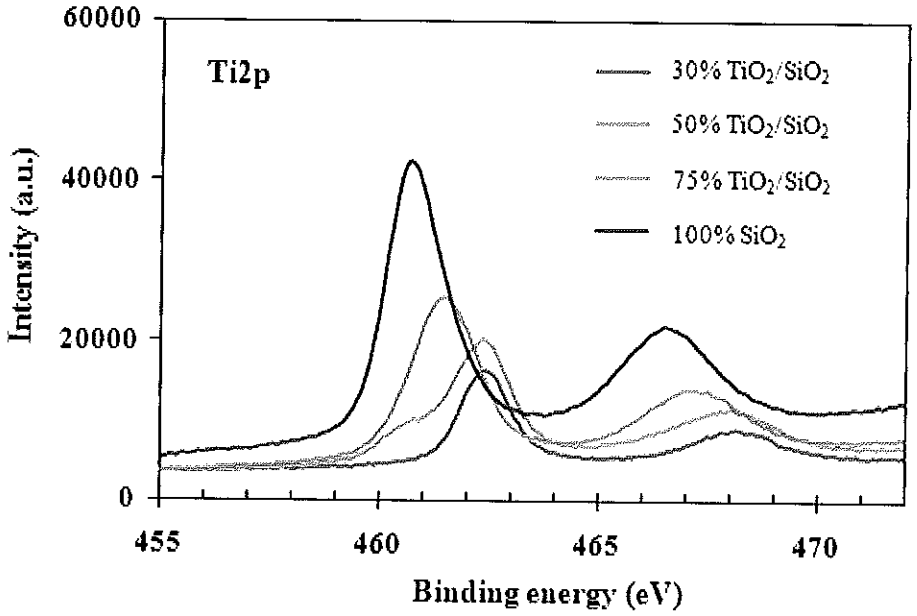

Figure 34. X-ray photoelectron spectroscopy multiplex high-resolution scans over O(1s), Si(2p), and Ti($2p_{3/2}$) spectra regions of nanosized TiO_2 grafted on SiO_2 sphere.

The trends of BE shift observed above support the incorporation of TiO_2 into the bulk of SiO_2 by the grafting method. Starting with pure SiO_2, when TiO_2 was introduced the formation of Si-O-Ti took place as evidenced by the BE shift. Ti has lower electronegativity than Si (and likewise for Ti(IV) to Si(IV)). By forming such bridge Si becomes more electron rich hence its BE shifting to lower energy while Ti becomes more positive with its BE shifting to higher energy. This effect passes on to oxygen atoms as we can see BE of Ti-linked oxygens shift to higher energy and Si-linked oxygens shift to lower energy. The intensities of these XPS peaks also reflect the percentages of TiO_2 grafted into SiO_2.

3.2 Photocatalytic study

3.2.1 Effect of TiO_2/SiO_2 ratio on photocatalytic decolorization of methylene blue

The photocatalytic oxidation of as-prepared pure TiO_2 and decorated TiO_2/SiO_2 are shown in Fig. 35 as percentage of decolorization of methylene blue by nanoparticle TiO_2 and decorated TiO_2/SiO_2 samples. The concentration of methylene blue decreased exponentially with irradiation time and the highest decolorization of methylene blue belongs to 50% TiO_2/SiO_2. The kinetics of this reaction can be approximated as a first-order process, and the rate constants can be used to compare the relative efficiency of the different materials under essentially identical conditions. The rate constants of the products were obtained from the plots of $\ln(A_0/A)$ versus time – example of the plot is shown in the appendix A. Rate constants obtained from these data as a function of percent TiO_2/SiO_2 is shown in Fig. 36. The methylene blue in the absence of semiconductor particles or pure SiO_2 shows negligible photodecomposition. The results show that the rate of decomposition of methylene blue depends on the TiO_2/SiO_2 ratio and was largest at 50% TiO_2/SiO_2 which showed an activity about 6 times higher than that of pure TiO_2. The result for this could be due to the high surface area of photocatalyst and the small crystallite size of TiO_2 decorated on SiO_2 sphere. Nevertheless, the appropriate percentage of TiO_2 dispersed on SiO_2 sphere is also a marked factor for the good performance of photocatalyst as the result of 50% TiO_2/SiO_2 above.

The enhanced photocatalytic activity of the TiO_2/SiO_2 composite might be attributed to the unique physicochemical properties of TiO_2/SiO_2 nanocomposites which result from the strong interaction of TiO_2 and SiO_2 particles at molecular level, such as the increased specific surface area of TiO_2/SiO_2 nanocomposites (Hong, *et al.*, 2003; Shibata, *et al.*, 2006; Yu, *et al.*, 2006; Zhou, *et al.*, 2006). The increase in specific surface area facilitates more effective adsorption sites which might promote the photocatalytic activity by increasing the concentration of contaminants and

reaction intermediates near the TiO_2 (Anderson and Bard, 1995; Kim, *et al.*, 2005; Arai, *et al.*, 2006).

The increasing in reactivity can partly be attributed to an increased surface area, and also the beneficial effect of SiO_2, which indicates no photoactivity, but is probably relates to the preferential adsorption of R-6G on SiO_2. The preferential adsorption effectively increases the surface concentration of R-6G at or near the TiO_2 sites promoting more efficient oxidation by photogenerated species (Anderson and Bard, 1995). Since methylene blue is cationic dye as R-6G, the results in photodecomposition of methylene blue by irradiated TiO_2/SiO_2 particle can be summarized in the same way.

In addition to the increased specific surface area of TiO_2/SiO_2 nanocomposites, mixed metal oxides often generate additional surface acidity over their individual members because of an increase in the polarizability of the hydroxide group present in the mixed oxide (Nakabayashi, 1992). The amine titration method is a means of determining surface acidity of metal oxides (Papp, *et al.*, 1994). Qi and his co-worker (2007) investigated the *N-butylamine* titration method to confirm that the acidity of TiO_2/SiO_2 nanocomposite powders was stronger than that of pure TiO_2 powder. Many previous research works reported that the stronger acidity would contribute to the increase in the photocatalytic activity (Papp, *et al.*, 1994; Fu, *et al.*, 1996). In the TiO_2/SiO_2 nanocomposites, a complex oxide may form at the interfaces due to the existence of Ti-O-Si vibration in the IR spectrum detected in previous works (Liu and Davis, 1994; Seok and Kim, 2004). Ti-O-Si bonds enhance surface acidity of the TiO_2/SiO_2 nanocomposites and in turn improve the photocatalytic activity of the TiO_2/SiO_2 nanocomposites fabricated in this study. Although, *N-butylamine* titration method was not used to confirm the acidity of TiO_2/SiO_2 nanocomposite powders in this work, but the method to characterize the physical properties of all powders (FTIR, BET, TEM and XPS) and the study of photodecolorization of methylene blue give significant details to prove that a mixed oxide TiO_2/SiO_2 is a more efficient photocatalyst for the degradation of methylene blue than TiO_2 alone.

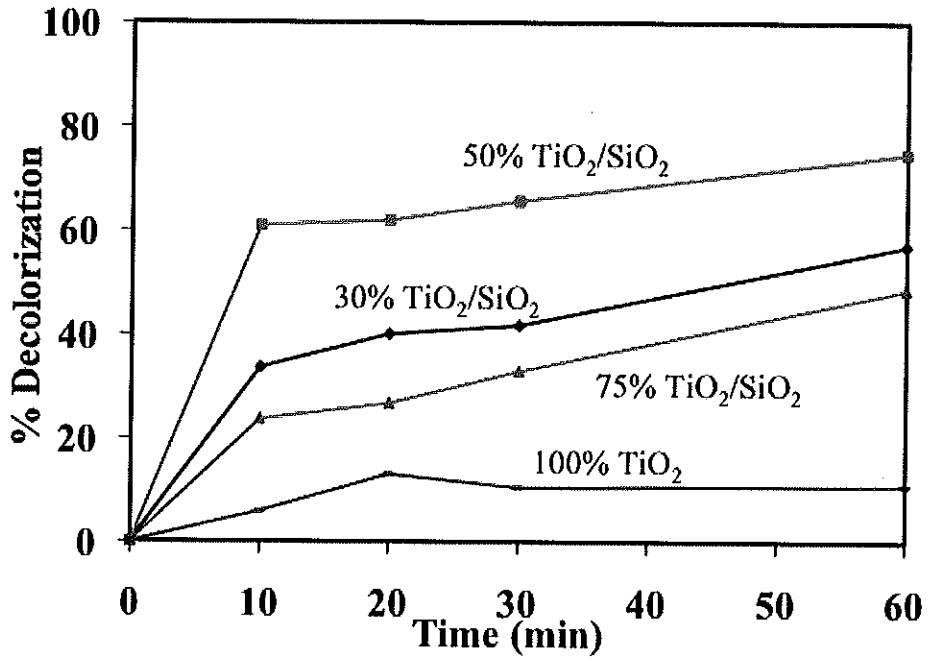

Figure 35. Decolorization of methylene blue solution with different ratio of nanoparticle TiO_2 decorated on SiO_2 sphere.

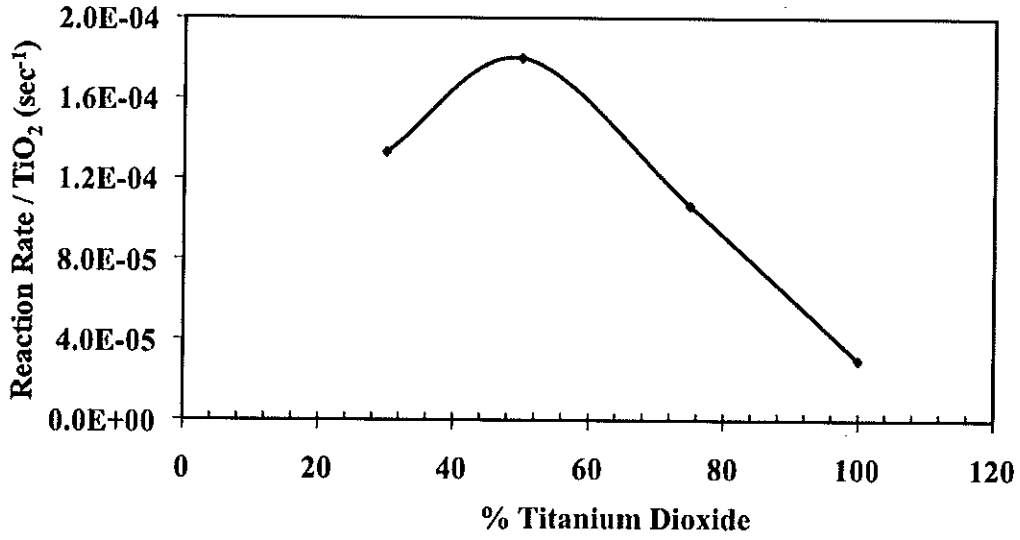

Figure 36. The reaction rate per titanium dioxide belongs to different ratio of nanoparticle TiO_2 decorated on SiO_2 sphere.

In this work, the controlled decoration or grafting of photoactive TiO_2 semiconductor on SiO_2 microsphere was explored as a means to increase photoefficiency. SiO_2 was chosen as the supporting oxide because it is inexpensive and the previous work (Qi, *et al.*, 2007) suggests that the Lewis acidity of the SiO_2 helps increase the photoreaction rates. Furthermore, there is evidence to suggest that the electronic binding energies of the overlying oxide is affected by the underlying SiO_2 and hence opens up the possibility of tuning the position of the valence and/or the conduction band of the TiO_2 (Guiu and Grange, 1995; Lassaletta, *et al.*, 1995; Wachs, 1996), to better match the absolute values of the redox couple of the compound being decomposed in water.

3.2.2 Photocatalytic degradation pathway of methylene blue from literatures

Houas, *et al.*, (2001) studied the TiO_2/UV photocatalytic degradation of methylene blue in aqueous heterogeneous suspensions. A detailed reaction mechanism was presented from the initial step of adsorption involving the cationic functional group of methylene blue molecule, which was probably adsorbed perpendicularly to the surface down to the final products (CO_2, SO_4^{2-}, NH_4^+, and NO_3^-). The degradation intermediates originated from the initial opening of the central aromatic ring and their subsequent metabolites were formed in agreement with general rules already put in evidence in the degradation of other complex molecules in water. It can be concluded that photocatalysis can decontaminate colored used waters. Photocatalysis appears as the only sub-discipline of heterogeneous catalysis, which is able to convert organic pollutants to CO_2 in water without heating nor using high pressure of oxygen nor requiring chemical reactants or additives.

The main aromatic metabolites resulting from methylene blue decomposition are presented in Scheme 2, where they are logically reported according to their decreasing molecular weight. The initial step of methylene blue degradation can be ascribed to the cleavage of the bonds of the $C\text{-}S^+\text{=}C$ functional group in methylene blue. The electrophilic attack of $^\bullet OH$ concerned the free doublet of

heteroatom S, making its oxidation degree pass from -2 to 0. However, the passage from C-S^{+}=C to C-S(=O)-C requires the conservation of double bond conjugation, which induces the opening of the central aromatic ring containing both heteroatoms, S and N. The origin of H atoms necessary to C-H and N-H bond formation can be proposed from the proton reduction by photogenerated electrons as already observed in alcohol dehydrogenation and pesticide degradation. An alternative rearrangement of the phenothiazine structure is presented in Scheme 3. The sulfoxide group can undergo a second attack by an $^{\bullet}$OH radical producing the sulfone (non-detected) and causing the definitive dissociation of the two benzenic rings.

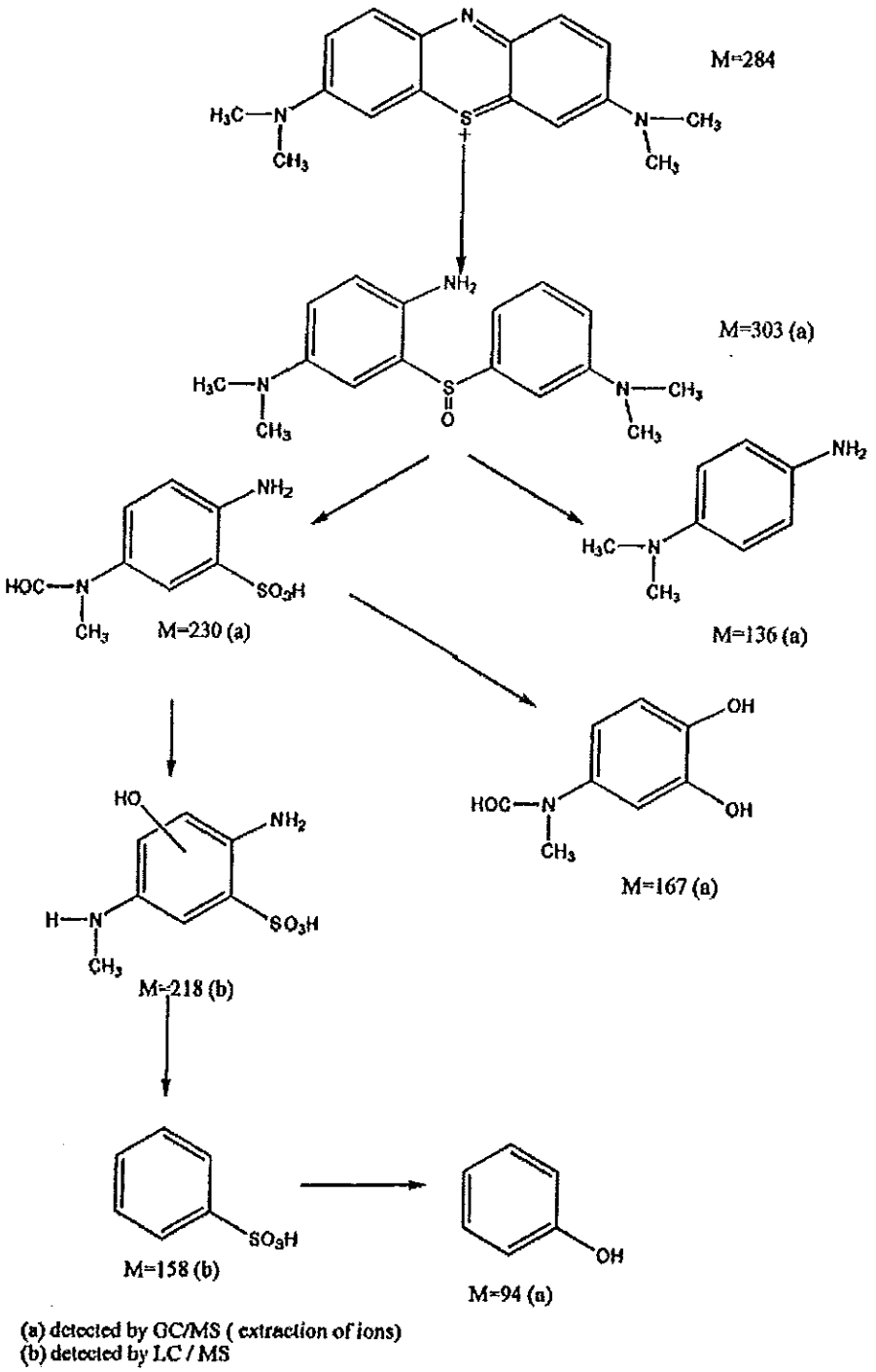

Scheme 2. Photocatalytic degradation pathway of methylene blue (Houas, *et al.*, 2001).

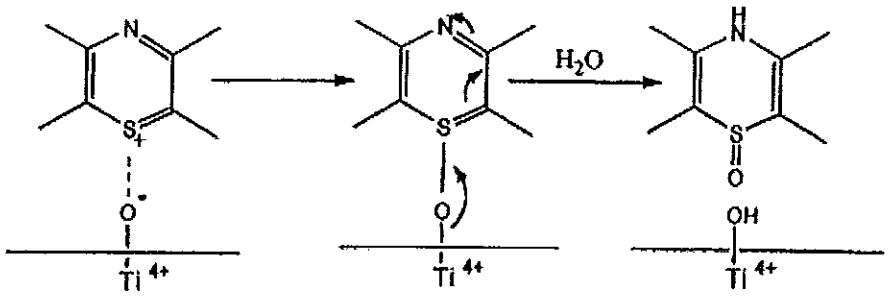

Scheme 3. Electronic reorganization during the passage of adsorbed methylene blue to the sulfoxide form (Houas, *et al.*, 2001).

CHAPTER 4

CONCLUSIONS

The nanosized TiO_2 decorated on SiO_2 sphere was prepared by a low temperature sol-gel process and simple electrostatic attraction strategy. The major phase of the pure TiO_2 particle and deposited TiO_2 on SiO_2 sphere are of the anatase structure. The XRD, BET, FTIR, TEM and XPS method were used to characterize the physical properties of all powders. The results show that the higher amount of SiO_2 resulting in smaller crystallite size and larger surface area of TiO_2 particles.

In photodecomposition, a fixed bed reactor was used to study the degradation of methylene blue by TiO_2/SiO_2 and pure TiO_2 particles. A mixed oxide TiO_2/SiO_2 is a more efficient photocatalyst for the degradation of methylene blue than TiO_2 alone. The decomposition rate of methylene blue of 50% TiO_2/SiO_2 is largest in this comparison. The result show that the appropriate percentage of TiO_2 dispersed on SiO_2 is also important factor for photodecolorization reaction. The presence of an adsorbent, SiO_2, can act to elevate the efficiency by increasing the quantity of methylene blue near the TiO_2 sites relative to the solution concentration of methylene blue.

In conclusion, the enhanced photoactivity can be related to the increased specific surface area, the small crystallite size, and the appropriate percentage of TiO_2 decorated onto SiO_2 sphere.

REFERENCES

Adams, L. K.; Lyon, D. Y. and Alvarez, P. J. J. 2006. "Comparative Eco-toxicity of Nanoscale TiO_2, SiO_2, and ZnO Water Suspensions." *Water Research* **40**, 3527-3532.

Akiba, N.; Hayakawa, I.; Keh, E. S. and Watanabe, A. 2005. "Antifungal Effects of a Tissue Conditioner Coating Agent with TiO_2 Photocatalyst." *J. Med. Dent. Sci.* **52**, 223-227.

Amézaga-Madrid, P.; Nevárez-Moorillón, G. V.; Orrantia-Borunda, E. and Miki-Yoshida, M. 2002. "Photoinduced Bactericidal Activity against *Pseudomonas aeruginosa* by TiO_2 Based Thin Films." *FEMS. Microbiol. Lett.* **211**, 183-188.

Amézaga-Madrid, P.; Silveyra-Morales, R.; Córdoba-Fierro, L.; Nevárez-Moorillón, G. V.; Miki-Yoshida, M.; Orrantia-Borunda, E. and Solís, F. J. 2003. "TEM Evidence of Ultrastructural Alteration on *Pseudomonas aeruginosa* by Photocaalytic TiO_2 Thin Films." *J. Photochem. Photobiol. B: Biol.* **70**, 45-50.

Anderson, C and Bard, A. J. 1995. "An Improved Photocatalyst of TiO_2/SiO_2 Prepared by a Sol-Gel Synthesis." *J. Phys. Chem.* **99**, 9882-9885.

Andrulevicius, M.; Tamulevicius, S.; Gnatyuk, Y.; Vityuk, N.; Smirnova, N. and Eremenko, A. 2008. "XPS Investigation of $TiO_2/ZrO_2/SiO_2$ Films Modified with Ag/Au Nanoparticles." *Mater. Sci.* **14**, 8-14.

Anpo, M. and Takeuchi, M. 2003. "The Design and Development of Highly Reactive Titanium Dioxide Photocatalysts Operating under Visible Light Irradiation." *J. Catal.* **216**, 505-516.

Approved standard M7-A4. 2002. Reference methods for dilution antimicrobial susceptibility tests for bacteria that grow aerobically, Clinical and Laboratory Standards Institute (CLSI), Wayne, PA, USA.

Arai, Y.; Tanaka, K. and Khlaifat, A. L. 2006. "Photocatalysis of SiO_2-loaded TiO_2." *J. Mol. Catal. A: Chem.* **243**, 85-88.

Asahara, T.; Koseki, H.; Tsurumoto, T.; Shiraishi, K.; Shindo, H.; Baba, K.; Taoda, H. and Terasaki, N. 2009. "The Bactericidal Efficacy of a Photocatalytic TiO_2 Particle Mixture with Oxidizer against *Staphylococcus aureus*." *Jpn. J. Infect. Dis.* **62**, 378-380.

Awati, P. S.; Awate, S. V.; Shah, P. P. and Ramaswamy, V. 2003. "Photocatalytic Decomposition of Methylene Blue Using Nanocrystalline Anatase Titania Prepared by Ultrasonic Technique." *Catal. Commun.***4**, 393-400.

Balch, A. and Smith, R. 1994. "*Pseudomonas Aeruginosa*: Infections and Treatment." *Informa Health Care.* pp. 83-84.

Baolong, Z.; Baishun, C.; Keyu, S.; Shangjin, H.; Xiadong, L.; Zongjie, D. and Kelian, Y. 2003. "Preparation and Characterization of Nanocrystal Grain TiO_2 Porous Microspheres." *Appl. Catal. B.* **40**, 253-258.

Benabbou, A. K.; Derriche, Z.; Felix, C.; Lejeune, P. and Guillard, C. "Photocatalytic Inactivation of *Escherichia coli* Effect of Concentration of TiO_2 and Microorganism, Nature, and Intensity of UV Irradiation." *Appl. Catal. B: Environ.* **76**, 257-263.

Bently, R. and Meganathan R. 1982. "Biosynthesis of vitamin K (menaquinone) in bacteria." *Microbiol. Rev.* **46**, 241-280. PMID 6127606

Bergna, H. E. and Roberts, W. O. 2006. "Colloidal Silica: Fundamentals and Applications." CRS Press, pp.386; ISBN 0824709675.

Bicanic, T. and Harrison, T. S. 2004. "Cryptococcal meningitis." *Br. Med. Bull.* 72, 99-118.

Biofuelcell, Helsinki University of Technlogy, 2007.

Blake, D. M.; Maness, P.-C.; Huang, Z.; Wolfrmum, E. J. and Huang, J. 1999. "Application of the Photocatalytic Chemistry of Titanium Dioxide to Disinfection and the Killing of Cancer Cells." *Sep. Purif. Methods.* **28**, 1-50.

Bond, G. C. and Tahir, S. F. 1991. "Vanadium Oxide Monolayer Catalysts Preparation, Characterization and Catalytic Activity." *Appl. Catal.* **71**, 1-31.

Brinker, C. J. and Scherer, G. W. 1990. "Sol-Gel Science: The Physics and Chemistry of Sol-Gel Processing." New York, Academic Press. ISBN 0121349705

Brunet, F. and Cabane, B. 1993. "Populations of Oligomers in Sol-gel Condensation." *J. Non-Crystalline Solids.* **163**, 211-225.

Carp, O.; Huisman, C. L. and Reller, A. 2004. "Photoinduced Reactivity of Titanium Dioxide." *Progress in Solid State Chemistry.* **32**, 33-177.

Castillo, R.; Koch, B.; Ruiz, P. and Delmon, B. 1996. "Influence of the Amount of Titania on the Texture and Structure of Titania Supported on Silica." *J. Catal.* **161**, 524-529.

Chandler, R. R.; Bigham, S. R. and Coffer, J. L. 1993. "Spectroscopic Analysis of Semiconductor Colloids." *J. Chem. Edu.* **70**, A7-A10.

Chandrasekharan, R. 2008. "Study of Transport Properties of Ta_2O_5 for High Temperature Thermal Management and Photocatalytic Water Purification Systems." Ph.D. Dissertation, University of Illinois at Urbana-Champaign, IL, USA.

Chemat. 1998. Sol-Gel Technology. http://www.chemat.com/html/solgel.html Chemat Technology, Inc.

Cheng, C.-L.; Sun, D.-S.; Chu, W.-C.; Tseng, Y.-H.; Ho, H.-C.; Wang, J.-B.; Chung, P.-H.; Chen, J.-H.; Tsai, P.-J.; Lin, N.-T.; Yu, M.-S. and Chang, H.-H. 2009. "The Effect of the Bactericidal Interaction with Visible-Light Responsive Titania Photocatalyst on the Bactericidal Performance." *J. Biomed. Sci.* **16**, 7-16.

Cheng, P.; Zheng, M. P.; Jin, Y. P.; Huang, Q. and Gu, M. Y. 2003. "Preparation and Characterization of Silica-doped Titania Photocatalyst through Sol-gel Method." *Mater. Lett.* **57**, 2989-2994.

Cho. I.-H.; Moon, I.-Y.; Chung, M.-H.; Lee, H.-K. and Zoh, K.-D. 2002. "Disinfection Effects on *E. coli* Using TiO_2/UV and Solar Light System." *Water Supply.* **2**, 181-190.

Cho, M.; Chung, H.; Choi, W. and Yoon, J. 2005. "Different Inactivation Behaviors of MS-2 Phage and *Escherichia coli* in TiO_2 Photocatalytic Disinfection." *Appl. Environ. Microbiol.* **71**, 270-275.

Choychangtong, W. 2004. "Synthesis and Characterization of Titanium Dioxide." Master of Science Thesis, Prince of Songkla University, Thailand.

Christner, B.C.; Morris, C.E.; Foreman, C.M.; Cai, R. and Sands, D.C. 2008. "Ubiquity of biological ice nucleators in snowfall." *Science.* **319**, 1214.

Dadachova E.; Bryan, R. A.; Huang, X.; Moadel, T.; Schweitzer, A. D.; Aisen, P.; Nosanchuk, J. D. and Casadevall, A. 2007. "Ionizing Radiation Changes the Electronic Properties of Melanin and Enhances the Growth of Melanized Fungi." *PLoS One* **2**, e457. doi:10.1371/journal.pone.0000457. PMID 17520016.

Daneshvar, N.; Salari, D. and Khataee, A. R. 2003. "Photocatalytic Degradation of Azo Dye Acid Red 14 in Water: Investigation of the Effect of Operational Parameters." *J. Photochem. Photobiol. A: Chem.* **157**, 111-116.

Deo, G.; Turek, A. M.; Wachs, I. E. and Jacobs, P. A. 1993. "Characterization of Titania Silicalites." *Zeolytes.* **13**, 365-373.

Ding, X. –Z. and Liu, Z. –H. 1997. "Synthesis and Microstructure Control of Nanocrystalline Titania Powders via a Sol-Gel Process." *Mater. Sci. Eng. A* **224**, 210-215.

Djebbar, K. and Sehili, T. 1998. "Kinetics of Heterogeneous Photocatalytic Decomposition of 2,4-Dichlorophenoxyaceticacid over Titanium Dioxide and Zinc Oxide in Aqueous Solution." *Pestic. Sci.* **54**, 269-276.

Duran, A.; Serna, C.; Fornes, V. and Fernández-Navarro, J. M. 1986. "Structural Considerations about SiO_2 Glasses Prepared by Sol-gel." *J. Non-Cryst. Solids.* **82**, 69-77.

Dutoit, D. C. M.; Schneider, M. and Baiker, A. 1995. "Titania-Silica Mixed Oxides: I. Influence of Sol-gel and Drying Conditions on Structural Properties." *J. Catal.* **153**, 165-176.

Epling, G. A. and Lin, C. 2002. "Photoassisted Bleaching of Dyes Utilizing TiO_2 and Visible Light." *Chemosphere.* **46**, 561-570.

Feng, P.; Weagant, S. and Grant, M. 2002. "Enumeration of *Escherichia Coli* and the Coliform Bacteria." *Bacteriological Analytical Manual*, 8th ed., FDA/Center for Food Safety and Applied Nutrition.

Fox, M. A. and Dulay, M. T. 1993. "Heterogeneous Photocatalysis" *Chem. Rev.* **93**, 341- 357.

Freuze, I.; Brosillon, S.; Laplanche, A.; Tozza, D. and Cavard, J. 2005. "Effect of Chlorination on the Formation of Odorous Disinfection By-Products." *Water Res.* **39**, 2636-2642.

Fu, X. A. and Qutubuddin, S. 2001. "Synthesis of Titania-coated Silica Nanoparticles Using Ono-ionic Water-in-oil." *Colloids Surf. A: Physicochemical and Engineering Aspects.* **178**, 151-156.

Fu, X. Z.; Clark, L. A.; Yang, Q. and Anderson, M. A. 1996. "Enhanced Photocatalytic Performance of Titania-Based Binary Metal Oxides: TiO_2/SiO_2 and TiO_2/ZrO_2." *Environ. Sci. Technol.* **30**, 647-653.

Fujishima, A.; Hashimoto, K. and Watanabe, T. 1999. "TiO_2 Photocatalysis Fundamentals and Applications." Tokyo, Japan : BKC Inc.

Fujishima, A.; Rao, T. N. and Tryk, D. A. 2000. "Titanium Dioxide Photocatalysis." *J. Photochem. Photobiol.* C: *Photochem. Rev.* **1**, 1-21

Gaskell, P. H. and Johnson, D. W. 1976. "The Optical Constants of Quartz, Vitreous Silica and Neutron-Irradiated Vitreous Silica: (II) Analysis of the Infrared Spectrum of Viterous Silica." *J. Non-Cryst. Solids.* **20**, 171-191.

Girotti, A. W. and Thomas, J. P. 1984. "Damaging Effects of Oxygen Radicals on Resealed Erythrocyte Ghosts." *J. Biol. Chem.* **259**, 1744-1752.

Gómaz, R.; López, T.; Ortiz-Islas, E.; Navarrete, J.; Sánchez, E.; Tzompanztzi, F. and Bokhimi, X. 2003. "Effect of Sulfation on the Photoactivity of TiO_2 Sol-Gel Derived Catalysts." *J. Mol. Catal. A: Chem.* **193**, 217-226.

Gopal, M.; Chan, W. J. M. and De Jonghe, L. C. 1997. "Room Temperature Synthesis of Crystalline Metal Oxides." *J. Mater. Sci.* **32**, 6001-6008.

Guiu, G. and P. Grange, P. 1995. "Acidic and Catalytic Properties of SiO_2-Ta_2O_5 Mixed Oxides Prepared by the Sol-Gel Method." *J. Catal.* **156**, 132-138.

Gumy, D., Morais, C., Bowen, P., Pulgarin, C., Giraldo, S., Hajdu, R., and Kiwi, J. 2006a. "Catalytic Activity of Commercial of TiO_2 Powders for the Abatement of the Bacteria (*E. coli*) under Solar Simulated Light: Influence of the Isoelectric Point." *Appli. Catal. B: Environ.* **63**, 76-84.

Gumy, D., Rincon, A.G., Hajdu, R., and Pulgarin, C. 2006b. "Solar Photocatalysis for Detoxification and Disinfection of Water: Different Types of Suspended and Fixed TiO_2 Catalysts Study." *Solar Energy.* **80**, 1376 – 1381.

Han, J. and Kumacheva, E. 2001. "Monodispersed Silica-Titanyl Sulfate Microspheres." *Langmuir.* **17**, 7912-7917.

Hench, L. L. and West, J. K. 1990. "The Sol-Gel Process." *Chem. Rev.* **90**, 33-72.

Hidaka, H.; Horikoshi, S.; Serpone, N. and Knowland, J. 1997. "In Vitro Photchemical Damage to DNA, RNA and Their Bases by an Inorganic Sunscreen Agent on Exposure to UVA and UVB Radiation." *J. Photochem. Photobiol. A: Chem.* **111**, 205-213.

Hoffman, M. R.; Martin, S. T.; Choi, W. and Bahnemann, D. W. 1995. "Environmental Applications of Semiconductor Photocatalysis." *Chem. Rev.* **95**, 69-96.

Holgado, M.; Cintas, A.; Ibisate, M.; Serna, C. J.; Lopez, C. and Meseguer, F. 2000. "Three-Dimensional Arrays Formed by Monodisperse TiO_2 Coated on SiO_2 Spheres." *J. Colloid. Interface Sci.* **229**, 6-11.

Hong, S. S.; Lee, M. S.; Park, S. S. and Lee, G. D. 2003. "Synthesis of Nanosized TiO_2/SiO_2 Particles in the Microemulsion and Their Photocatalytic Activity on the Decomposition of *p*-nitrophenol." *Catal. Today* **87**, 99-105.

Houas, A.; Lachheb, H.; Ksibi, M.; Elaloui, E.; Guillard, C. and Herrmann, J. –M. 2001. "Photocatalytic Degradation Pathway of Methylene Blue in Water." *Appl. Cat. B.* **31**,145-147, and references cited therein.

http://en.wikipedia.org/wiki/Escherichia_coli (accessed March 10th, 2010).

http://en.wikipedia.org/wiki/Candida_albicans (accessed March 15th, 2010).

http://en.wikipedia.org/wiki/Cryptococcus_neoformans (accessed March 15th, 2010).

http://en.wikipedia.org/wiki/MRSA (accessed March 10th, 2010)

http://micro.digitalproteuscom/morphology2.php (accessed March 10th, 2010).

http://sariyusriati.files.wordpress.com/2008/10/flowchat-sol-gel1.jpg (accessed June 1st, 2010).

http://www.advancedenviro.net/fungi.htm (accessed March 14th, 2010).

http://www.astrographics.com (access March 10th, 2010).

http://www.dailytech.com (accessed March 10th, 2010).

http://www.fungusfocus.com/html/candida_info.htm (accessed March 14th, 2010).

http://www.randstarteam.blogspot.com (accessed March 10th, 2010).

http://www.swampie.wordpress.com (accessed March 10th, 2010).

Hu, L.; Yoko, T.; Kozuka, H. and Sakka, S. 1992. "Effects of Solvent on Properties of Sol-gel Derived TiO_2 Coating Films." *Thin Solid Films*. **219**, 18-23.

Huang, N.; Min-huaa, X.; Yuana, C. and Rui-rong, Y. 1997. "The Study of the Photokilling Effect and Mechanism of Ultrafine TiO_2 Particles on U937 Cells." *J. Photochem. Photobiol. A: Chem.* **108**, 229-233.

Huang, W. J.; Fang, G.-C and Wang, C. C. 2005. "The Determination and Fate of Disinfection By-Products from Ozonation of Polluted Raw Water." *Sci. Total Environ.* **345**, 261-272.

Huang, Z.; Maness, P.-C.; Blake, D. M.; Wolfrum, E. J.; Smolinski, S. L. and Jacoby, W. A. 2000. "Bactericidal Mode of Titanium dioxide Photocatalysis." *J. Photochem. Photobiol. A: Chem.***130**, 163-170.

Hudault, S;. Guignot, J. and Servin, A. L. 2001. "*Escherichia Coli* Strains Colonizing the Gastrointestinal Tract Protect Germfree Mice against *Salmonella Typhimurium* Infection." *Gut.* **49**, 47-55.

Ibánez, J. A.; Litter, M. I. and Pizarro, R. A. 2003. "Photocatalytic Bactericidal Effect of TiO_2 on *Enterobacter cloacae* Comparative Study with Other Gram (-) Bacteria." *J. Photochem. Photobiol. A: Chem.* **157**, 81-85.

Iengo, P.; Aprile, G.; Di Serio, M. and Santacesaria, E. 1999. "Preparation and Properties of New Acid Catalysts Obtained by Grafting Alkoxides and Derivatives on the Most Common Supports. Part III-Grafting Titanium Alkoxides and Sulphate Derivatives on Silica." *Appl. Catal. A: Gen.* **178**, 97-109.

Islam, M. A.; Alam, M. M.; Choudhury, M. E.; Kobayashi, N. and Ahmed, M. U. 2008. "Determination of Minimum Inhibitory Concentration (MIC) of Cloxacillin for Selected Isolated of Methicillin-Resistant *Staphylococcus Aureus* (MRSA) with Their Antibiogram." *Bangl. J. Vet. Med.* **6**, 121-126

Jawetz, E; Melnick, J. L. and Adelberg, E. A. 1984. Review of Medical Microbiology, 16th ed., Lange Medical Publication, California, USA., p.4.

Jernigan, J. A.; Arnold, K.; Helipern, K.; Kainer, M.; Woods, C. and Hughes, J. M. 2006. "Methicillin-Resistant *Staphylococcus Aureus* as Community Pathogen." Symposium on Community Associated Methicillin-Resistant *Staphylococcus Aureus* (Atlanta, Georgia, USA). Cited in *Emerg. Infect. Dis.* http://www.cdc.gov/ncidod/EID/vol12no11/06-0911.htm (accessed June 1st, 2010).

Jung, W. Y.; Baek, S. H.; Park, S. S.; Lee, G.-D.; Jeong, E. D.; Kim, H.G. and Hong, S.-S. 2007. "Synthesis of Nanosized TiO_2/SiO_2 Particles Using Microwave Processes and Their Photocatalytic Activity on the Decomposition of Orange II." *React. Kinet. Catal. Lett.* **91**, 233-240.

Kanna, M. 2008. "Comparison of Various Titanium Dioxide for the Photocatalytic Degradation of Dyes." Ph.D. Thesis, Prince of Songkla University, Thailand.

Kanna, M. and Wongnawa, S. 2008. "Mixed amorphous and nanocrystalline TiO_2 powders prepared by sol-gel method: characterization and photocatalytic study." *Mater. Chem. Phys.* **110**, 166-175.

Khalil, K. M. S. and Zaki, M. I. 1997. "Synthesis of High Surface Area Titania Powders via Basic Hydrolysis of Titanium (IV) Isopropoxide." *Powder Technol.* **92**, 233-239.

Khalil, K. M. S.; Elsamahy, A. A. and Elanany, M. S. 2002. "Formation and Characterization of High Surface Area Thermally Stabilized Titania/Silica Composite Materials via Hydrolysis of Titanium(IV) *tetra*-Isopropoxide in Sols of Spherical Silica Particle." *J. Colloid. Interface Sci.* **249**, 359-365.

Kikuchi, Y.; Sunada, K.; Iyoda, T.; Hashimoto, K. and Fujishima, A. 1997. "Photocatalytic Bactericidal Effect of TiO_2 Thin Films: Dynamic View of the Active Oxygen Species Responsible for the Effect." *J. Photochem. Photobiol. A: Chem.* **106**, 51-56.

Kim, H. J.; Shul, Y. G. and Han, H. 2005. "Photocatalytic Properties of Silica-supported TiO_2." *Chem. Mater. Sci.* **35**, 287-293.

Kim, S.; Taguchi, T.; Nishioka, M. and Taya, M. 2004. "Quantitative Assessment of DNA Damage Accompanied With no Substantial Loss in its Molecular Weight During Exposure to Oxidative Stress." *Biochem. Eng. J.* **22**, 81-87.

Kimura, I.; Kase, T.; Taguchi, Y. and Tanaka, M. 2003. "Preparation of Titania/Silica Composite Microspheres by Sol-gel Process in Reverse Suspension." *Mater. Res. Bull.* **38**, 585-597.

Kiriakidou, F.; Kondarides, D. I. And Verykios, X. E. 1999. "The Effect of Operational Parameters and TiO_2-Doping on the Photocatalytic Degradation of Azo-Dyes." *Catalysis Todays.* **54**, 119-130.

Kiwi, J. and Nadtochenko, V. 2005. "Evidence for the Mechanism of Photocatalytic Degradation of the Bacterial Wall Membrane at the TiO_2 Interface by ATR-FTIR and Laser Kinetic Spectroscopy." *Langmuir.* **21**, 4631-4641.

Kluytmans, J.; Van Belkum, A. and Verbugh, H. 1997. "Nasal Carriage of *Staphylococcus aureus*: Epidemiology, Underlying Mechanisms, and Associated Risks." *Clin. Microbiol. Rev.* **10**, 505-520.

Kurtzman C. P. and Fell J. W. 2005. "Biodiversity and Ecophysiology of Yeasts (in: The Yeast Handbook, Gábor P., de la Rosa C. L., eds.)." Berlin: Springer. p.11–30.

Kurtzman, C. P. and Piškur, J. 2006. "Taxonomy and Phylogenetic Diversity Among the yeasts (in Cooperative Genomics; Using Fungi as Models, Sunneragen, P.; Piskur, eds.)." Berlin: Springer, p.29-46.

Lassaletta, G.; Fernández, A.; Espinós, J. P. and González-Elipe, A. R. 1995. "Spectroscopic Characterization of Quantum-sized TiO_2 Supported on Silica: Influence of Size and TiO_2-SiO_2 Interface Composition." *J. Phys. Chem.* **99**, 1484-1490.

Lee, S.; Nishida, K.; Otaki, M. and Ohgaki, S. 1997. "Photocatalytic Inactivation of Phage QB by Immobilized Titanium Dioxide Mediated Photocatalyst." *Wat. Sci. Technol.* **35**, 101-106.

Legras, J.-L.; Merdinoglu, D.; Cornuet, J. –M. and Karst, F. 2007. "Bread, Beer and Wine: *Saccharomyces Cerevisiae* Diversity Reflects Human History." *Molecular Ecology.* **16**, 2091–2102.

Lenza, R. F. S. and Vasconcelos, W. L. 2000. "Synthesis and Properties of Microporous Sol-gel Silica Membranes." *J. Non-Crystalline Solids.* **273**, 164-169.

Li, Q. and Dong, P. 2003. "Preparation of Nearly Monodisperse Multiply Coated Submicrospheres with a High Refractive Index." *J. Colloid Interf. Sci.* **261**, 325-329.

Lin, C.-Y and Li, C.-S. 2003. "Effectiveness of Titanium Dioxide Photocatalyst Filters for Controlling Bioaerosols." *Aerosol Science and Technology* **37**, 162-170.

Liu, Z. and Davis, R. J. 1994. "Investigation of the Structure of Microporous Ti-Si Mixed Oxides by X-ray UV Reflectance, FT-Raman, and FT-IR Spectroscopies." *J. Phys. Chem.* **98**, 1253-1261.

Loftus B. J., *et al.* (2005). "The Genome of the Basidiomycetous Yeast and Human Pathogen Cryptococcus Neoformans." *Science* 307, 1321-1324.

doi:10.1126/science.1103773. PMID 15653466.

Lucarelli, L., Nadtochenko, V., and Kiwi, J. 2000. "Environmental Photochemistry: Quantitative Adsorption and FTIR Studies During the TiO_2-photocatalyzed Degradation of Orange II." *Langmuir.* **16**, 1102–1108.

Madigan, M. and Martinko, J. 2005. Brock Biology of Microorganisms, 11th ed. Prentice Hall, USA.

Mahmoodi, N. M.; Arami, M.; Limaee, N. Y. and Tabrizi, N. S. 2005. "Decolorization and Aromatic Ring Degradation Kinetics of Direct Red 80 by UV Oxidation in the Presence of Hydrogen Peroxide Utilizing TiO_2 as a Photocatalyst." *Chem. Eng. J.* **112**, 191-196.

Maness, P. –C.; Smolinski, S.; Blake, D. M.; Huang, Z.; Wolfrum, E. J. and Jacoby, W. A. 1999. "Bactericidal Activity of Photocatalytic TiO_2 Reaction: toward an Understanding of Its Killing Mechanism." *Appl. Environ. Microbiol.* **65**, 4094-4098.

Martinez-Gutierrez, F.; Olive, P.; Banuelos, A.; Orrantia, E.; Nino, N.; Sanchez, E. M.; Ruiz, F.; Bach, H. and Av-Gay, Y. 2010. "Synthesis, Characterization and Evaluation of Antimicrobial and Cytotoxic Effect of Silver and Titanium Nanoparticles." *Nanomedicine: Nanotechnology, Biology and Medicine.* Article in Press; doi:10.1016/j.nano.2010.02.001

Masschelin, W. J. 2002. "Ultraviolet Light in Water and Wastewater Sanitation." Lewis, Boca Raton, FL, USA., pp. 59-112.

Matsunaga, T.; Tomada, R.; Nakajima, T. and Wake, H. 1985. "Photoelectrochemical Sterilization of Microbial Cells by Semiconductor Powders." *FEMS Microbiol. Lett.* **29**, 211-214.

McKane, L. and Kandel J. 1985. "Microbiology: Essentials and Applications" 1st ed., McGrawhill, CA., USA., pp.4 and 21.

Miao, L.; Jin, P.; Kaneko, K.; Terai, A.; Nabatova-Gabain, N. and Tanemura, S. 2003. "Preparation and Characterization of Polycrystalline Anatase and Rutile TiO_2 Thin Films by rf Magnetron Sputtering." *Appl. Surf. Sci.* **212-213**, 255-263.

Mills, A. and Hunte, L.S. 1997. "An Overview of Semiconductor Photocatalysis." *J. Photochem. Photobiol. A: Chem.* **108**, 1-35.

Mills, A. and Sawunyama, P. 1994. "Photocatalytic Degradation of 4-Chlorophenol Mediated by TiO_2: a Comparative Study of the Activity of Laboratory Made and Commercial TiO_2 Samples." *J. Photochem. Photobiol. A*: *Chem.* **84**, 305-309.

Mills, A. and Wang, J. 1999. "Photobleaching of Methylene Blue Sensitised by TiO_2: an Ambiguous System?" *J. Photochem. Photobiol. A*: Chem. **127**, 123-134.

Min, C.; Hyenmi, C.; Wonyong, Y. and Jeyong, Y. 2004. "Linear Correlation between Inactivation of *E. coli* and OH Radical Concentration in TiO_2 Photocatalytic Disinfection." *Water Res.* **38**, 1069-1077.

Nadtochenko, V. A.; Rincon, A. G.; Stanca, S. E. and Kiwi, J. 2005. "Dynamics of *E. coli* Membrane Cell Peroxidation during TiO_2 Photocatalysis Studied by ATR-FTIR Spectroscopy and AFM Microscopy." *J. Photochem. Photobiol. A: Chem.* **169**, 131-137.

Nakabayashi, H. 1992. "Properties of Acid Sites on TiO_2-SiO_2 and TiO_2-Al_2O_3 Mixed Oxides Measured by Infrared Spectroscopy." *Bull. Chem. Soc. Jpn.* **65**, 914-916.

Nakamoto, K. 1986. Infrared and Raman Spectra of Inorganic and Coordination Compounds, 4th ed., Wiley, New York.

Nakano M. M. and Zuber P. 1998. "Anaerobic Growth of a "strict aerobe" (*Bacillus Subtilis*)." *Annu. Rev. Microbiol.* **52**, 165-190.

Neppolian, B.; Choi, H. C.; Sakthivel, S.; Arabindoo, B. and Murugesan, V. 2002. "Solar Light Induced and TiO_2 Assisted Degradation of Textile Dye Reactive Blue 4." *Chemosphere*. **46**, 1173-1181.

Ogston A. 1984. "On Abscesses: Classics in Infectious Disease." *Rev. Infect Dis.* **6**, 122-128.

Ohno, T., Haga, D., Fujihara, K., Kaizaki, K., and Matsumura, M. 1997. "Unique Effects of Iron(III) ions on Photocatalytic and Photoelectrochemical Properties of Titanium Dioxide." *J. Phys. Chem. B.* **101**, 6415 – 6419.

Ohtani, B.; Ogawa, Y. and Nishimoto, S. -I. 1997. "Photocatalytic Activity of Amorphous-Anatase Mixture of Titanium (IV) Oxide Particles Suspended in Aqueous Solutions." *J. Phys. Chem. B.* **101**, 3746-3752.

Okuma, K.; Iwakawa, K.; Turnidge, J. D.; Grubb, W. B.; Bell, J. M.; O'Brien, F. G.; Coombs, G. W.; Pearman, J. W.; Tenover F. C.; Kapi, M. Tiensasitorn, C.; Ito, T. and Hiramatsu, K. 2002. "Dissemination of new Methicillin-resistant *Staphylococcus aureus* Clones in the Community." *J. Clin. Microbiol.* **40**, 4289-4294.

Ostergaard, S.; Olsson, L. and Nielsen, J. 2000. "Metabolic engineering of *Saccharomyces cerevisiae*." *Microbiology and Molecular Biology Reviews* **64**, 34-50.

Otaki, M.; Hirata, T. and Ohgaki, S. 2000. "Aqueous Microoganisms Inactivation by Photocatalytic Reaction." *Wat. Sci. Technol.* **42**, 103-108.

Papp, J.; Soled, S.; Dwight, K. and Wold, A. 1994. "Surface Acidity and Photocatalytic Activity of TiO_2, WO_3/TiO_2, and MoO_3/TiO_2 Photocatalysts." *Chem. Mater.* **6**, 496-500.

Pelizetti, E. and Minero, C. 1993. "Mechanism of the Photo-Oxidative Degradation of Organic Pollutants over TiO_2 Partiles." *Electrochem. Acta* **38**, 47-55.

Perkowski, J.; Bzdon, S.; Bulska, A. and Jozwiak, W. K. 2006. "Decomposition of Detergents Present in Carwash Sewage by Titania Photo-assisted Oxidation." *Polish J. Environ. Stud.* **2006**, 457-465.

Pichat. P.; Guillard C.; Laurence, A.; Renard, A. –C. and Plaidy, O. 1995. "Assessment of the Importance of the Role of H_2O_2 and O_2^- in the Photocatalytic Degradation of 1,2-Dimethoxybenzene." *Sol. Energy Mater. Sol. Cells.* **38**, 391-399.

Qi, K.; Chen, X.; Liu, Y.; Xin, J. H.; Mak, C. L. and Daou, W. A. 2007. "Facile Preparation of Anatase/SiO_2 Spherical Nanocomposites and Their Application in Self-cleaning Textiles." *J. Mater. Chem.* **17**, 3504-3508.

Qumar, M.; Saquib, M. and Muneer, M. 2005. "Photocatalytic Degradation of Two Selected Dye Derivatives, Chromotrope 2B and Amido Black 10B, in Aqueous Suspensions of Titanium Dioxide." *Dyes and Pigments.* **65**, 1-9.

Randorn, C.; Wongnawa, S. and Boonsin, P. 2004. "Bleaching of Methylene Blue by Hydrated Titanium Dioxide." *ScienceAsia.* **30**, 149-156.

Raygada, J. L. and Levine, D. P. 2009. "Managing CA-MRSA Infections: Current and Emerging Options." *Infection in Medicine*. **26**, 49-58.

Reddy, K. M.; Reddy, C. V. G. and Manorama, S. V. 2001. "Preparation, Characterization, and Spectral Studies on Nanocrystalline Anatse TiO_2." *J. Solid State Chem*. **158**, 180-186.

Reid, G.; Howard, J. and Gan, B. S. 2001. "Can Bacterial Interference Prevent Infection?" *Trends Microbiol.* **9**, 424-428.

Retuert, J.; Quijada, R. and Fuenzalida, V. M. 2000. "Titania Coatings on High and Low Surface Area Spherical Silica Particles by a Sol-gel Method." *J. Mater. Chem.* **10**, 2818-2822.

Rincón, A.G. and Pulgarin, C. 2003. "Phtocatalytic Inactivation of *E. coli*: Effect of (Continuous-intermittent) Light Intensity and of (Suspended-fixed) TiO_2 Concentration." *Appl. Catal. B: Environ.* **44**, 263-284.

Rincón, A. G. and Pulgarin, C. 2004. "Effect of pH, Inorganic Ions, Organic Matter and H_2O_2 on *E. coli* K12 Photocatalytic Inactivation by TiO_2 Implications in Solar Water Disinfection." *Appl. Catal. B: Environ.* **51**, 283-302.

Roark, R. D.; Kohler, S. D.; Ekerdt, J. G.; Kim, S. D. and Wachs, I. E. 1992. "Monolayer Dispersion of Molybdenum on Silica." *Catal. Lett.* **16**, 77-83.

Robertson, J. M. C.; Robertson, P. K. J. and Lawton, L. A. 2005. "A Comparison of the Effectiveness of TiO_2 Photocatalysis and UVA Photolysis for the Destruction of Three Pathogenic Micro-organisms." *J. Photochem. Photobiol. A: Chem.* **175,** 51-56.

Rubio, J.; Oteo, J. L.; Villegas, M. and Duran, P. 1997. "Characterization and Sintering Behavior of Submicrometre Titanium Dioxide Spherical Particles Obtained by Gas-phase Hydrolysis of Titanium Tetrabutoxide." *J. Mater. Sci.* **32,** 643-652.

Ryan, K. J. and Ray, C. G. 2004. "Sherris Medical Microbiology." 4th ed., McGraw Hill. ISBN 0-8385-8529-9.

Saito, T.; Iwase, T. Horis, J. and Morioka, T. 1992. "Mode of Photocatalytic Bactericidal Action of Powdered Semiconductor TiO_2 on Mutants Streptococci." *J. Photochem. Photobiol. B:Biol.* **14,** 369-379.

Samantaray, S. K.; Mohapatra, P. and Parida, K. 2003. "Physico-Chemical Characterization and Photocatalytic Activity of Nanosized SO_4^{2-}/TiO_2 towards Degradation of 4-Nitrophenol." *J. Mol. Catal. A: Chem.* **198,** 277-287.

Sanchez, E.; Lopez, T.; Gomez, R.; Morales, A. And Novaro, O. 1996. "Synthesis and Characterization of Sol-Gel Pt/TiO_2 catalyst." *J. Solid State Chem.* **122,** 309-314.

Sato, T. and Taya, M. 2006. "Enhancement of Phage Inactivation Using Photocatalytic Titanium Dioxide Particle with Different Crystalline Structures." *Biochem. Eng. J.* **28,** 303 – 308.

Sclafani, A. and Herrmann, J.M. 1996. "Comparison of the Photoelectronic and Photocatalytic Activities of Various Anatase and Rutile Forms of Titania in Pure Liquid Organic Phase and in Aqueous Solutions." *J. Phys. Chem.* **100**, 13655–3661.

Sclafani, A.; Palmisano, L. and Schiavello, M. 1990. "Influence of the Preparation Methods of TiO_2 on the Photocatalytic Degradation of Phenol in Aqueous Dispersion." *J. Phys. Chem.* **94**, 829-832.

Seok, S. I. and Kim, J. H. 2004. "TiO_2 Nanoparticles Formed in Silica Sol-gel Matrix." *Mater. Chem. Phys.* **86**, 176-179.

Seven, O.; Dindar, B.; Aydemir, S.; Metin, D.; Ozinel, M. A. and Icli, S. 2004. "Solar Photocatalytic Disinfection of a Group of Bacteria and Fungi Aqueous Suspensions with TiO_2, ZnO and Sahara Desert Dust." *J. Photochem. Photobiol. A: Chem.* **165**, 103-107.

Shi, L.; Zhao, Y.; Zhang, X.; Su, H. and Tan, T. 2008. "Antibacterial and Anti-mildew Behavior of Chitosan/nano-TiO_2 Composite Emulsion." *Korean J. Chem. Eng.* **25**, 1434-1438.

Shibata, T.; Hamada, N.; Kimoto, K.; Kawada, T.; Sawada, T.; Kumada, H.; Umemoto, T. and Toyoda, M. 2007. "Antifungal Effect of Acrylic Resin Containing Apatite-coated TiO_2 Catalyst." *Dent. Mater. J.* **26**, 437-447.

Shiraishi, K; Koseki, H.; Tsurumoto, T.; Baba, K.; Naito, M.; Nakayama, K. and Shindo, H. 2008. "Antibacterial Metal Implant with a TiO_2-conferred Photocatalytic Bactericidal Effect against *Staphylococcus aureus*." *Surface and Interface Analysis.* **41**, 17-22.

Sivalingam, G.; Nagavei, K.; Hegde, M. S. and Madras, G. 2003. "Photocatalytic Degradation of Various Dyes by Combustion Synthesized Nano Antase TiO_2." *Appl. Catal. B: Environ.* **45**, 23-28.

Sjogren, J. C. and Sierka, R. A. 1994. "Inactivation of Phage MS2 by Iron-aided Titanium Dioxide Photocatalysis." *Appl. Environ. Microbiol.* **60**, 344-347.

Stylidi, M., Kondarides, D.I., and Verykios, X.E. 2004. "Visible Light-induced Photocatalytic Degradation of Acid Orange 7 in Aqueous TiO_2 Suspensions." *Appl. Catal. B: Environ.* **47**, 189 – 201.

Sunada, K.; Kikuchi, Y.; Hashimoto, K. and Fujishima, A. 1998. "Bactericidal and Detoxification Effects of TiO_2 Thin Film Photocatalyst." *Environ. Sci. Technol.* **32**, 726-728.

Sunada, K.; Watanabe, T. and Hashimoto, K. 2003. "Studies on Photokilling of Bacteria on TiO_2 Thin Film." *J. PhotoChem. Photobiol. A: Chem.* **156**, 227-233.

Suresh, C.; Biju, V.; Mukundan, P. and Warrier, K. G. K. 1998. "Anatase to Rutile Transformation in Sol-Gel Titania by Modification of Precursor." *Polyhedron.* **17**, 3131-3135.

Suwanchawalit, C. 2005. "The Effect of Metal-doping on the Physical and Photocatalytic Properties of Nanosized TiO_2 Powder." Master of Science Thesis, Prince of Songkla University, Thailand.

Tortora, G., Funke, R.B., and Case, L.C. 2001. Microbiology: An Introduction, Addison-Wesley Longman, Inc., New York, USA.

Urbansky, E. T. and Magnuson, M. L. 2002. "Analyzing Drinking Water for Disinfection Byproducts." *Anal. Chem.* **74**, 260-267.

Velasco, M. J.; Rubio, F.; Rubio, J. and Oteo, J. L. 1999. "DSC and FT-IR Analysis of the Drying Process of Titanium Alkoxide Derived Precipitates." *Thermochim. Acta*. **326**, 91-97.

Verran, J., Sandoval, G., Allen, N.S., Edge, M., and Stratton, J. 2007. "Variables Affecting the Antibacterial Properties of Nano and Pigmentary Titania Particles in Suspension." *Dyes and Pigments.* **73**, 298–304.

Vohra, A.; Goswami, D. Y.; Deshpande, D. A. and Block S. S. 2005. "Enhanced Photocatalytic Inactivation of Bacterial Spores on Surfaces in Air." *J. Ind. Microbiol. Biotechnol.* **32**, 364-370.

Wachs, I. E. 1996. "Raman and IR Studies of Surface Metal Oxide Species on Oxide Supports: Supported Metal Oxide Catalysts." *Catal. Today* **27**, 437-455.

Wang, Z. C.; Chen, J. F. and Hu, X. F. 2000. "Preparation of Nanocrystalline TiO_2 Powder at near Room Temperature from Peroxo-Polytitanic Acid Gel." *Mater. Lett.* **43**, 87-90.

Wolfrum, E. J. Huang, J.; Blake, D. M.; Maness, P.-C.; Huang, Z. and Fiest, J. 2002. "Photocatalytic Oxidation of Bacteria, Bacterial and Fungal Spores, and Model Biofilm Components to Carbon Dioxide on Titanium Dioxide-Coated Surfaces." *Environ. Sci. Technol.* **36**, 3412-3419.

Xie, Y. and Yuan, C. 2003. "Photocatalytic Activity and Recycle Application of Titanium Dioxide Sol for X-3B Photodegradation." *J. Photochem. Photobiol. A: Chem.* **206**, 419-428.

Xu, N.; Shi, Z.; Fan, Y.; Dong, J.; Shi, J. and Hu, M. Z.-C. 1999. "Effects of Particle Size of TiO_2 on Photocatalytic Degradation of Methylene Blue in Aqueous Suspensions" *Ind. Eng. Chem. Res.* **38**, 373-379.

Yamazaki, S.; Fujinaga, N. and Araki, K. 2001. "Effect of Sulfate Ions for Sol-Gel Synthesis of Titania Photocatalyst." *Appl. Catal. A.* **210**, 97-102.

Youn, H. –J.; Ha, P. S.; Jung, H. S.; Hong, K. S.; Park, Y. H. and Ko, K. H. 1999. "Alcohol Rinsing and Crystallization Behavior of Precipitated Titanium Oxide." *J. Coll. Inter. Sci.* **211**, 321-325.

Yu, J.; Zhao, L. and Cheng, B. 2006. "Facile Preparation of Monodispersed SiO_2/TiO_2 Composite Microspheres with High Surface Area." *Mater. Chem. Phys.* **96**, 311-316.

Yu, J. G.; Zhao, X. J.; Yu, J. C.; Zhong, G. R.; Han, J. J. and Zhao Q. N. 2001. "The Grain Size and Surface Hydroxyl Content of Super-hydrophillic TiO_2/SiO_2 Composite Nanometer Thin Films." *J. Mater. Sci. Lett.* **20**, 1745-1748.

Zaban, A.; Aruna, S. T.; Tirosh, S.; Gregg, B. A. and Mastai, Y. 2000. "The Effect of the Preparation Condition of TiO_2." *J. Phys. Chem. B.* **104**, 4130-4133.

Zeltner, W. A. and Tompkin, D. T. 2005. "Shedding Light on Photocatalysis." *Ashrae Trans.* **111**, 532-534.

Zhang, F.; Zhao, J.; Shen, T.; Hidaka, H.; Pelizzetti, E. and Serpone, N. 1998. "TiO_2-Assisted Photodegradation of Dye Pollutants II. Adsorption and Degradation Kinetics of Eosin in TiO_2 Dispersions under Visible Light Irradiation." *Appl. Catal. B.* **45**, 147-156.

Zhang, H.; Penn, R. L.; Hamers, R. J. and Banfield, J. F. 1999. "Enhanced Adsorption of Molecules on Surfaces of Nanocrystalline Particles." *J. Phys. Chem. B.* **103**, 4656-4662.

Zhang, Q., Gua, J., and Gao, L. 2000. "Effect of Hydrolysis Conditions on Morphology and Crystallization of Nanosized TiO_2 Powder." *J. Eur. Ceram. Soc.* **20**, 2153-2158.

Zhang, Q.; Gao, L. and Guo, J. 2000. "Effects of Calcination on the Photocatalytic Properties of Nanosized TiO_2 Powders Prepared by $TiCl_4$ Hydrolysis." *Appl. Catal. B.* **26**, 207-215.

Zhang, Q. –H.; Gao, L. and Guo, J. –K. 1999. "Preparation and Charaterization of Nanosized TiO_2 Powders from Aqueous $TiCl_4$ Solution." *NanoStruct. Mater.* **11**, 1293-1300.

Zhang, R. and Gao, L. 2001. "Effect of Peptization on Phase Transformation of TiO_2 Nanoparticles." *Mater. Res. Bull.* **36**, 1957-1965.

Zhou, L. J.; Yan, S. S.; Tian, B. Z.; Zhang, J. L. and Anpo. M. 2006. "Preparation of TiO_2-SiO_2 Film with High Photocatalytic Activity on PET Substrate." *Mater. Lett.* **60**, 396-399.

Zhu, C.; Wang, L.; Kong, L.; Yang, X.; Wang, L.; Zheng, S.; Chen, F.; MaiZhi, F. and Zong, H. 2000. "Photocatalytic Degradation of AZO Dyes by Supported TiO_2 + UV in Aqueous Solution." *Chemosphere.* **41**, 303-309.

Zielińska, B.; Grzechulska, J.; Grzmil, B. and Morawski, A. W. 2001. "Photocatalytic Degradation of Reactive Black 5 A Comparison between TiO_2-Tytanpol A11 and TiO_2-Degussa P25 Photocatalysts." *Appl. Catal. B.* **35**, L1-L7.

Zielińska, B.; Grzechulska, J.; Grzmil, B. and Morawski, A. W. 2003. "The pH Influence on Photocatalytic Decomposition of Organic Dyes over A11 and P25 Titanium Dioxide." *Appl. Catal. B.* **45**, 293-300.

Zielińska, B.; Grzechulska, J. and Morawski, A. W. 2003. "Photocatalytic Decomposition of Textile Dyes on TiO_2-Tytanpol A11 and TiO_2-Degussa P25." *J. Photochem. Photobiol. A: Chem.* **157**, 65-70.

APPENDIX

APPENDIX A

EXAMPLES FOR KINETICS STUDY

For the kinetics study, the photodegradation of methylene blue has been established to follow the Langmuir-Hinshelwood first order rate law which has the simplified form as (Houas, *et al.*, 2001)

$$\ln\left(\frac{A_0}{A}\right) = k \cdot t.$$

The plots of $\ln(A_0/A)$ versus time yielded straight lines for all TiO_2/SiO_2 samples indicating the degradation of methylene blue is a first order process.

Data of the 50% TiO_2/SiO_2 and 75% TiO_2/SiO_2 are used to illustrate the plot of $\ln(A_0/A)$ versus time as shown in Fig. 37. The rate constants as obtained from the slope of the straight lines are 9.2×10^{-3} and 8.2×10^{-3} min^{-1} for the 50% TiO_2/SiO_2 and 75% TiO_2/SiO_2 samples, respectively.

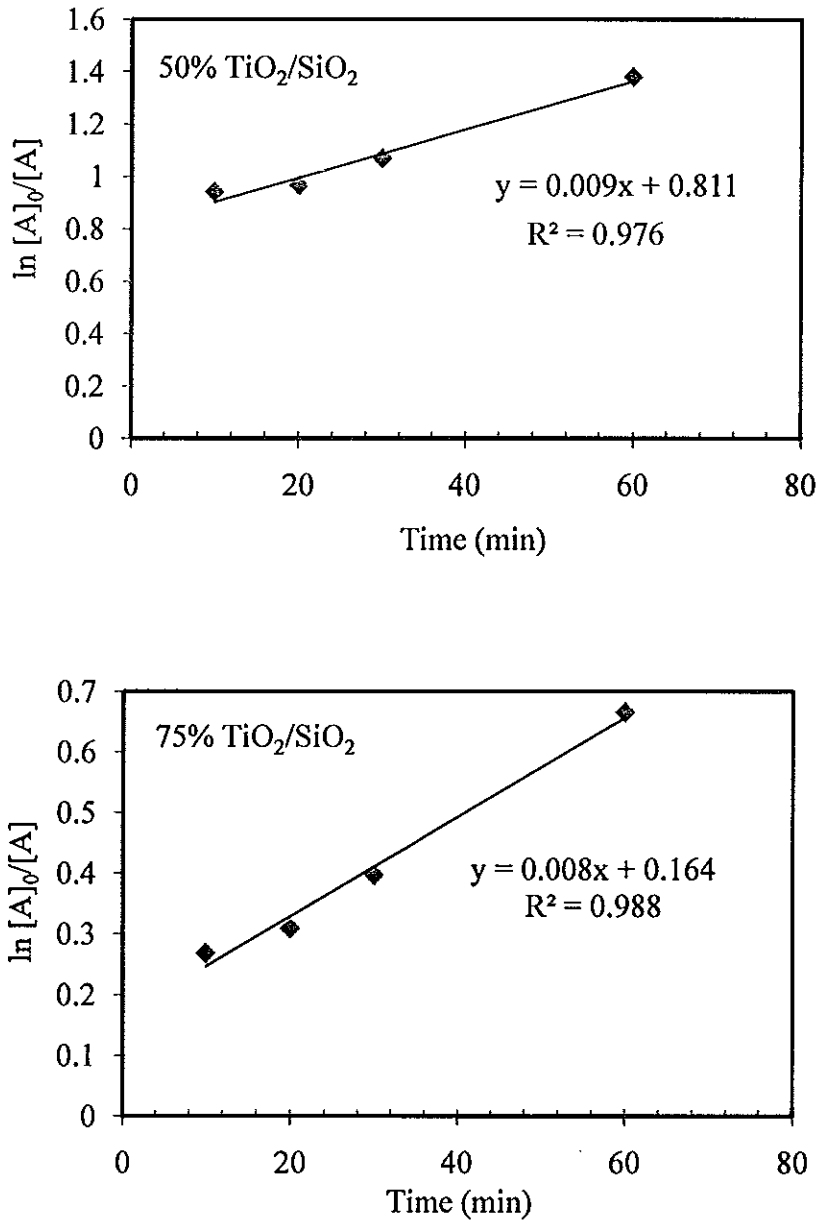

Figure 37. The kinetics of decolorization of methylene blue under UV irradiation by the TiO_2/SiO_2 samples; a) 50% TiO_2/SiO_2 and b) 75% TiO_2/SiO_2.

APPENDIX B

PUBLICATIONS FROM THIS WORK

Songklanakarin J. Sci. Technol.
31 (5), 517-525, Sep. - Oct. 2009

Songklanakarin Journal of Science and Technology
http://www.sjst.psu.ac.th

Original Article

Evaluation of bactericidal activity of TiO_2 photocatalysts: a comparative study of laboratory-made and commercial TiO_2 samples

Uraiwan Sirimahachai[1], Souwalak Phongpaichit[2] and Sumpun Wongnawa[1]*

[1] *Department of Chemistry.*

[2] *Department of Microbiology, Faculty of Science.*
Prince of Songkla University, Hat Yai, Songkhla, 90112 Thailand.

Received 17 February 2009; Accepted 25 May 2009

Abstract

Titanium dioxide photocatalysts were synthesized by sol-gel process, by varying the reaction conditions, acids, water content, and trivalent (Al, B) dopants. The characterizations of products were determined by XRD, SEM, BET, and UV-vis spectroscopy. The samples were mainly amorphous with a small amount of anatase, rutile, or a mixture of anatase and rutile, with a crystallite sizes of about 5-10 nm. The antibacterial activity of the synthesized TiO_2 samples were investigated qualitatively and semi-quantitatively. Five types of bacteria, *Escherichia coli* ATCC25922, *Psudomonas aeruginosa* ATCC27853, *Bacillus subtilis* BGA, *Saphylococcus aureus* ATCC25923, and *methicillin-resistant S. aureus* (MRSA) DMST 2054, were used for the inactivation experiment employing the agar dilution method. All the synthesized samples showed inactivation activity with varying degree of efficiency. Two of them showed a much higher activity than Degussa P25.

Keywords: titanium dioxide photocatalyst, antibacterial activity, photocatalytic process, sol-gel method, amorphous titanium dioxide

1. Introduction

Photocatalytic processes are rapidly developing as potential techniques for the purification of water and air (Legrini *et al.*, 1993; Mills and Hunte, 1997; Jacoby *et al.*, 1998; Lin and Li 2003). Among various metal oxide semiconductor photocatalysts, titanium dioxide is a very important photocatalyst due to its strong oxidizing power, nontoxicity, and photostability. The titania photocatalytic performance has been known to be dependent on several variables, such as, preparation method, particle size, reactive surface area, and ratio between anatase and rutile phases (Hoffmann *et al.*, 1995). Attempts have been made to improve the activity of titania photocatalyst through modified synthesis methods in order to alter the morphology and crystallinity, while dopings with ions of other elements are also another promising method.

Titania has three different crystalline phases: rutile, anatase, and brookite. Rutile is thermodynamically stable, while the latter two phases are in metastable states (Gopal *et al.*, 1997). Titania in anatase crystalline form behaves as a classical semiconductor. When a TiO_2 photocatalyst was illuminated by photons with energy greater than its band gap, an electron can be excited to the conduction band thus creating an electron-hole pair. With holes (h^+) and hydroxyl radicals (OH^*) generated in the valence band, and electrons and superoxide anions (O_2^{*-}) generated in the conduction band, irradiated TiO_2 photocatalysts can decompose and mineralize organic compounds by a series of oxidation reactions leading to carbon dioxide. It is also documented that inactivation of bacteria is caused by exposure to reactive oxygen intermediates, such as hydroxyl radicals (OH^*), superoxide anion (O_2^{*-}), and hydrogen peroxide (H_2O_2), which can damage proteins, nucleic acids, and cell membranes

*Corresponding author.
Email address: sumpun.w@psu.ac.th

(Ireland *et al.*, 1993; Ibanez *et al.*, 2003). In addition to water and wastewater disinfection, the semiconductor photocatalysis has received considerable attention over the past few years with emphasis given on the inactivation of bacteria, viruses, and protozoan parasites (Otaki *et al.*, 2000; Cho *et al.*, 2004; Rincon and Pulgarin 2004; Fernandez *et al.*, 2005; Lonnen *et al.*, 2005; Gumy *et al.*, 2006; Rincon and Pulgarin 2006). In terms of antibacterial effects of photocatalysts, Matsunaga *et al.* first reported the sterilization of microbial cells in water by a TiO_2/Pt powder in 1985. Since then, much research has been performed on the antibacterial effects of TiO_2 thin film, as well as TiO_2 powder (Huang *et al.*, 2000; Rincon and Pulgarin 2003; Yao *et al.*, 2007).

Until today, most of the work involving the disinfection of microorganisms by TiO_2 utilized commercial products, such as Degussa P25, anatase, rutile (Maness *et al.*, 1999; Rincon and Pulgarin 2003; Dadjour *et al.*, 2006; Benabbou *et al.*, 2007; Pal *et al.*, 2007; Sichel *et al.*, 2007; Sökmen *et al.*, 2007). In our laboratory, several modifications of titania nanoparticle have been synthesized for the dye degradation purpose, such as the acid catalysed nanosized TiO_2, Al(III)- and B(III)-doped TiO_2. Some data on the characterizations and physical properties of these synthesized TiO_2 powders have been reported elsewhere (Kanna and Wongnawa, 2008). In order to extend the usefulness of these photocatalysts, the antibacterial activities have been investigated in comparison with the commercial products and are reported in this article.

2. Materials and Methods

2.1 Materials

The main chemicals are titanium tetrachloride ($TiCl_4$, Merck, Germany), Degussa P25 (Degussa AG, Frankfurt, Germany), anatase (Carlo Erba, Italy), and rutile (R706, Dupont, USA). All other reagents were of reagent grade and used without further purification. Deionized water was used throughout the experiment. All solutions and materials in testing disinfection of TiO_2 were sterilized by autoclaving. The bacteria, *E. coli* ATCC25922, *P. aeruginosa* ATCC 27853, *B. subtilis* BGA, *S. aureus* ATCC25923 and MRSA SK1 were obtained from the laboratory stock of the Department of Microbiology, Faculty of Science, Prince of Songkla University.

2.2 Preparation of acid catalyzed nanosized TiO_2

Nanosized TiO_2 was synthesized from titanium tetrachloride. 20 mL of $TiCl_4$ was added slowly to 200 mL of cold deionized water (2°C), which had been placed in an ice-water bath at least 10 minutes prior to the addition. The solution was then mixed with 2 mL of conc. acid (HCl and H_2SO_4) and refluxed at 80°C for 1 h under vigorous stirring. The solution was then treated with ammonia solution until pH ≈ 7 and maintained at the same temperature for 24 hrs. The white precipitate formed was filtered and then washed with deionized water until no chloride ion was found by $AgNO_3$ solution test. The product was dried overnight at 105°C and ground to fine powder, until a final white powder was obtained. These samples are designated as TiO_2-200w-80HCl and TiO_2-200w-80H_2SO_4 (Kanna and Wongnawa, 2008).

2.3 Preparation of Al(III)- and B(III)-doped TiO_2

$TiCl_4$ was slowly added to deionized water ($TiCl_4$:H_2O volume ratios was 1:7.5 and 1:2.5) at room temperature. For the Al(III)-doped titania, $Al_2(SO_4)_3.18H_2O$ (0.04 mol% Al) and 2 mL of conc. HCl were added into the solution; then the mixture was kept over night without stirring. After that the resulting clear solution was refluxed at 95°C for 13 hrs. The solution was treated with ammonia solution to adjust the pH to 7 and continually refluxed for 13 hrs. This treatment produced a milky white TiO_2 suspensions. Afterwards the suspension was filtered, washed, and dried to obtain the final product as white powder. In the case of B (III)-doped titania, B_2O_3 (0.08 mol% B) was used instead of $Al_2(SO_4)_3.18H_2O$. These samples are designated as: TiO_2-Al150w, TiO_2-Al50w, TiO_2-B150w, and TiO_2-B50w (Suwandchawalit, 2005). The suffixes 150w and 50w correspond to high and low volume of water used.

2.4 Products characterization

Powder X-ray diffraction (XRD, PHILIPS X' Pert MPD with Ni-filtered and Cu Ka radiation) was used for crystal phase identification. The crystallite size has been calculated by using the Scherrer's formula,

$$L = \frac{K\lambda}{\beta_{hkl}\cos\theta} \qquad (1)$$

where L is the average crystallite size in nm, K is a constant usually taken as 0.9, λ is the wavelength of the X-ray radiation (using CuK_α = 0.154056 nm), β_{hkl} is the line width at half-maximum height in radians, and θ is the diffracting angle (Zielinska *et al.*, 2001; Sivalingam *et al.*, 2003).

The Brunauer-Emmett-Teller (BET) surface area of TiO_2 powders were determined using Coulter, model SA 3100. The infrared spectra were investigated by a Bruker EQUINOX 55, in the range 4000-400 cm^{-1}. Scanning electron microscopy (SEM) images were obtained using a JEOL JSM-5800LV electron microscope.

The diffuse reflectance spectra of the solid catalysts were performed on a Shimadzu UV-2401PC spectrophotometer. $BaSO_4$ was used as reference and the spectra were recorded in the range of 200-600 nm. The bandgap energy (E_g) of the catalyst was calculated by the Planck's equation,

$$E_g = \frac{hc}{\lambda} = \frac{1240}{\lambda} \qquad (2)$$

where E_g is the bandgap energy (eV), h is the Planck's constant, c is the light velocity (3×10^8 m/s), and λ is the

wavelength of the absorption edge (nm).

2.5 Culture of microorganisms

The bacteria, *E. coli* ATCC25922, *P. aeruginosa* ATCC27853, *B. subtilis* BGA, *S. aureus* ATCC25923, and MRSA DMST2054, were used for the antibacterial activity test for the photocatalyst. All bacteria were cultured overnight at 37°C in nutrient agar (NA). The density of final inocula contained 10^4 organisms/spot on the titanium dioxide. A bacterial inoculum was prepared by picking couple colonies of overnight growth culture into 1 mL nutrient broth and incubated them with agitation under aerobic condition at 35°C for 3 hrs. A 0.5 McFarland standard was used for visual comparison to adjust the suspension to a density equivalent to approximately 10^8 CFU/mL by using 0.85% saline solution. Then the suspensions of organisms was diluted in 0.85% saline solution to give 10^7 CFU/mL. Plates have been inoculated within 30 min to avoid any changes in the inoculum density.

2.6 Antibacterial activity test

Commercial anatase, rutile, Degussa P25, and the synthesized TiO_2 samples were used for all experiments. The method for testing the antibacterial activity is the agar dilution method to determine the minimal inhibitory concentration (MIC) of antimicrobial agents. The MIC is the lowest concentration of the agent that completely inhibits visible growth as judged by the naked eyes, disregarding a single colony or a thin haze within the area of the inoculated spot. The procedure, based on the recommendations from the Clinical and Laboratory Standard Institute (CLSI) for this method using a suspension of TiO_2 photocatalyst, was adapted to the agar dilution susceptibility test in this work (Approved standard M7-A4, 2002).

In each antibacterial test experiment, titanium dioxide agar plates were prepared in four concentrations 100, 50, 25, and 12.5 mg/ml in Mueller-Hinton agar (MHA). The weighed titanium dioxide powders were incorporated in 10 mL of melted MHA and poured into Petri dishes. The pH of each batch of medium was about 6.9. By using inoculum-replicating apparatus, the final inocula contained 10^4 CFU/spot, three spots/bacterial strain as shown in Figure 1. After inoculation, test plates were allowed to dry at room temperature before irradiation under UV light for a predetermined time was carried out.

The synthesized titanium dioxide agar plates were irradiated in an UV box, which contained five fluorescent blacklight tubes, 20 W each, with λ_{max} 366 nm (Random *et al.*, 2004). The sample plates were collected immediately after the titanium dioxide agar plates were exposed to UV light and subsequently every 30 min. The test plates were incubated at 35°C for 18 hrs. The results then were inspected visually and MIC values were recorded. All tests and inoculation on each plate were run in duplicate.

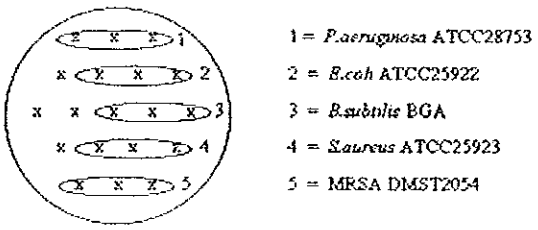

Figure 1. Titanium dioxide agar plate inoculated with various types of bacteria.

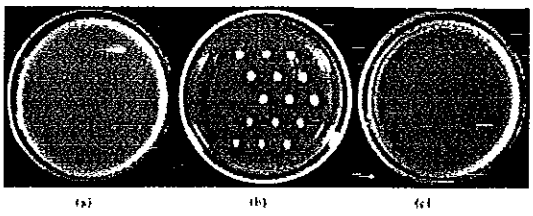

Figure 2. a) Agar plate with 25 mg/mL of TiO_2-200w-80H$_2SO_4$ irradiated under UV light for 30 min, b) control plate without TiO_2, and c) agar plate with 12.5 mg/mL of TiO_2-200w-80H$_2SO_4$ irradiated under UV light for 30 min.

A control plate was carried out under the same conditions with antibacterial activity test but without TiO_2 powders. Photographs of typical agar plates are shown in Figure 2.

3. Results and discussion

3.1 Physical properties of nanosized TiO_2 and Al(III)-, B(III)-doped TiO_2

The sol-gel method was used to synthesized the TiO_2 samples with two different acids, HCl and H_2SO_4, as catalysts in the hydrolysis process. The XRD results in Figure 3 show that varying the synthesis parameters affected the growth of anatase and rutile to some extent. When using H_2SO_4 or Al (III)-doped and prepared with a large amount of water the products were mainly amorphous TiO_2 with small amount of anatase phase. However, with HCl acid or Al(III)-doped and prepared with a small amount of water or B(III)-doped and prepared with a large amount of water mixtures of mainly amorphous titania with small amounts of both anatase and rutile phase were obtained. The presence of sulfate has been known to accelerate the growth of the TiO_2 cluster in the anatase phase. In this study, when H_2SO_4 was added as an acid catalyst in the hydrolysis process, the formation of anatase could be observed, since the SO_4^{2-} ion induced the growth of anatase phase (Zhang *et al.*, 1999; Zhang *et al.*, 2000; Karna and Wongnawa, 2008).

The surface area of these synthesized samples are relatively high (Table 1, last column) due to its low crystallinity.

Table 1. Physical properties of commercial and synthesized TiO_2 samples.

Sample	Crystallinity [a] (%)	Crystallite size [b] (nm)		BET (m^2/g)
		Anatase	Rutile	
Anatase	100 (A)	13.4	-	11.3
Rutile	100 (R)	-	11.6	13.1
Degussa P25	80 (A), 20 (R) [c]	10.1	11.6	65.9
TiO_2-200w-80HCl	13 (A), 6 (R)	6.7	6.7	250.2
TiO_2-200w-80H_2SO_4	15 (A)	5.4	-	320.1
TiO_2-Al-150w	23.4 (A)	6.7	-	277.1
TiO_2-Al-50w	9.1 (A), 11.5 (R)	5.4	4.5	244.9
TiO_2-B-150w	6.3 (A), 6.8 (R)	6.7	10.1	234.8
TiO_2-B-50w	48.3 (R)	-	6.4	106.6

[a] Determined by XRD using standard addition method, the rest is amorphous phase. A denotes anatase and R denotes rutile. [b] Calculated from XRD data.
[c] Stylidi *et al.* (2004)

It is the aim of our project to study the samples right from the synthesis without calcinations (Kanna and Wongnawa, 2008). Therefore, without the calcination, the samples remain mostly in the amorphous form with a small amount of crystalline phases (anatase and rutile) as shown by the XRD patterns in Figure 3. The small amount of each anatase phase or rutile phase was determined by using XRD data combined with the standard addition method and shown in the second column of Table 1. The crystallite sizes of anatase and rutile (column 3 and 4 of Table 1) were calculated from the Sherrer's formula (Equation 1). According to these sizes they can be classified as nanoparticles. The bandgap energies were obtained from the absorption edge wavelengths in Figure 4 and calculated by Equation 2. The corresponding numerical data are shown in Table 2. None of the bandgap energies show a significant deviation from the normal values of anatase and rutile.

The SEM images (Figure 5 and 6) show the morphology of the samples and appear to be constituted of spherical building units. The synthesized samples, which exist mostly in amorphous phase, show higher aggregation with the formation of bigger chunks than the commercial samples. This could be the result from the non-calcination at high temperature being applied.

3.2 Evaluation of antibacterial activity of TiO_2

The bactericidal activity of synthesized and commercial TiO_2 nanoparticles were evaluated by growth inhibition of *P. aeruginosa*, *E. coli* (the Gram-negative bacteria), and *B. subtilis*, *S. aureus*, MRSA (the Gram-positive bacteria). The Gram-positive bacteria have a relatively thick wall composed of many layers of peptidoglycan polymer and only one layer of membrane. The Gram-negative bacteria have only a thin layer of peptidoglycan and a more complex cell wall with two cell membranes, an outer membrane, and a plasma

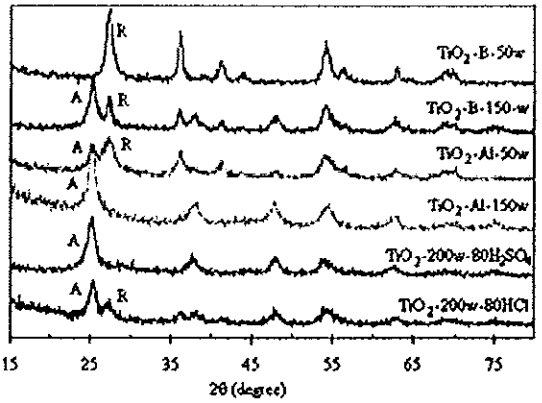

Figure 3. XRD patterns of all the synthesized TiO_2 samples; A denotes anatase and R denotes rutile.

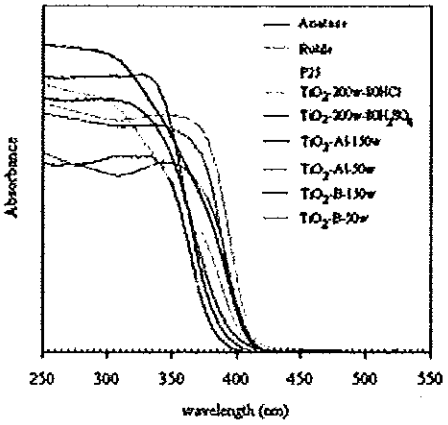

Figure 4. The diffused reflectance spectra of the commercial and the synthesized TiO_2 samples

Table 2. Absorption edge and band gap energy of commercial TiO_2 and synthesized TiO_2 samples.

Sample	Absorption edge (nm)	Bandgap energy [a] (eV)	
		This work	Literature
Anatase	383	3.24	3.20 [b]
Rutile	411	3.02	3.00 [b]
Degussa P25	395	3.14	3.14 [c]
TiO_2-200w-80HCl	406	3.05	-
TiO_2-200w-80H_2SO_4	394	3.15	-
TiO_2-Al-150w	385	3.22	-
TiO_2-Al-50w	405	3.06	-
TiO_2-B-150w	410	3.02	-
TiO_2-B-50w	411	3.02	-

[a] Calculated by Plank's equation: $E_g = 1240/\lambda$.
[b] Sclafani *et al.* (1990); Miao *et al.* (2003).
[c] Zielinska *et al.* (2003)

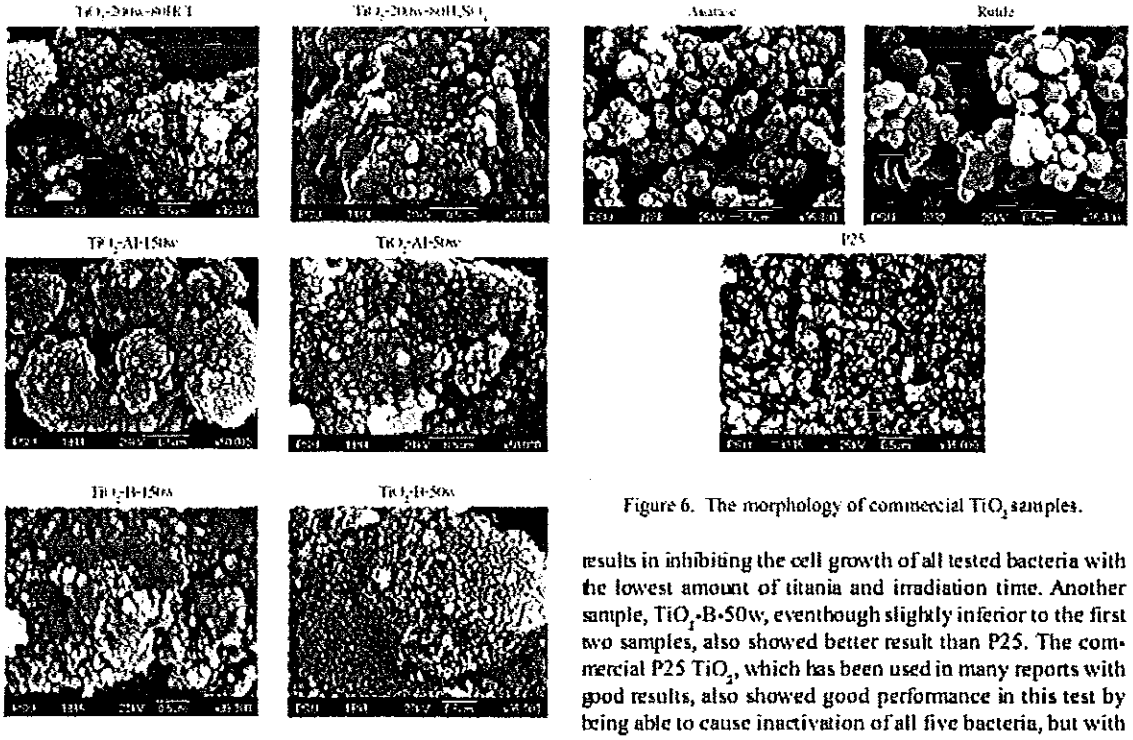

Figure 6. The morphology of commercial TiO_2 samples.

Figure 5. The morphology of synthesized TiO_2 samples.

membrane. Under certain conditions, the Gram-negative bacteria are more resistant to many chemical agents than the Gram-positive cells (Tortora *et al.*, 2001).

As shown in Table 3, two of the synthesized samples, TiO_2-200w-80H_2SO_4 and TiO_2-Al-150w, showed the best results in inhibiting the cell growth of all tested bacteria with the lowest amount of titania and irradiation time. Another sample, TiO_2-B-50w, eventhough slightly inferior to the first two samples, also showed better result than P25. The commercial P25 TiO_2, which has been used in many reports with good results, also showed good performance in this test by being able to cause inactivation of all five bacteria, but with higher MIC values than the first three samples. The commercial anatase TiO_2, usually showing slightly lower activity than P25 in the dye degradation study, fails to inactivate *S. aureus* and MRSA bacteria in this test. The commercial rutile did not show any activity at all for all the five bacteria, which is consistent with its poor performance found in the dye degradation study (Kanna and Wongnawa, 2008). Another two of the synthesized samples, TiO_2-Al-50w, TiO_2-B-150w,

Table 3. MIC values of TiO_2 samples with various bacteria.

TiO_2 samples	Irradiation time (min)	MIC (mg·mL)				
		P.aeruginosa	*E.coli*	*B.subtilis*	*S.aureus*	MRSA
Anatase	30	·	·	·	·	·
	60	12.5	·	·	·	·
	90	12.5	100	·	·	·
	120	12.5	12.5	100	·	·
Rutile	30	·	·	·	·	·
	60	·	·	·	·	·
	90	·	·	·	·	·
	120	·	·	·	·	·
Degussa P25	30	·	·	100	·	·
	60	100	100	50	100	100
	90	100	100	25	100	100
	120	100	100	25	100	100
TiO_2-200w-80HCl	30	·	·	·	·	·
	60	·	·	·	·	·
	90	·	·	·	·	·
	120	100	100	100	100	100
TiO_2-200w-80H_2SO_4	30	25	50	25	25	25
	60	25	25	25	25	25
	90	25	25	25	25	25
	120	25	25	25	25	25
TiO_2-Al-150w	30	50	100	50	50	50
	60	25	50	50	50	50
	90	25	50	25	25	25
	120	25	25	25	25	25
TiO_2-Al-50w	30	100	·	·	·	·
	60	100	100	100	·	·
	90	100	100	100	·	·
	120	50	50	50	100	100
TiO_2-B-150w	30	100	·	·	·	·
	60	100	100	100	·	·
	90	100	100	100	·	·
	120	50	50	50	100	100
TiO_2-B-50w	30	100	·	12.5	25	100
	60	100	·	12.5	25	50
	90	50	·	12.5	25	50
	120	50	100	12.5	25	50

* (·) represent the bacterial growth equal to the control (no inhibition)

showed respectable results with all five bacteria. The last one, TiO_2-200w-80HCl, eventhough it could inactivate all five bacteria, it needed a long irradiation time with high MIC values compared with all the synthesized samples in this study. In summary, it is interesting to see that all of the six synthesized samples could inactivate all five bacteria in this screening test albeit with varying MIC values. In comparison with P25, three samples showed better antibacterial activity than P25. The order of performance can be arranged as follows:

TiO_2-200w-80H_2SO_4 > TiO_2-Al-150w > TiO_2-B-50w > P25 > TiO_2-Al-50w ≈ TiO_2-B-150w > TiO_2-200w-80HCl > anatase > rutile.

With regard to the photocatalytic activity, there have been

many reports that the anatase shows higher activivty than the rutile in many photocatalytic reactions in air and water (Mills and Sawunyama, 1994; Sclafani and Herrmann, 1996; Lucarelli *et al.*, 2000; Sato and Taya, 2006) except in some cases (Ohno *et al.*, 1997). The effect of crystalline structures on biocidal activity of TiO_2 particles has been clarified by investigating the photocatalytic deactivation of phage MS2 in suspensions of anatase TiO_2 and rutile TiO_2 as well as their mixtures. The results showed that the contact between both types of TiO_2 particles in aggregations caused the enhancement of the quantum yield of the TiO_2 suspension, thereby the generation of reactive oxygen species from photocatalytic reaction, which leads to the enhancement of biocidal activity of the photocatalytic particles (Sato and Taya, 2006). In another study, the photocatalytic process of anatase has been shown to produce highly reactive species, such as hydroxyl radical, hydrogen peroxide, and superoxide, which, in principle, can cause fatal damage to microorganisms by injury of the cell membranes when bacteria come into contact with the TiO_2 surface (Sunada *et al.*, 1998).

Most of the recent research on the inhibition of bacterial cell growth (Gumy *et al.*, 2006a; Gumy *et al.*, 2006b; Verran *et al.*, 2007) have been studied by using the suspended-TiO_2 in solution. In suspension, TiO_2 nanoparticles were trapped onto the bacteria surface resulting in the adsorption of TiO_2 particles on the bacteria surface, which could lead to the inactivation of bacteria in coopte with the photocatalytic oxidation reaction described above. In this study, the agar dilution method was chosen to eliminate the possibility of inactivation by surface adsorption, hence the inactivation results could be said to come solely from the photocatalytic property of the photocatalysts. In this method, the TiO_2 nanoparticles were fixed in agar and would not be adsorbed onto the bacterial surface. The disadvantage of this method is that, due to the fixed TiO_2 particles in the agar matrix, a higher concentration of the photocatalyst is required, and, hence, the MIC values from this method would be higher than that from the suspension method.

Our results as mentioned above showed that the antibacterial activity of the synthesized anatase-type TiO_2, TiO_2-200w-$80H_2SO_4$ and TiO_2-Al-150w, are more effective than the commercial P25. It is rather difficult to rationalize this surprising behavior. When discussing the photocatalytic activity, the parameters such as bandgap energy, surface area, crystallinity, and phases are usually of prime concerns. The bandgap energy, however, does not seem to be a major factor in this case since the bandgap of TiO_2-B-50w, the third best performer, is only 3.02 eV, which is low compared to the top two performers, TiO_2-200w-$80H_2SO_4$ and TiO_2-Al-150w, with 3.15 and 3.22 eV, respectively. A pure single anatase phase is active while a pure rutile phase does not show any activity, whereas in the TiO_2-B-50w case it is a mixture of amorphous and rutile phase. Although the clear explanation for the high activity of P25 is still unknown, there seems to have a belief that it is the result of a synergetic effect between the mixed phases of anatase and rutile plus the high crystallinity (Ohno *et al.*, 2001; Ohno *et al.*, 2003). The generally good performance shown by all the six synthesized samples in this work can be narrowed down to their uncalcined nature during the syntheses. Without the calcination, (1) the products are mainly amorphous with a small amount of anatase and/or rutile mixed in, (2) the products have low crystallinity and small crystallite sizes, hence large surface areas. The small crystallite sizes may help disperse the particles within the agar matrix better than the larger ones, ensuring an evenly high concentration of photocatalysts within the agar matrix as well as the agar surface resulting in good inactivation activities. When irradiated with UV light, the reactive oxygen species are generated from the TiO_2 centers at the agar surface and come into contact with bacteria, and by this operate in concert to attack the polyunsaturated phospholipids in the bacteria. The lipid peroxidation reaction causes a breakdown function is the mechanism underlying cell death. The attack by reactive species generated by the photocatalytic process outside the cell is very likely the initial mode of killing that is observed for bacteria and other cell types (Maness *et al.*, 1999).

4. Conclusions

In this study, photocatalyst TiO_2 powders in anatase or rutile or a mixture of anatase and rutile phases have been synthesized from an aqueous solution of $TiCl_4$ by sol-gel process. No calcination at high temperature was applied to these syntheses. The product TiO_2 composed of mainly amorphous phase with a small amount of anatase or rutile or a mixture of both. These samples were tested for antibacterial activity in comparison with the commercial products, anatase, rutile, and Degussa P25. All the six synthesized samples showed inactivation activity towards bacteria, two of them showed a higher activity than Degussa P25.

Acknowledgements

This work was supported by the Songklanagarind Scholarship for Graduate Studies from the Prince of Songkla University.

References

Approved standard M7-A4. 2002. Reference methods for dilution antimicrobial susceptibility tests for bacteria that grow aerobically, Clinical and Laboratory Standards Institute (CLSI), Wayne, PA, USA.

Benabbou, A.K., Derriche, Z., Felix, C., Lejeune, P., and Guillard, C. 2007. Photocatalytic inactivation of *Escherischia coli*: effect of concentration of TiO_2 and microorganism, nature, and intensity of UV irradiation. Applied Catalysis B: Environmental. 76, 257-263.

Cho, M., Chung, H., Choi, W., and Yoon, J. 2004. Linear correlation between inactivation of *E.coli* and OH radical concentration in TiO_2 photocatalytic disinfec-

tion. Water Research. 38, 1069-1077.

Dadjour, M.F., Ogino, C., Matsumura, S., Nakamura, S., and Shimizu, N. 2006. Disinfection of *Legionella pneumophila* by ultrasonic treatment with TiO_2. Water Research. 40, 1137-1142.

Fernández, P., Blanco, J., Sichel, C., and Malato, S. 2005. Water disinfection by solar photocatalysis using compound parabolic collectors. Catalysis Today. 101, 345-352.

Gopal, M., Chan, W.J.M., and Jonghe, L.C.D. 1997. Room temperature synthesis of crystalline metal oxides. Journal of Materials Science. 32, 6001-6008.

Guisy, D., Morais, C., Bowen, P., Pulgarin, C., Giraldo, S., Hajdu, R., and Kiwi, J. 2006a. Catalytic activity of commercial of TiO_2 powders for the abatement of the bacteria (*E. coli*) under solar simulated light: influence of the isoelectric point. Applied Catalysis B: Environmental. 63, 76-84.

Guisy, D., Rincon, A.G, Hajdu, R., and Pulgarin, C. 2006b. Solar photocatalysis for detoxification and disinfection of water: different types of suspended and fixed TiO_2 catalysts study. Solar Energy. 80, 1376-1381.

Hoffmann, M.R., Martin, S.T., Choi, W., and Bahnemann, D.W. 1995. Environmental applications of semiconductor photocatalysis. Chemical Reviews. 95, 69-96.

Huang, Z., Maness, P.C., Blake, D.M., Wolfrum, E.J., Smolinski, S.L., and Jacoby, W.A. 2000. Bactericidal mode of titanium dioxide photocatalysts. Journal of Photochemistry and Photobiology A: Chemistry. 130, 163-170.

Ibanez, J.A., Litter, M. I., and Pizarro, R.A. 2003. Photocatalytic bactericidal effect of TiO_2 on *Enterobacter cloacae*: comparative study with other Gram (+) bacteria. Journal of Photochemistry and Photobiology A: Chemistry. 157, 81-85.

Ireland J.C., Klostermann P., Rice E.W., and Clark R.M. 1993. Inactivation of *Escherichia coli* by titanium dioxide photocatalytic oxidation. Applied and Environment Microbiology. 59, 1668-1670.

Jacoby, W.A., Maness, P.C., Wolfrum, E.J., Blake, D.M., and Fennell, J.A. 1998. Mineralization of bacterial cell mass on a photocatalytic surface in air. Environmental Science and Technology. 32, 2650-2653.

Kanna, M. and Wongnawa, S. 2008. Mixed amorphous and nanocrystalline TiO_2 powders prepared by sol-gel method: characterization and photocatalytic study. Materials Chemistry and Physics. 110, 166-175.

Legrini, O., Oliveros, E., and Braun, A.M. 1993. Photochemical processes for water treatment. Chemical Reviews. 93, 671-679.

Lin, C.Y. and Li, C.S. 2003. Inactivation of microorganisms on the photocatalytic surfaces in air. Aerosol Science and Technology. 37, 939-946.

Lonnen, J., Kilvington, S., Kehoe, S.C., Al-Touati, F., and McGuigan, K.G. 2005. Solar and photocatalytic disinfection of protozoan, fungal and bacterial microbes in drinking water. Water Research. 39, 877-883.

Lucarelli, L., Nadtochenko, V., and Kiwi, J. 2000. Environmental photochemistry: quantitative adsorption and FTIR studies during the TiO_2-photocatalyzed degradation of Orange II. Langmuir. 16, 1102-1108.

Maness, P.C., Smolinski, S., Blake, D.M., Huang, Z., Wolfrum, E.J., and Jacoby, W.A. 1999. Bactericidal activity of photocatalytic TiO_2: toward an understanding of its killing mechanism. Applied and Environment Microbiology. 65, 4094-4098.

Matsunaga, T., Tomoda, R., Nakajima, T., and Wake, H. 1985. Photoelectrochemical sterilization of microbial cells by semiconductor powders. Federation of European Microbiological Societies Microbiology Letters. 29, 211-214.

Miao, L., Jin, P., Kaneko, K., Terai, A., Nabatova-Gabain, N., and Tanemura, S. 2003. Preparation and characterization of polycrystalline anatase and rutile TiO_2 thin films by rf magnetron sputtering. Applied Surface Science. 212-213, 255-263.

Mills, A. and Sawunyama, P. 1994. Photocatalytic degradation of 4-chlorophenol mediated by TiO_2: a comparative study of the activity of laboratory made and commercial TiO_2 samples. Journal of Photochemistry and Photobiology A: Chemistry. 84, 305-309.

Mills, A. and Hunte, L.S. 1997. An overview of semiconductor photocatalysis. Journal of Photochemistry and Photobiology A: Chemistry. 108, 1-35.

Ohno, T., Haga, D., Fujihara, K., Kaizaki, K., and Matsumura, M. 1997. Unique effects of Iron(III) ions on photocatalytic and photoelectrochemical properties of titanium dioxide. Journal of Physical Chemistry B. 101, 6415-6419.

Ohno, T., Sarukawa, K., Tokieda, K., and Matsumura, M. 2001. Morphology of a TiO_2 photocatalyst (Degussa, P-25) consisting of anatase and rutile crystalline phases. Journal of Catalysis. 203, 82-86.

Ohno, T., Tokieda, K., Higashida, S., and Matsumura, M. 2003. Synergism between rutile and anatase TiO_2 particles in photocatalytic oxidation of naphthalene. Applied Catalysis A: General. 244, 383-391.

Oaki M., Hirada T., and Ohgaki S. 2000. Aqueous microorganisms inactivation by photocatalytic reaction. Water Science and Technology. 42, 103-108.

Pal, A., Pehkonen, S.O., Yu, L.E., and Ray, M.B. 2007. Photocatalytic inactivation of Gram-positive and Gram-negative bacteria using fluorescent light. Journal of Photochemistry and Photobiology A: Chemistry. 186, 335-341.

Random, C., Wongnawa, S., and Boonsin, P. 2004. Bleaching of methylene blue by hydrated titanium dioxide. Science Asia. 30, 149-156.

Rincón, A.G. and Pulgarin, C. 2003. Photocatalytic inactivation of *E. coli*: effect of (continuous-intermittent) light

intensity and of (suspended-fixed) TiO_2 concentration. Applied Catalysis B: Environmental. 44, 263-284.

Rincón, A.G. and Pulgarin, C. 2004. Effect of pH, inorganic ions, organic matter and H_2O_2 on *E. coli* K12 photocatalytic inactivation by TiO_2: implications in solar water disinfection. Applied Catalysis B: Environmental. 51, 283-302.

Rincón, A.G. and Pulgarin, C. 2006. Comparative evaluation of Fe^{3+} and TiO_2 photoassisted process in solar photocatalytic disinfection of water. Applied Catalysis B: Environmenta.. 63, 222-231.

Sato, T. and Taya, M. 2006. Enhancement of phage inactivation using photocatalytic titanium dioxide particle with different crystalline structures. Biochemical Engineering Journal. 28, 303-308.

Sclafani, A., Palmisano, L., and Schiavello, M. 1990. Influence of the preparation methods of titanium dioxide on the photocatalytic degradation of phenol in aqueous dispersion. Journal of Physical Chemistry. 94, 829-832.

Sclafani, A. and Herrmann, J.M. 1996. Comparison of the photoelectronic and photocatalytic activities of various anatase and rutile forms of titania in pure liquid organic phase and in aqueous solutions. Journal of Physical Chemistry. 100, 13655-13661.

Sichel, C., de Cara, M., Tello, J., Blanco, J., and Fernandez-Ibáñez, P. 2007. Solar photocatalytic disinfection of agricultural pathogenic fungi: *Fusarium* species. Applied Catalysis B: Environmental. 74, 152-160.

Sivalingam, G., Nagaveni, K., Hegde, M.S., and Madras, G. 2003. Photocatalytic degradation of various dyes by combustion synthesized nano anatase TiO_2. Applied Catalysis B: Environmental. 45, 23-38.

Sökmen, M., Değerli, S., and Aslan, A. 2008. Photocatalyite disinfection of *Giardia intestinalis* and *Acanthamoeba castellani cysts* in water. Experimental Parasitology. 119, 44-48.

Stylidi, M., Kondarides, D.I., and Verykios, X.E. 2004. Visible light-induced photocatalytic degradation of acid orange 7 in aqueous TiO_2 suspensions. Applied Catalysis B: Environmental. 47, 189-201.

Sunada, K., Kikuchi, Y., Hashimoto, K., and Fujishima, A. 1998. Bactericidal and detoxification effects of TiO_2 thin film photocatalysts. Environmental Science and Technology. 32, 726-728.

Suwanchawalit, C. 2005. The effect of metal-doping on the physical and photocatalytic properties of nanosized TiO_2 powder. M.S. Thesis, Prince of Songkla University, Thailand.

Tortora, G., Funke, R.B., and Case, L.C. 2001. Microbiology: An Introduction, Addison-Wesley Longman, Inc., New York, USA.

Verran, J., Sandoval, G., Allen, N.S., Edge, M., and Stratton, J. 2007. Variables affecting the antibacterial properties of nano and pigmentary titania particles in suspension. Dyes and Pigments. 73, 298-304.

Yao, K.S., Wang, D.Y., Ho, W.Y., Yan, J.J., and Tzeng, K.C. 2007. Photocatalytic bactericidal effect of TiO_2 thin film on plant pathogens. Surface and Coatings Technology. 201, 6886-6888.

Zhang, Q.H., Guo, J.K., and Gao, L. 1999. Preparation and characterization of nanosized TiO_2 powders from aqueous $TiCl_4$ solution. Nanostructured Materials. 11, 1293-1300.

Zhang, Q., Guo, J., and Gao, L. 2000. Effect of hydrolysis conditions on morphology and crystallization of nanosized TiO_2 powder. Journal of European Ceramic Society. 20, 2153-2158.

Zielińska, B., Grzechulska, J., Grzmil, B., and Morawski, A.W. 2001. Photocatalytic degradation of Reactive Black 5: a comparison between TiO_2-Tytanopol A11 and TiO_2 Degussa P25 photocatalysts. Applied Catalysis B: Environmental. 35, L1-L7.

Zielińska, B., Grzechulska, J., Kaleńczuk, R.J., and Morawski, A.W. 2003. The pH influence on photocatalytic decomposition of organic dyes over A11 and P25 titanium dioxide. Applied Catalysis B: Environmental. 45, 293-300.

J Sol-Gel Sci Technol (2010) 56:53–58
DOI 10.1007/s10971-010-2272-z

ORIGINAL PAPER

Nanosized TiO_2 particles decorated on SiO_2 spheres (TiO_2/SiO_2): synthesis and photocatalytic activities

Uraiwan Sirimahachai · Nicholas Ndiege · Ramesh Chandrasekharan · Sumpun Wongnawa · Mark A. Shannon

Received: 30 November 2009 / Accepted: 19 June 2010 / Published online: 31 August 2010

Abstract Nanosized TiO_2 and nano-anatase TiO_2 decorated on SiO_2 spherical core shells were synthesized by using a sol–gel method. The synthesized pure TiO_2 nano particle and TiO_2 grafted on SiO_2 sphere with various ratios have been characterized for their structure and morphologies by X-ray diffraction (XRD), X-ray photoelectron spectroscopy (XPS), Fourier transform infrared spectrophotometry (FTIR) and transmission electron microscopy (TEM). Their surface areas were measured using the BET method. The photocatalytic activity of all nanocomposites was investigated using methylene blue as a model pollutant. The synthesized TiO_2/SiO_2 particles appeared to be more efficient in the degradation of methylene blue pollutant, as compared to pure TiO_2 particles.

Keywords Nanosized TiO_2/SiO_2 · Sol–gel · TiO_2 photocatalyst · SiO_2 core shell · Methylene blue degradation

U. Sirimahachai · S. Wongnawa
Department of Chemistry, Faculty of Science, Prince of Songkla University, 15 Kanjanavanich Road, Ko-hong, Hat Yai, Songkhla 90112, Thailand

N. Ndiege · M. A. Shannon
School of Chemical Sciences, University of Illinois at Urbana-Champaign, 600 South Mathews Avenue, Urbana, IL 61801, USA

R. Chandrasekharan · M. A. Shannon (✉)
Mechanical Science and Engineering, University of Illinois at Urbana-Champaign, 1206 West Green Street, Urbana, IL 61801, USA
e-mail: mshannon@illinois.edu

1 Introduction

Titanium dioxide (TiO_2) has been extensively employed as a photocatalytic material for solving environmental problems, especially for eliminating toxic chemicals from wastewater [1, 2]. Many applications and uses of supported metal oxides on silica have recently attracted much attention as advanced support materials substituting pure TiO_2 because of their higher mechanical strength, thermal stability and specific surface area [3, 4]. Silica-modified TiO_2 was reported to exhibit a better photocatalytic performance than TiO_2 itself. This improved performance was believed to have come from multiple sources, namely: the interaction between TiO_2 and SiO_2, improved adsorption of the pollutant on the silica over pure TiO_2, as well as the TiO_2 supported on silica having a different structure from bulk TiO_2. These materials have been considered for use not only as catalytic supports, but also as catalysts through the generation of new catalytic active sites [5–7]. It is well known that silica surface is fairly inert, however, the silica surface hydroxyls generally act as adsorptive/reactive sites because of their hydrophilic character. Thus, the preparation of highly dispersed metal oxides on silica often involves highly reactive precursors, such as titanium alkoxides or $TiCl_4$, which readily react with the surface hydroxyls of the silica support [4, 6]. The effect of incorporation of silica on the behavior of titania-based photocatalysts prepared by a sol–gel technique showed that the decomposition of rhodamine-6G by the titania/silica mixed oxide with a ratio 30/70 produced the highest activity, about three times higher than the Degussa P25 Titania [8].

It is well-known that the preparation method, the surface area, and the concentration of the surface hydroxyls on the silica surface can strongly influence the dispersion capacity

and the maximum surface coverage of surface titanium oxide species on silica. Depending on the titanium loading, often indicated as percentage by weight of TiO_2, different types of titanium species could be present, ranging from dispersed surface TiO_x species, both in tetrahedral and octahedral coordination, to small TiO_2 crystallites. The relative amount depends on the preparation conditions and chemical compositions.

In this work, nanosized pure TiO_2 and nanosized TiO_2 grafted on SiO_2 sphere (TiO_2/SiO_2) were prepared by the sol–gel method using titanium tetraisopropoxide (TTIP) and methyl-trimethoxysilane (MTMS) as precursors. The morphologies of these compounds comprised of nanosized TiO_2 decorated on SiO_2 spheres, but were different from previous literature [9], as will be later described. The physical properties of TiO_2/SiO_2 particles were investigated by FT-IR, XRD, and XPS. We also determined the effect that the amount of TiO_2 grafted on SiO_2 had on the physical properties of nanosized TiO_2/SiO_2 particles. In addition, their photocatalytic activities on the decomposition of methylene blue was also investigated. The effect of this particular decoration of titanium metal oxide onto the silicon metal oxide will be discussed with respect to the observed enhanced photocatalytic activity.

2 Experimental

2.1 Catalysts preparation

2.1.1 Preparation of TiO_2 sols

TiO_2 sols were prepared according to the method previously reported [9]. 5 ml of titanium tetraisopropoxide (TTIP, Aldrich, 99.99%) was added dropwise into 100 mL acidic water containing 1 mL nitric acid and 10 mL acetic acid under vigorous stirring. Then the mixture was refluxed at 60 °C while stirring for 20 h.

2.1.2 Preparation of SiO_2 spheres

Silica spherical core–shell structure with particle size around 400 nm was prepared as follows: 2.5 mL of methyl-trimethoxysilane (MTMS, Sigma 98%) was added to 100 mL of 1×10^{-4} M nitric acid aqueous solution that was heated to 60 °C while vigorous stirring was maintained. Then 2.5 mL ammonia was added to the solution. A milky silica solution was attained. SiO_2 powder was extracted by centrifuging the milky suspension of silica, and the supernatant removed.

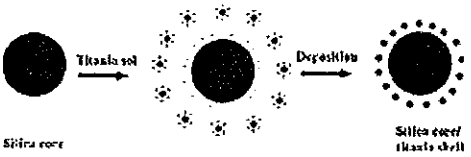

Scheme 1 The formation mechanism of TiO_2 grafted on SiO_2 sphere [9]

2.1.3 Synthesis of TiO_2 decorated on SiO_2 particles

The as-synthesized SiO_2 powder was added to different relative weight percentages of TiO_2 sols. Then the mixture was dispersed in an ultrasonic bath for 15 min. The TiO_2/SiO_2 mixture was kept for 24 h to form TiO_2 grafted on SiO_2 spherical core–shell structure. The formation mechanism of TiO_2 grafted on SiO_2 sphere was shown in Scheme 1. The suspension mixture then was filtered and calcined in air at 500 °C for 3 h. Different amounts of titania decorated on SiO_2 sphere formed different grafted patterns related to spacing and clumping of TiO_2 particles on SiO_2 surface.

2.2 Products characterization

The crystal structure of powder was analyzed by X-ray diffraction (XRD). XRD study was done on a Rigaku D-Max X-ray powder diffractometer (Rigaku Corporation, Tokyo, Japan) with Ni-filtered CuKα (0.15418 nm) radiation at 45 kV and 20 mA. The crystallite size was calculated by using the Scherrer formula.

$$L = \frac{K\lambda}{\beta_{hkl}\cos\theta} \quad (1)$$

where L is the average crystallite size in nm, K is a constant usually taken as 0.9, λ is the wavelength of the X-ray radiation (using CuK_α = 0.154056 nm), β_{hkl} is the line width at half-maximum height in radians, and θ is the diffracting angle [10, 11].

The Brunauer-Emmett-Teller (BET) surface area of TiO_2 powders was determined using a Coulter model SA3100 analyzer. The infrared spectra were investigated by a Bruker EQUINOX 55, in the range 4000–400 cm^{-1}. Scanning Electron Microscopy (SEM) observations were carried out using a JEOL JSM-5800LV electron microscope.

The composition of the powder was determined by X-ray photoelectron spectroscopy (XPS). XPS measurements were performed on a Physical Electronics PHI 5400 X-ray Photoelectron Spectrometer (Perkin-Elmer Corporation, Eden Prairie, MN) with an Mg K anode (1253.6 eV photon energy, 15 kV, 300 W) at a take-off angle of 45°.

Multiplex XPS spectra of O 1 s, Ti 2p, Si 2p were recorded using a band-pass energy of 178.95 eV corresponding to an energy resolution of 1.0 eV. The atomic concentrations of these elements were obtained by comparing the peak areas of their spectra.

The morphology of the powder was investigated by scanning electron microscopy (SEM) and transmission electron microscopy (TEM). A SEM sample was made by applying powder sample on the a conductive carbon tape, the sample was sputtered with gold for 25 s (Emitech K575 Sputter Coater, Emitech Ltd., Ashford, U.K.) before imaging. The SEM image was performed on a Hitachi S-4700 scanning electron microscope (Hitachi Ltd., Tokyo, Japan). A TEM sample was made by dispersing a thin film of powder sample on a Cu grid. The TEM observation was performed on a JEOL 2010LaB6 transmission electron microscope (JEOL Ltd., Tokyo, Japan) operated at 200 kV, with a point-to-point resolution of 0.28 nm.

2.3 Photodegradation of methylene blue

In order to quantify the effectiveness of a photocatalyst for water decontamination and also to explore techniques to increase photo efficiency, it is necessary to come up with methodologies to quantify the photochemical and photoelectrical properties of photocatalysts. Usually, photocatalyst decontamination performance is evaluated by quantifying the photochemical degradation rate for either an actual pollutant or a model pollutant such as a dye with a specific absorption peak in the visible, e.g. methylene blue. The photoreactions are done by shining UV light on slurry of the photocatalyst powder and measuring the degradation rate of the pollutant. The limitation of such a system lies in the difficulty of quantifying transport of light and the reactants and products to and from the surface of the photocatalysts. The actual amount of light that reaches each individual photocatalyst particle is hard to quantify given the scattering of UV off the photocatalyst powder particles and absorption by the water and the pollutant in them. Similarly, the reactive-diffusion of pollutants and products is hard to quantify given the lack of knowledge of light intensity at the particle and also the distribution of the particles in the slurry. Given this limitation in correctly quantifying transport properties, accurately comparing photocatalysts that are different from each other in particle size and optical (scattering) characteristics is not possible. In this work, we used a fixed bed reactor in order to be able to compare photocatalysts undergoing the same photon flux and attenuation within the fixed bed, instead of having large variations in flux that occurs with slurry. The fixed bed makes it possible to maintain similar light and species transport conditions across samples thus enabling more direct comparison in photocatalytic activity.

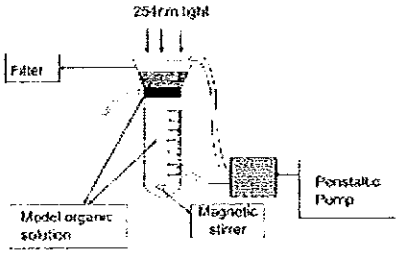

Fig. 1 Experimental setup to measure photochemical degradation of methylene blue [12]

A schematic of the experimental system is shown in Fig. 1. A packed bed of ~1–2 mm of the photocatalyst is spread on top of a nanoporous filter and an aqueous solution of the target pollutant is circulated through this bed. The light source used was a 254 nm UV lamp.

The initial concentration of the methylene blue was 10^{-5} M. The aqueous solution of the organic molecules is re-circulated through the photocatalyst bed using a peristaltic pump. Prior to illumination using UV light, the aqueous solutions are circulated through the samples for at least 2 h in the dark. This dark adsorption helps to differentiate between the photodegradation and the adsorption of the pollutant onto the samples. Subsequent to irradiation by UV light, samples are collected once every 10 min and the concentration of the methylene blue was determined using a Cary 5G UV–Vis spectrometer. The 660 nm methylene blue peak along with Beer Lambert's law is used to quantify the methylene blue concentration.

3 Results and discussion

Figure 2 shows the XRD patterns of SiO_2, TiO_2, and nanosized TiO_2/SiO_2 (with varying weight percentage of TiO_2) samples. All were calcined under the same condition in air at 500 °C for 3 h. TiO_2 and nanosized TiO_2/SiO_2 showed a clear anatase-type crystal structure. The sharp peaks and strong intensities indicated that crystallization was present, and the higher the percentage of TiO_2 gave higher intensity of peaks. The peak associated with SiO_2 show that it is an amorphous form of silica. The crystallite sizes of Titania and TiO_2/SiO_2 are listed in Table 1.

From the crystallite size and BET surface area data in Table 1, it appears that the amount of SiO_2 sphere has an effect on the crystallite size of grafted nanosized TiO_2, with higher amount of SiO_2 resulting in smaller crystallite size, and larger surface area of TiO_2 particles. This effect may be due to the SiO_2 limiting the agglomeration of TiO_2 particles.

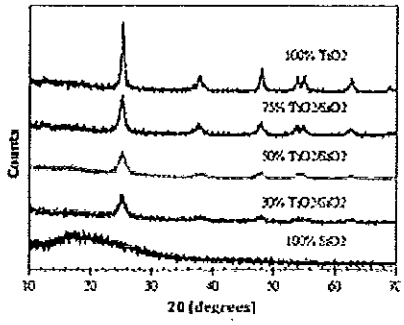

Fig. 2 X-ray diffraction patterns of SiO_2, TiO_2, and TiO_2/SiO_2 (with various relative weight percent of TiO_2 on SiO_2) obtained by calcining powder samples in air for 3 h at 500 °C

Table 1 The crystallite size and BET surface area of TiO_2 and TiO_2 grafted on SiO_2

Catalysis	Phase	Crystallite size (nm)	BET surface area (m^2/g)
100% SiO_2	Amorphous	–	11.57
30% TiO_2/SiO_2	Anatase	6.8	367.58
50% TiO_2/SiO_2	Anatase	6.0	211.87
75% TiO_2/SiO_2	Anatase	8.5	148.47
100% TiO_2	Anatase	16.2	54.491

3.1 FTIR

In Fig. 3, the transmittance spectra of nanosized TiO_2 and TiO_2 grafted on SiO_2 sphere with various relative weight percent of TiO_2 are presented. The band centered near 3,740 cm^{-1} which shows up in the case of pure SiO_2 and 75% TiO_2/SiO_2, has been assigned to silanols (single Si–OH groups and geminal $Si(OH)_2$ group) that are completely unassociated, or very weakly associated sites. The feature near 3,670 cm^{-1} is due to vicinal silanols that undergo mutual hydrogen bonding. The broad band centered near 3,500 cm^{-1} has been assigned to sites that interact with residual physisorbed water [13]. The band at 1,630 cm^{-1} observed in all spectra are attributed to stretching mode of hydroxyl [14, 15]. In pure SiO_2, the bands at 820 cm^{-1} and 1,120 cm^{-1} are ascribed to the symmetric vibration of Si–O–Si and the asymmetric stretching vibration of Si–O–Si, respectively [14, 16]. In the nanosized TiO_2/SiO_2 samples, the peaks of Si–O–Si asymmetric stretching mode are split into 2 peaks (1,140; 1,040 cm^{-1}) when disorder of the structure is introduced [17]. The wavenumber of 940–960 cm^{-1} indicate the band for Ti–O–Si, while the vibration Si–O–Si stretching are in

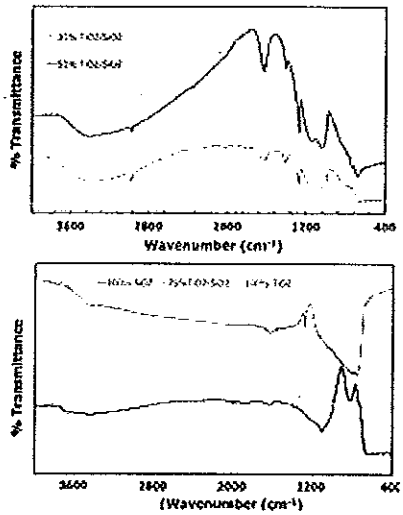

Fig. 3 The FTIR spectra of as-synthesized TiO_2 and different ratio of TiO_2/SiO_2

the range 1,050–1,120 cm^{-1} [18]. The spectrum of 75% TiO_2/SiO_2 sample observed was similar to pure TiO_2.

3.2 TEM

Morphology and size of the silica and Titania particles were examined using TEM. Figure 4 shows the TEM images of calcined 30, 50 and 75% of TiO_2 grafted on SiO_2 spheres. This result shows that the particle size of silica is about 100 times bigger than TiO_2 particles. The average particle size of the Titania particles was around 3 nm while the SiO_2 sphere core shell averaged around 350 nm. TiO_2 particles were deposited on the surface of SiO_2 sphere only partially, without complete coverage (Fig. 4a). On a closer inspection, TiO_2 particle agglomeration can be seen in Fig. 4b, while in Fig. 4c, with the highest percentage of TiO_2, deposition of particles became denser leading to higher order of crystallinity (less defect/grain boundary concentration) as evidenced by the smoother surface on the TiO_2.

The intensities of XRD peaks increased directly with increasing amount of TiO_2 deposited on SiO_2 sphere. It is interesting to note that the specific surface area decreased as the percentage of TiO_2 increased. The reason for this could be that as the amount of TiO_2 increases, it selectively deposits on the TiO_2 already present. Hence, complete coverage of SiO_2 sphere was not observed (Fig. 4a). Furthermore, at 75% TiO_2 the deposited chunk of TiO_2

J Sol-Gel Sci Technol (2010) 56:53–60

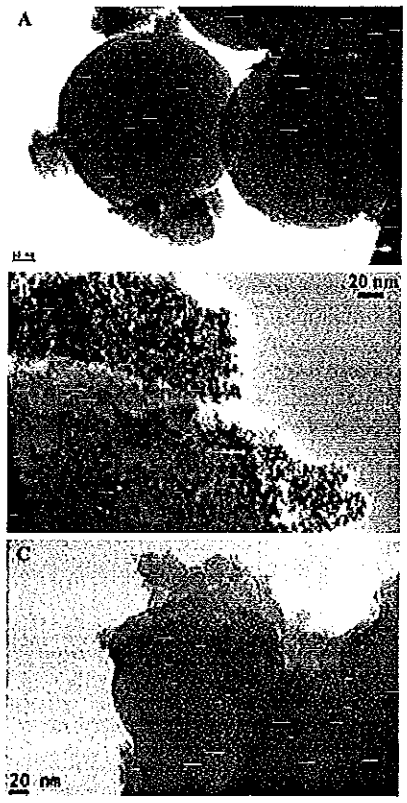

Fig. 4 TEM images for nanosized a 30%, b 50% and c 75% of TiO_2 on SiO_2 sphere core shell

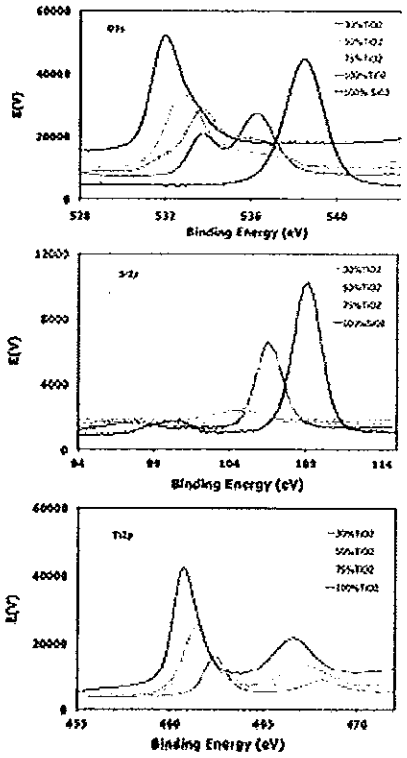

Fig. 5 X-ray photoelectron spectroscopy multiplex high-resolution scans over Si(2p), Ti($2p_{3/2}$) and O(1 s) spectra regions of nanosized TiO_2 grafted on SiO_2 sphere

became more crystalline (as mentioned above) resulting in lower surface area and also slightly larger crystallite size (Table 1).

3.3 XPS

Si(2p), Ti(2p) and O(1 s) photoelectron peaks of nanosized TiO_2 grafted on SiO_2 sphere annealed at 500 °C for 3 h are presented in Fig. 5. The binding energy (BE) of Si(2p) peak was at 108.9 eV for pure SiO_2 sphere. The BE of Si(2p) are shifted towards lower values as the amount of TiO_2 increased in the grafting. The BE of the Ti($2p_{3/2}$) for the pure TiO_2 was 460.7 eV, which shifted upwards as the amount of SiO_2 increased. The major O(1 s) peak was at 531.9 eV and 538.4 eV for the pure TiO_2 and pure SiO_2, respectively. Both peaks are shown in TiO_2 grafted on SiO_2. The intensity of O(1 s) peak, which belongs to SiO_2 was decreased with increasing the percentage of TiO_2 grafted on SiO_2 as expected. The trends of BE shift observed above support the incorporation of TiO_2 onto the surface of SiO_2 by the grafting method. When TiO_2 was introduced onto the pristine SiO_2 surface, the formation of Si–O–Ti took place as evidenced by the BE shift. Ti has lower electronegativity than Si (and likewise for Ti(IV) to Si(IV)). By forming such bridges, Si becomes more electron rich, hence its BE shifting to lower energy while Ti becomes more positive with its BE shifting to higher energy. This effect passes onto oxygen atoms as we can see the BE of Ti-linked oxygens shift to higher energy and Si-linked oxygens shift to lower energy. The intensities of these XPS peaks also reflect the percentages of TiO_2 grafted into SiO_2.

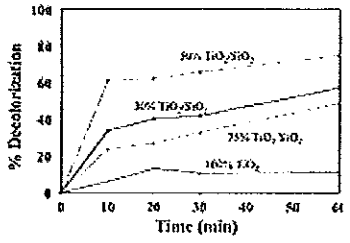

Fig. 6 Decolorization of methylene blue solution with different ratio of nanoparticle TiO_2 decorated on SiO_2 sphere

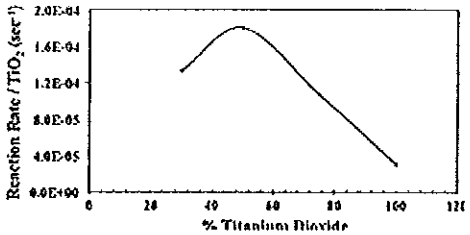

Fig. 7 The reaction rate per titanium dioxide belongs to different ratio of nanoparticle TiO_2 decorated on SiO_2 sphere

3.4 Effect of TiO_2/SiO_2 ratio on photocatalytic oxidation with methylene blue

The photocatalytic oxidation of as-prepared pure TiO_2 and decorated TiO_2/SiO_2 are shown in Fig. 6 as percentage of decolorization of methylene blue by nanoparticle TiO_2 and decorated TiO_2/SiO_2 samples. The concentration of methylene blue decreased exponentially with irradiation time and the highest decolorization of methylene blue belongs to 50% TiO_2/SiO_2. The kinetics of this reaction can be approximated as a first-order process, and the rate constants can be used to compare the relative efficiency of the different materials under essentially identical conditions. Rate constants obtained from this data as a function of percent TiO_2/SiO_2 is shown in Fig. 7. The methylene blue in the absence of semiconductor particles or pure SiO_2 shows negligible photodecomposition. The results show that the rate of decomposition of methylene blue depends on the TiO_2/SiO_2 ratio and was largest at 50% TiO_2/SiO_2, which show an activity about 6 times higher than that of pure TiO_2.

Adsorption behaviour of rhodamine 6G (R-6G) on SiO_2 has been studied extensively. Given that both R-6G and methylene blue are cationic dyes and both have large molecular dimensions, some parallels can be drawn between the two dyes regarding their adsorption onto SiO_2 surfaces [19]. The increase in reactivity can partly be attributed to an

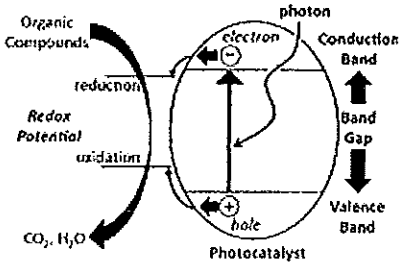

Fig. 8 Schematic representation of the photocatalytic oxidation mechanism of semiconductor materials. *VB* valence band and *CB* conduction bands. Note that for the desired oxidation–reduction reaction to occur for organic compounds, the redox potential needs to be smaller than the band gap, and the reduction potential below in absolute position with respect the conduction band potential, and above for the oxidation and the valence band

increased surface area, and also the beneficial effect of SiO_2, which indicates no photo activity, but is probably related to the preferential adsorption of R-6G on SiO_2. The preferential adsorption effectively increases the surface concentration of R-6G at or near the TiO_2 sites promoting more efficient oxidation by photo generated species [8]. Since methylene blue is a cationic dye as R-6G, then the results in photodecomposition of methylene blue by irradiated TiO_2/SiO_2 particle can be summarized in the same way.

The usefulness of metal oxide for water purification lies in the ability of the photo generated electrons and holes to participate in reactions with the pollutants that have been mineralized to harmless products. Most organic pollutants can be removed by oxidation reactions. As shown in Fig. 8, either the photogenerated hole directly reacts with the pollutant or the hole reacts with water forming hydroxyl species, which oxidize the pollutants. The photocatalytic mechanism of TiO_2 has been well documented and can be summarized as follows [20, 21].

$$TiO_2 + h\nu \rightarrow e_{cb}^- + h_{vb}^+ \quad (2)$$

$$O_{2(ads)} + e_{cb}^- \rightarrow O_2^{\cdot -} \quad (3)$$

$$O_2^{\cdot -} + H^+ \rightarrow {}^{\cdot}OOH \quad (4)$$

$$2\,{}^{\cdot}OOH \rightarrow H_2O_2 + O_2 \quad (5)$$

$$H_2O_2 + e^- \rightarrow {}^{\cdot}OH + OH^- \quad (6)$$

$$H_2O_{2(ads)} + h_{vb}^+ \rightarrow H^+ + {}^{\cdot}OH \quad (7)$$

$$\text{Organic pollutants} + {}^{\cdot}OH \rightarrow \text{degradation products} \quad (8)$$

$$\text{Organic pollutants} + h_{vb}^+ \rightarrow \text{degradation products} \quad (9)$$

The reaction begins with TiO_2 particles being excited with UV light resulting in the formation of electron–hole pair, as displayed in Eq. (2). The electron in the conduction band, e_{cb}^-, and the hole in the valence band, h_{vb}^+, may

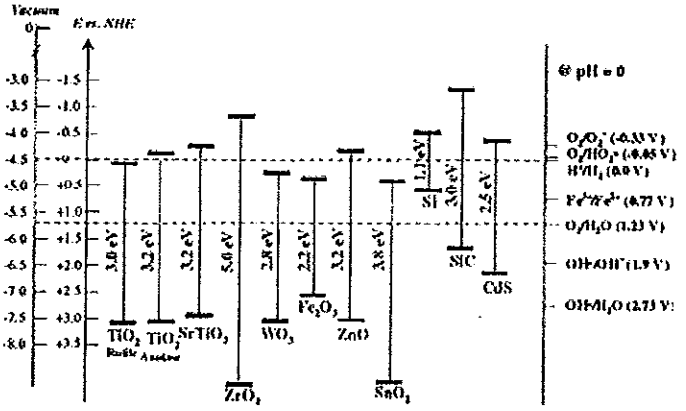

Fig. 9 Conduction band and valence band energy positions for common semiconductors at pH = 0. The value noted on the right axis are the redox potentials for certain common redox couples of interest in water purification. [12]

recombine and nullify further reactions. The e_{cb}–h_{vb} pair, if they do not recombine, will eventually diffuse to the bulk surface and react with other molecules nearby. The e_{cb} can react with molecular O_2 adsorbed at the bulk surface and after few more steps will lead to the formation of OH^* radical at the surface, Eq. (3–6), which plays a major role in photocatalytic reaction. The h_{vb} can react with H_2O at the bulk surface leading to formation of OH^* radical as well, Eq. (7). The OH^* radical can react with adsorbed dye molecules to completely mineralize them, Eq. (8). In addition, the h_{vb} itself can also attack and mineralize dye molecules at the photocatalyst surface, Eq. (9). This cycle continues when light is available.

The relative positions of the redox potentials for the formation of hydroxyl species and the valence band for some common semiconductors are shown in Fig. 9. A semiconductor such as Si with a valence band above the redox potential required for hydroxyl radical formation is not useful for photocatalytic oxidation. Conversely, titanium dioxide has valence bands below the redox potential required for hydroxyl radical formation making it suitable for photocatalytic oxidation. Furthermore, the difference between the redox potential for the desired reaction and the valence and conduction bands acts as the driving potential for the desired reaction. The higher this driving potential is, the faster the oxidation (valence) and reduction (conduction) reactions. Note too in Fig. 8 that the redox couple is generally asymmetric with respect to the band gap, and that if either the reduction or oxidation potential is above or below the conduction and valence band of the photocatalyst, the reaction will not go forward.

However, the limitations of photocatalysts for water purification is the low photoefficiency of photocatalysts and the high energy required for the photon (near UV or UV) to generate electrons and holes. Previous literature has explored multiple ways to improve the photo efficiency of the decontamination and disinfection process for titanium dioxide and other semiconductors. Methods to reduce the energy bandgap and hence the required energy of the photon have also been investigated. Some of the proposed methods to increase photoefficiency focus on increasing the charge separation between the electrons and holes; thus reducing the recombination rates and increasing availability of the electrons and holes to participate in the redox reactions. These methods include the deposition of tiny metal particles on the photocatalyst surfaces that act as electron receptors or supporting of the photocatalyst on substrates as a means for increasing adsorption and photoreaction rates. [21].

In this work, the controlled decoration or grafting of photoactive TiO_2 semiconductor on SiO_2 microsphere was explored as a means to increase photo efficiency. SiO_2 was chosen as the supporting oxide because it is inexpensive and the previous work suggests that the Lewis acidity of the SiO_2 helps increase the photoreaction rates. Furthermore, there is evidence to suggest that the electronic binding energies of the overlying oxide is affected by the underlying SiO_2 and hence opens up the possibility of tuning the position of the valence and/or the conduction band of the TiO_2 [22–24], to better match the absolute values of the redox couple of the compound being decomposed in water.

4 Conclusions

The nanosized TiO_2 decorated on SiO_2 sphere was prepared by sol–gel process. The major phase of the pure TiO_2

particle and deposited TiO_2 on SiO_2 sphere are of the anatase structure. In photodecomposition, a fixed bed reactor was used to study the degradation of methylene blue by TiO_2/SiO_2 and pure TiO_2 particles. A mixed oxide TiO_2/SiO_2 is a more efficient photocatalyst for the degradation of methylene blue than TiO_2 alone. The decomposition rate of methylene blue of 50% TiO_2/SiO_2 is largest in this comparison. The presence of an adsorbent, SiO_2, can act to elevate the efficiency by increasing the quantity of methylene blue near the TiO_2 sites relative to the solution concentration of methylene blue and (though not shown in this study), possibly tunes the position of the valence and/or the conduction band of the TiO_2 to better match the absolute values of the redox couple of the methylene blue.

Acknowledgements This work was partially supported by the Singhalangarand Scholarship for Graduate Studies from Prince of Songkla University (to U.S.) and the NSF Science and Technology Center of Advanced Materials for Purification of Water with Systems (Water CAMPWS). Any opinions, findings, conclusions or recommendations expressed in this publication are those of the authors and do not necessarily reflect the views of NSF. TEM, XRD and XPS analysis were carried out in the Center for Microanalysis of Materials, University of Illinois, which is partially supported by the U.S. Department of Energy under grant DEFG02-91-ER45439.

References

1. Mills A, Hunte SL (1997) J Photochem Photobiol A Chem 108:1
2. Fujishima A, Rao TN, Tryk DA (2000) J Photochem Photobiol C Rev 1:1
3. Roark RD, Kohler SD, Ekerdt JG, Kim SD, Watts JE (1992) Catal Lett 16:37
4. Cunlife R, Koch B, Ruiz P, Delmon B (1995) J Catal 161:524
5. Iaggo P, Aprile G, Di Serio M, Gazzoli D, Santacesaria E (1999) Appl Catal A Gen 178:97
6. Deo G, Turek AM, Wachs IE, Huybrechts DRC, Jacobs PA (1993) Zeolites 13:365
7. Sheldon RA (1980) J Mol Catal 7:107
8. Anderson C, Bard AJ (1995) J. Phys Chem 99:9882
9. Qi K, Chen X, Liu Y, Xin JH, Mak CL, Daoud WA (2007) J Mater Chem 17:3568
10. Sivalingam G, Nagaveni K, Hegde MS, Madras G (2003) Appl Catal B Environ 45:23
11. Zielińska B, Grzechulska J, Grzmil B, Morawski AW (2001) Appl Catal B Environ 35:L1
12. Chandrasekharan R (2008) Doctoral dissertation, University of Illinois at Urbana-Champaign, IL, USA
13. Bergna HE, Roberts WO (2006) Colloidal silica: fundamentals and applications, CRS Press, p 388, ISBN 0824709675
14. Datteo DCM, Schneider M, Bäßler A (1995) J Catal 153:165
15. Rubio J, Oteo JL, Villegas M, Duran P (1997) J Mater Sci 32:643
16. Duran A, Serna C, Fornes V, Fernández-Navarro JM (1986) J Non-Cryst Solids 82:69
17. Gaskell HP, Johnson WD (1976) J Non-Cryst Solids 20:171
18. Jung WY, Baek SH, Park SS, Lee G-D, Jeong ED, Kim HG, Hong S-S (2007) React Kinet Catal Lett 91:233
19. Ohlice SM, Lee S, Williams S, Chang C (2001) Chem Phys Lett 345(1–2):9
20. Houas A, Lachheb H, Ksibi M, Elaloui E, Guillard C, Herrmann JM (2001) Appl Catal B 31:145
21. Arpac M (2003) M Takeuchi J Catal 216:505
22. Wachs IE (1996) Catal Today 27:437
23. Guru G, Grange P (1995) J Catalysis 156:132
24. Lassaletta G, Fernández A, Espinós JP, Gonzáles AR (1995) J Phys Chem 99:1484

VITAE

Name Mrs. Uraiwan Sirimahachai

Student ID 4823018

Education Attainment

Degree	Name of Institution	Year of Graduation
B. Sc. (Chemistry)	Prince of Songkla University	1996
M.Sc. (Inorganic Chemistry)	Prince of Songkla University	2000

Scholarship Awards during Enrolment

1. Songklanagarind Scholarship for Graduate Study from the Prince of Songkla University.
2. Partial support fund from the NSF Science and Technology Center of Advanced Materials for Purification of Water with Systems (WaterCAMPWS), University of Illinois at Urbana-Champaign, for working in U.S.A. (3 months).

Work -position and address

Lecturer, Department of Chemistry, Faculty of Science, Prince of Songkla University.

List of Publication

Uraiwan Sirimahachai, Souwalak Phongpaichit, and Sumpun Wongnawa, 2009. "Evaluation of Bactericidal Activity of TiO_2 Photocatalysts: a Comparative Study of the Laboratory-made and Commercial TiO_2 Samples." *Songklanakarin J. Sci Technol.* **31**, 517-525.

Uraiwan Sirimahachai, Nicholas Ndiege, Ramesh Chandrasekharan, Sumpun Wongnawa and Mark A. Shannon, 2010. "Nanosized TiO_2 Particles Decorated on SiO_2 Spheres (TiO_2/SiO_2): Synthesis and Photocatalytic Activities." *J. Sol-gel Sci. Technol.* **56**, 5653-5660.